NASA Contractor Report 191069

Nonlinear Probabilistic Finite Element Models of Laminated Composite Shells

S.P. Engelstad and J.N. Reddy
Virginia Polytechnic Institute and State University
Blacksburg, Virginia

February 1993

Prepared for
Lewis Research Center
Under Contract NAG3–933

National Aeronautics and Space Administration

TABLE OF CONTENTS

TABLE OF CONTENTS (CONTINUED)

NONLINEAR PROBABILISTIC FINITE ELEMENT MODELS OF LAMINATED COMPOSITE SHELLS

S. P. Engelstad and J. N. Reddy
Department of Engineering Science and Mechanics
Virginia Polytechnic Institute and State University, Blacksburg, VA 24061

SUMMARY

A probabilistic finite element analysis procedure for laminated composite shells has been developed. A total Lagrangian finite element formulation, employing a degenerated 3–D laminated composite shell element with the full Green–Lagrange strains and first–order shear deformable kinematics, forms the modeling foundation. The first–order second–moment technique for probabilistic finite element analysis of random fields is employed and results are presented in the form of mean and variance of the structural response. The effects of material nonlinearity are included through the use of a rate–independent anisotropic plasticity formulation with the macroscopic point of view. Both ply–level and micromechanics–level random variables can be selected, the latter by means of the Aboudi micromechanics model. A number of sample problems are solved to verify the accuracy of the procedures developed and to quantify the variability of certain material type/structure combinations. Experimental data is compared in many cases, and the Monte Carlo simulation method is used to check the probabilistic results. In general, the procedure is quite effective in modeling the mean and variance response of the linear and nonlinear behavior of laminated composite shells.

1. INTRODUCTION

1.1 Motivation

The use of fiber reinforced composite materials in modern engineering structural design has become a common practice. Organic matrix composite materials such as graphite–epoxy have been used extensively with substantial weight savings along with additional benefits such as dimensional stability. More advanced materials such as metal matrix composites are being developed for use in aerospace structures where temperature requirements exceed the limits of typical organic matrix composites. Analytical methods for metal matrix composites are a "hot" item in current research, and in order to use these materials, methods for determining design limitations are necessary.

In the area of structural analysis, the finite element method (FEM) has become the most widely used analysis tool. Developments and improvements have progressed over the last two decades to the point where many families of reliable finite element codes are in place. For a typical FEM analysis, it is a fair statement to say that uncertainties caused by modeling inaccuracies are far outweighed by uncertainties in the material properties, geometry, and loading of the problem. This is the primary reason for the development of probabilistic finite element methods, so that these uncertainties can be modeled within the framework of statistical methods.

The benefits from the use of statistical methods in design are numerous. They include: 1) a reduction in design conservatism, so that materials can be used to their true capacity; 2) the ability to quantify the amount of variability itself, and 3) the estimation of the risk of exceeding design variables. As opposed to a deterministic yes–no failure analysis, risk of failure or "reliability"

of a structure can be much more meaningful to the designer. This reliability can only be determined if the uncertainties of the problem are included in the model.

As composite materials are incorporated into modern structural components, lack of an experience base induces a trend towards conservatism in the design. Thus much of the available savings in weight and long term costs are lost. Since more design variables exist when composites are involved, and the manufacturing processes for producing composite materials themselves are more complex, then more variability can exist in a design produced with composites versus conventional materials. Thus the motivation of this research is to develop methods for probabilistic structural analysis of composite materials. Laminated shell type structures are selected as the focus, and both geometric and material nonlinearities are included.

In the following section, a summary of the selected methods used in the present study, along with some discussions involving orginality are presented.

1.2 Present Study

The main objective of this study is to develop a probabilistic finite element procedure to be used for reliability analysis of laminated composite shells. Since these structures often exhibit both geometric and material nonlinear behavior, these nonlinearities have been included in the development. The discussion to follow describes the deterministic and probabilistic methods incorporated into the computational procedure.

A degenerated 3–D shell element formulation, incorporating the first–order shear deformable kinematics, has been chosen to model laminated composite shell structures. For organic matrix composites, the importance of shear deformation has been covered in the literature quite extensively. An example has been given in this work which illustrates this importance in the postbuckling range, both for determining postbuckling response and failure.

The second–moment technique for probabilistic finite element analysis has been employed. The random variables built into the model include the ply stiffnesses, orientation angles, and ply thicknesses. Using a micromechanics theory, micromechanics level random variables such as fiber and matrix stiffnesses and volume ratios can be selected.

Geometric nonlinearity is based on the total Lagrangian approach with the full Green–Lagrange strains. Material nonlinearity is incorporated using classical rate–independent plasticity and a general orthotropic yield function. The radial return algorithm for plane stress has been extended to calculate the elastic–plastic stresses with the orthotropic yield function.

The probabilistic responses in the computer program, developed during this study, are the first and second probabilistic moments of the structural responses, which include deflection, strain, and stress. It was decided that verification of the second–moment methods using Monte Carlo procedures would be made easier if these moments (mean and variance) were calculated. Also, the variability of the response due to individual random variables can be quantified (sensitivity analysis) by estimating the variance. In order to become familiar with all the computational subtleties in the probabilistic finite element

method, the mean and variance calculations are the natural first step. Obviously, future work involves incorporation of the reliability estimation techniques.

The originality in this study lies in the application of the second–moment method for probabilistic finite element analysis to geometric and material nonlinear composite shells. Previous work in the literature for composites only involved linear analysis of plates, in which classical lamination theory was used. Other works involved geometric or material nonlinearities in a probabilistic finite element format, but only for isotropic materials and usually only for plates. It is of interest here to analyze more realistic laminated composite structures, so the shell element with shear deformation theory has been employed. The computational difficulties in analyzing actual laminated composite panels, involving models with large numbers of layers and degrees of freedom, and also that proceed deep into the postbuckling range, have been investigated. Several comparisons have been made with experimental results as well.

A review of the literature involving several areas of research of importance to this study is presented in Sec. 2. Section 3 contains the theoretical development of the degenerated 3–D shell element for laminated composite shells and the finite element formulation of the incremental equations of motion including geometric nonlinearity. The Aboudi micromechanics theory is developed in Sec. 4, and the anisotropic plasticity formulation is presented in Sec. 5. Section 6 contains the development of the second–moment probabilistic finite element method, including discussions on computational saving techniques. A number of illustrative problems are solved

in Sec. 7, which demonstrate various aspects and capabilities of the overall procedure. Section 8 provides a summary, conclusions, and recommendations for future work.

Throughout this study it has been assumed that the reader has a basic understanding of probability concepts and terms. However, to aid in this area, a review of reliability estimation theory, along with a brief explanation of basic terms is presented in Appendix A. Appendix B describes the Monte Carlo simulation technique.

2. LITERATURE REVIEW

The purpose of this review is to assess the current state of probabilistic finite element methods in general, and in particular to include any work in relation to composite materials. A brief discussion of various micromechanics models, macroscopic anisotropic plasticity theories, and reliability estimation methods will be given as well.

2.1 Probabilistic Finite Element Methods

Probabilistic finite element methods have generally evolved along two major paths [33]. The first one uses standard statistical methods in conjunction with the finite element code. The second method involves non–statistical techniques and differs little from deterministic methods. These two categories will be discussed, with emphasis on the second one since it contains the primary concentration of effort in current research.

2.1.1 Statistical Approach

Typically these methods involve statistical sampling procedures known as Monte Carlo simulation. Sampling from a known multivariate distribution function is conducted and due to the 'weak law of large numbers' [1], large sample sizes must be used in order to converge to the approximately correct statistical parameters of the response. These methods therefore become very expensive, as finite element solutions must be produced for each sample. When correlation of the random variables exist, transformations must be performed prior to simulation since simulation involves independent sampling. In order to cut down on the number of samples required for the direct Monte Carlo

simulation technique, other methods of sampling such as stratified sampling and Latin hypercube sampling are often used [1–3]. Since the literature in this category is quite extensive, a few of the most important and widely used statistical methods are reviewed.

An example of the use of Monte Carlo techniques to study a spatial stochastic process is given by Ma and Wei [4]. They considered homogeneous and inhomogeneous processes, and a Choleski decomposition of the covariance matrix was used to correlate the Monte Carlo sampling. The direct sampling method, coupled with the finite element procedure were used to study porous random fields for groundwater flow.

The Neumann expansion technique proposed by Shinozuka et al. [5,6] used sampling techniques that successfully reduced the computational effort in solving the finite element equations independently for each sample. The Neumann expansion method effectively employs a perturbation expansion in conjunction with the Monte Carlo simulation so that only a single stiffness matrix factorization is required. The method allows for large variability of the random variables to be modeled without loss of accuracy. It can be easily adapted to an existing finite element code with little change.

Contreras [7] proposed a different method in which stochastic differential and difference theory is applied to structures discretized using the finite element method. A semi–discretized formulation is employed in which a finite difference method is used for the time domain and the finite element method is used for the spatial domain. This technique involves a complete reformulation of an existing finite element program in order to model the stochastic differential equations.

A method known as stochastic linearization [8,9] has been used to solve nonlinear stochastic differential equations of random vibration in which the loading is the only random process. Recently, Mohammadi and Amin [10] and Casciati and Faravelli [11–15] employed it for dynamic analysis of material nonlinear continua. The stochastic linearization technique is used to linearize the nonlinear hysteresis behavior in the model. In addition, Chen and Yang [16] used a finite element formulation combined with stochastic linearization and normal mode methods to study geometrically nonlinear random vibration of plate and shell structures. In general, this method has only been applied to random loading problems, and not to problems in which uncertainties exist in the properties.

Faravelli [17] has demonstrated another statistical approach in which a planned set of experiments around the space of the central values of the different random vectors is performed using a standard finite element code to determine the response to the different inputs. A regression analysis is then used to fit the response to an appropriate polynomial of the input variables. A level–2 reliability approach is introduced to obtain approximations of the cumulative distribution functions of the response variables. Nonlinear problems can be solved as well as linear. In order to minimize the number of numerical experiments necessary, experimental design theory is used. It seems that this method would be computationally costly when a large number of random variables is involved. In reference [18], the method was applied to an automotive impact problem. A similar method was used by Chryssanthopoulos et al. [19] to perform a reliability–based design of stringer stiffened cylinders under axial compression.

Larder [20] developed a method for studying failure in parallel fiber composites. A deterministic finite element formulation was used to model the fiber and matrix of a representative cell, and then Monte Carlo simulation methods were used to simulate randomly occurring damage. The program however, could not model general structural level problems.

Deodatis and Shinozuka [21] developed a probabilistic model for the spatial strength variation in laminated orthotropic composites. Monte Carlo simulation techniques were coupled with Tsai–Hill and Tsai–Wu failure criteria and assumed failure mechanisms.

Finally, Ditlevsen et al. [22] have conducted research in improving the efficiency of the Monte Carlo method. An off–mean centered directional importance sampling procedure is compared to other uniform directional sampling methods. The aim was to further reduce the number of samples required as compared to other improved Monte Carlo procedures.

2.1.2 Non–Statistical Approaches

Non–statistical finite element approaches seem to be getting the most attention in current research. These approaches include second–moment analysis, numerical integration, and the new iterative perturbation methods, which use multiple regression as a post–processor. These techniques will be discussed and compared in detail in the following review.

Ang and Tang [23], discussed a method of using the Taylor series expansion of a general function g(X) about the mean of the random variable X and truncating the series after the second order terms. They showed that the mean of g(X) can be estimated using a second–order approximation which uses

the first and second statistical moments of X, and that the variance of g(X) can be estimated using a first–order approximation which requires only the second moment of X. Since higher statistical moments of the original variate X would be required for a higher–order approximation to the variance of g(X), the variance was left at first–order. Higher moments of the original variates are generally not known. A major advantage of this method is that the multivariate distribution function does not need to be known, but only the first two moments. Since a first–order Taylor series approximation is used for the variance, then uncertainties in the original variates cannot be too large. This means that deviations from the mean of the random variables of the function cannot be large, typically not greater than 10 percent. However, they showed that acceptable results can still be obtained for coefficients of variation as high as 20 percent. An important point is that these approximations have proven to be adequate even when the function g(X) is nonlinear, as long as the variance of X is small relative to g(X). This leads directly to the works by Liu et al. [33–40] to be discussed later.

Handa and Andersson [24] used the above ideas combined with the finite element method to study linear truss structures and the effects of correlation. At about the same time Hisada and Nakagiri [25] used the same "perturbation" (second–moment) method to analyze structures with uncertain shapes. In this work the geometrical coordinates were allowed to be random variables. Nakagiri et al. [26–29] were the first, and to the author's knowledge, the only researchers to apply this method to the analysis of composites. In [26], probabilistic eigenvalue analysis of linear vibration of fiber reinforced laminated plates was studied, in which the fiber orientation angle and the layer thickness

were random variables. The effects of these random variables on the eigenvalues of the plate with and without correlation was investigated. In [27], reliability indices of a fiber reinforced laminated plate were calculated as the end result of the stochastic finite element technique. Here elastic constants of the layers were treated as the random variables, but no spatial correlation was considered. The strengths used in the failure criterion to determine reliability, were also variates. Cases in which flat plates under uniaxial tension, with and without holes, were analyzed to investigate the effect of the distributed stress on the reliability index. In [28], Tani and Nakagiri extended the method to perform design optimization of the reliability index of fiber reinforced plastic (FRP) laminated plates with probabilistic elastic constants and lamina strengths. The fiber orientation angle was the design parameter in the optimization, and failure of each lamina was determined by the Tsai–Hill criterion. Sato, Watanabe, and Nakagiri [29] used the second–moment method to perform a reliability analysis of a FRP pressure vessel with probabilistically distributed stacking parameters. Linear elastic material and geometrically linear behavior was studied in their work.

A different approach to the second–moment method was used by Lawrence [30]. Here expansions of random variables in terms of orthogonal Galerkin type functions became the core of his "basis random variable" technique. A Rayleigh–Ritz finite element model was derived, and the first and second moment statistics were obtained from a series of linear solutions. Lawrence [30] achieved the same accuracy as other second–moment FEM techniques; however, he stated that the greatest advantage of his method over others is the ease of application. Using the basis random variable

representation, the random character of the problem is treated "merely as an extra set of dimensions". Later, Lawrence [31] applied the method to probability based design, in which sensitivities of reliability indices to design variables are calculated to enhance the design process. Additionally, Ghanem and Spanos [32] developed an independent but similar Galerkin–based response surface approach. In these works only linear problems were studied.

Liu, Belytschko, and Mani [33–40] have carried out the most developmental work using the second–moment finite element method. They have applied the method to nonlinear structural dynamics for correlated or uncorrelated discrete random variables [34,35], and later to nonlinear structural dynamics problems with both homogeneous or inhomogeneous random fields [33]. They termed the method the Probabilistic Finite Element Method (PFEM), and applied it to geometric as well as material nonlinear problems. Good results were achieved since the coefficients of variations were kept around 10 percent. It is noted that the probabilistic density functions must also be considered to have decaying tails to maintain good results. Only isotropic materials were studied. Two methods for improving computational efficiency were developed: 1) transforming the correlated random variables to independent uncorrelated random variables thereby reducing the order of the tensor multiplications required, and 2) an adjoint method was introduced to reduce computations by allowing the statistics of the response to be calculated only in a reduced domain from the original problem.

Liu, Besterfield, and Belytschko [36] developed a probabilistic Hu–Washizu variational principle (PHWVP) for the PFEM. They applied it to both linear and nonlinear elasticity. Using this principle, the probabilistic

distributions for the constitutive law, compatibility condition, equilibrium, domain and boundary conditions can be incorporated into the PFEM. Thus all aspects of the problem were treated as random variables or fields.

The latest work by these authors involves an optimum fusion of PFEM and reliability analysis. Liu, et al. [41] applied the method to probabilistic fracture mechanics. Uncertainties in loads, material parameters, geometry, crack length, orientation and location can be incorporated into the problem to determine the probability of brittle fracture. The reliability analysis is performed using a Kuhn–Tucker optimization procedure. An enriched finite element with the embedded crack–tip singularity is employed in this overall reliability package. In [42], they extended the method to fatigue crack growth problems. Liu, Chen, and Lu [43] have also applied the reliability and PFEM fusion method to the fluid–structure interaction problem in which the influences of random parameters on the energy transfer between the structural system and the acoustic system were studied.

Several other authors have fused the first and second–order reliability methods with finite element methods. Here the differentiation of the finite element equations with respect to the random variables is performed as in the second–moment formulation, except that these are then blended directly into the first–order reliability equations. In this way the small probabilities of failure required in structural reliability calculations can be accurately predicted. These small probabilities at the tails of the distributions are poorly defined by first and second moments. Arnbjerg–Nielson and Bjerager [44] applied a form of the method to linear and nonlinear truss structures. Der Kiureghian et al. [45,46] applied it to linear and nonlinear beam and plate problems. The key

point is that while the PFEM methods evaluated statistical moments, this step is avoided altogether here in the process of estimating reliability.

Other non–statistical techniques have been developed and are discussed next. Liu et al. [34] developed a numerical integration procedure in which Hermite–Gauss quadrature is used for numerically evaluating the integrals involved in the definition of expectation and variance. The method assumes uncorrelated fields and has limited use, especially for problems involving large numbers of random variables (also see Gorman [47]). Takada and Shinozuka [48] have developed a new method in which local integrations of the continuous stochastic field are made on an element by element basis to form element stiffness matrices so that the random field is transformed into only a few random variables. This new method has been proven to allow much coarser meshes than the first–order second–moment methods, but requires more computational time for equivalent mesh sizes. It has only been applied to linear elastic problems. A similar idea is used by Weiqiu and Weiqiang [49], in which local averages of the random field are used to improve the accuracy of the second–order perturbation method. They applied it to random eigenvalue problems.

The best alternative to the first–order second–moment methods is one developed by Dias and Nagtegaal [50]. They introduced stochastic finite element techniques based on the Fast Probability Integration (FPI) algorithms developed by Wu and others [81–85]. Using FPI, and given a closed–form expression of the response variable as a function of the uncorrelated random variables (normalized to zero mean and unit standard deviation), an optimization algorithm is then used to determine the minimum distance from

the origin to a given limit state. This minimum distance is commonly referred to as the safety index, from which the probability of exceedance of the limit state can easily be computed. Thus what is needed is a method to relate the response of the structure to the uncorrelated random variables. By performing a spectral decomposition of the covariance matrix, the correlated random variables can be related to a set of uncorrelated random variables. In order to determine the response of the structure, the deterministic finite element model is used in conjunction with a prescribed set of perturbations of the input random variables. To obtain a closed–form expression of the response, a multiple regression procedure that fits the stored perturbations to a polynomial expression is used.

Obviously the method requires a multiple set of solutions of the finite element model which can become computationally expensive. In order to overcome this problem, an approach based on a modified Newton iteration method was developed. Basically it uses an iterative perturbation procedure about the known mean deterministic solution, so that multiple perturbation solutions can be obtained using only one factorization of the stiffness matrix. A notable advantage of this method is the lack of modifications required to incorporate it into an existing finite element program. In addition, the method is not limited to any specific probability distributions for the input random variables. What is needed is an efficient data storage structure to keep track of the multitude of perturbation solutions. Many other authors have worked with Dias in this arena (see [50–55]). It is of importance to mention that the Probabilistic Structural Analysis Methods (PSAM) being developed at NASA–Lewis Research Center use this technique, due to its ease of

incorporation into any finite element formulation by simply coupling it with existing modules for reliability computations.

Various examples exist in the literature of application of the previously discussed methods to specific problems. A recent book edited by Liu and Belytschko [56], contains a wealth of interesting examples. Recent works using the first–order second–moment stochastic FEM method for analysis of soil structures are given in references [57,58]. Various stochastic FEM methods for solving material nonlinear problems are reviewed in references [59–62].

2.1.3 Comparison of Approaches

From the literature review, it was quickly determined that the non–statistical techniques would prove to be the most promising for application to linear and nonlinear composite structures. It was also noticed immediately that little work has been done (only Nakagiri [26–29]) in the area of stochastic finite element procedures for composite structures. Out of all the works reviewed, the second–moment techniques have received the most attention for nonlinear applications, but only for isotropic behavior (see Liu et al. [33–40] and Liu and Der Kiureghian [46]). The iterative perturbation techniques also seem very promising. The following discussion is an attempt to compare the pros and cons of these two procedures.

The first–order second–moment approach is basically a mean–centered perturbation method since the Taylor series expansion is performed about the mean point. Since it is only a first–order approximation for the covariance, then the method does not allow for large variations of the input random variables from the mean. Typically coefficients of variation of 10 percent give

good results, however, and for most material property variations this range is well within the expected level of uncertainty.

In order to apply the second–moment technique to an existing finite element code, significant changes must be made in order to calculate partial derivatives of the stiffness matrices and loads with respect to the random variables. These derivatives can be obtained either using analytical differentiation of the formulation under consideration or finite difference techniques. The latter method should allow more generic programming techniques to be employed, making it more formulation independent. As the number of random variables in the problems increase, it becomes apparent that a significant amount of storage becomes necessary to retain all the partial derivatives.

An advantage of the second–moment method is that it has been previously demonstrated for nonlinear problems by Liu et al. [33–40], with good success. The authors also developed techniques for efficiency improvements to reduce the computational costs considerably.

Once the statistical moments of the response are determined using the second–moment formulation, any of the reliability estimation techniques can be employed. Recent work however, has shown that this is not necessary; in fact, it is more accurate not to calculate the moments but to evaluate the sensitivity derivatives in the finite element program and use them directly to estimate reliability. In any case, unlike the iterative perturbation methods, no regression curve fitting is required in this step.

The iterative perturbation methods involve a higher order perturbation than the strict first–order second–moment methods. Using the iterative

procedure, higher order terms are effectively captured. The stability of the algorithm is conditional however, and convergence is not assured for large stiffness perturbations. The method can be generalized so that any finite element formulation can be incorporated into the algorithm without any element level program changes. Like the previous second–moment methods, it requires significant storage in order to retain all the response solutions to the various perturbations of the random variables. This storage coordination must be very well organized and self contained as well.

The iterative methods have just recently been demonstrated for material nonlinear problems in the current literature. Convergence stability problems have been reported when constraint equations exist such as those for thin plates and shells allowing transverse shear deformation, deviatoric rate–independent plasticity, and incompressible or near–incompressible elastic materials. Currently, stability limits are being developed to alleviate these problems.

The results of the iterative perturbation finite element program are data files of response for various perturbed inputs. In order to make reliability calculations, the FPI reliability algorithms require a closed form equation involving the response variables as a function of the input random variables. Thus multiple regression techniques are employed at this step to obtain a polynomial equation from the response data files.

After reviewing all of the above facets of the two methods, it was decided to use the second–moment methods for the present application. Since an experience base exists for the nonlinear applications, and since large non–normal variations are not anticipated for the uncertainties, the methods should be acceptably accurate. As for the storage problems, it appears that

both methods will require considerable storage, so this really is not a factor. Since Liu et al. [33–40] has developed techniques for reducing computational costs, it was anticipated that the effort spent making significant programming changes would be rewarded by a reduction in CPU charges. This is very important since a rather large number of random variables are needed to model the uncertainties in a composite laminate.

2.2 Micromechanics Models

One of the goals of this research is to model from a micromechanics level the uncertainties in laminated composites, involving both linear and nonlinear behavior. It was discovered, however that certain algorithmic difficulties existed in coupling a micromechanics–based plasticity theory with the second–moment stochastic finite element methods. Thus the micromechanics model was limited to linear and geometric nonlinear elastic behavior for this study with the possibility of adding the material nonlinear case at a later date. In any case, it was desired to select a micromechanics theory that has proven to be effective in the literature. Arenburg [63] has given a very thorough review of this area of research, and has recommended the model by Aboudi [64]. This model is based on a higher–order continuum theory that can account for particulate or continuous fiber reinforcement, general mechanical and thermal load histories, and damage in the form of fiber–matrix debonding. Arenburg used this model to develop a finite element program for the analysis of metal–matrix composite plates. In his work, the unified theory of Bodner [65] was used to model the nonlinear viscoplastic behavior of the matrix. In the

present work, Aboudi's model will again be used, but in this case will be limited to elastic behavior.

2.3 Macroscopic Anisotropic Plasticity

In order to model the nonlinear material behavior existing in metal matrix composites, it was decided to use the macroscopic or smeared approach. This method proved to be more compatible with the probabilistic finite element method both from an algorithmic and a computational expense point of view. Many authors have made contributions in this area. Griffin [66] and Arenburg [63] have presented surveys of the theories of plasticity in anisotropic materials. It is not of interest here to review all of these, but to touch on the most notable and then explain the reasons for selecting the theory used in the present work.

Hill's anisotropic theory of plasticity [67,68] has received much attention. This theory was based on a generalization of the von Mises yield criterion which assumed yielding was independent of hydrostatic stress and that plastic flow was incompressible. Whereas these assumptions are standard and experimentally validated for metals, they have been shown to be incorrect for some materials by Lin et al. [69]. Griffin [66] and Chandrashekhara [70] have applied the theory in finite element formulations. While Griffin showed generally good agreement with off–axis test data, Chandrashekhara did not make any experimental comparisons.

An endochronic theory of plasticity of Valanis [71] was extended to transversely isotropic media by Pindera and Herakovich [72]. Various effects

such as cyclic loading and unloading and stress interaction were successfully demonstrated.

Recently, Sun et al. [74–77], presented a plasticity formulation based on the anisotropic plastic flow rule proposed by Kachanov [73]. The yield function they selected was quadratic in stresses and, in general, excludes the assumptions of incompressibility of plastic strains and that no yielding is caused by hydrostatic stresses. The formulation was installed in a finite element program, and much experimental validation work was performed for Boron/Aluminum composites [74–77]. Examples of off–axis uniaxial test specimens with holes, edge cracked panels, and cyclic loading and unloading under constrained plasticity conditions were demonstrated with good analytical/experimental comparisons. Due to the generality and amount of experimental work done by Sun and his coworkers, this plasticity formulation was selected for the present work. Algorithmic modifications were made for computational efficiency and compatibility with the second–moment probabilistic method.

2.4 Reliability Estimation

Orginally it was planned to estimate reliability as a post–processing function using the first and second moments of the stress or displacement response output from the probabilistic finite element analysis. However recent work [41–42,45–46], which fused the second–moment probabilistic finite element methods with the first and second–order reliability methods, have shown that direct use of the response derivatives with respect to the random variables (obtained from the finite element program) in the reliability

algorithms is much more accurate for small probabilities of failure. These small probabilities at the tails of the distributions are poorly defined by the first and second moments. For this reason, the reliability estimations in the present work are limited to approximations based on the first and second moments (these moments are still quite useful for sensitivity analysis). Future work will use the response derivatives already evaluated in the finite element program directly for reliability estimation. Appendix A gives a brief explanation of the reliability procedures.

In reviewing the vast literature in reliability computation, the first and second–order reliability methods are prominant. References [23,45,46,56] give a good description of these methods. The family of Fast Probability Integration (FPI) algorithms has also been found to be important in recent work. The origin of the FPI methods can be traced to the definition of a safety index proposed by Hasofer and Lind [78]. Rackwitz and Fiessler [79] later extended the algorithm to accommodate non–Gaussian distributions. Recent work by Wu et al. [81–85] contains further improvements in terms of accuracy and computational efficiency.

3. FINITE ELEMENT FORMULATION

In this chapter a review of the finite element formulation of the incremental equations of motion of a continuous medium including geometric nonlinearity will be presented. The degenerated 3–D shell element for composite laminates will then be reviewed. The formulation is based on the work by Liao and Reddy [86]. Summation convention on repeated indices is assumed throughout this study.

3.1 Principle of Virtual Displacements

The principle of virtual displacements requires that

$$\int_v \tau_{ij} \delta e_{ij} dv = R \tag{3.1}$$

where δ is the variational symbol,

τ_{ij} = the Cartesian components of the Cauchy stress tensor at time $t + \Delta t$ (i.e., configuration 2).

e_{ij} = the Cartesian components of the infinitesimal strain associated with the incremental displacements Δu_i in going from the configuration at time t to the configuration at time $t + \Delta t$, i.e. $e_{ij} = \frac{1}{2}\left(\frac{\partial \Delta u_i}{\partial x_j} + \frac{\partial \Delta u_j}{\partial x_i}\right)$ which are also referred to this unknown configuration at time $t + \Delta t$.

x_i = Cartesian components of a point in the configuration at time $t + \Delta t$,

and

$$R = \int_a t_k \delta u_k da + \int_v \rho f_k \delta u_k dv \tag{3.2}$$

In equation (3.2), t_k and f_k are the components of the externally applied surface and body force vectors respectively, and δu_k is a virtual variation in the current displacement components u_k, where

$$u_k = x_k - X_k,$$

X_k being the Cartesian coordinates of a point in the configuration at time $t = 0$.

3.2 Total Lagrangian Formulation

Equation (3.1) cannot be solved directly since the configuration at time $t + \Delta t$ is unknown. An approximate solution of equation (3.1) can be obtained by referring all variables to a previously calculated known equilibrium configuration and linearizing the resulting equation. The total Lagrangian (T.L.) formulation, in which all static and kinematic variables are referred to the initial configuration at time 0 of the body, is used here. The applied forces in equation (3.1) are evaluated using

$$\begin{aligned} T_k dA &= t_k da \\ \rho_0 F_k dV &= \rho f_k dv \end{aligned} \tag{3.3}$$

where T_k, F_k, dA, dV, ρ_0 refer to time $t = 0$ and t_k, f_k, da, dv, ρ refer to time $t + \Delta t$.

The volume integral of Cauchy stresses times variations in infinitesimal strains in equation (3.1) is transformed to an integral over a known volume (the initial volume) using the 2nd Piola–Kirchhoff stress tensor and the energetically conjugate Green–Lagrange strain tensor to give

$$\int_v \tau_{ij} \delta e_{ij} dv = \int_V S_{ij} \delta E_{ij} dV \tag{3.4}$$

where

S_{ij} = Cartesian components of the 2nd Piola–Kirchhoff stress tensor corresponding to configuration at time $t + \Delta t$ but measured in the configuration at time $t = 0$.

E_{ij} = Cartesian components of the Green–Lagrange strain tensor in the configuration at time $t + \Delta t$, referred to the configuration at time 0:

$$E_{ij} = \frac{1}{2}(u_{i,j} + u_{j,i} + u_{k,i}u_{k,j}) \text{ and } u_{i,j} = \frac{\partial u_i}{\partial X_j}$$

The 2nd Piola–Kirchhoff stress tensor referred to the configuration at time $t = 0$ is defined as

$$S_{ij} = \frac{\rho_o}{\rho} X_{i,s} \tau_{sr} X_{j,r} \tag{3.5}$$

Substituting equations (3.3) and (3.4) into (3.1) and (3.2), we obtain

$$\int_V S_{ij} \delta E_{ij} dV = R \tag{3.6}$$

which involves the equilibrium for the body in the configuration at time $t + \Delta t$ but referred to the configuration at time $t = 0$. In equation (3.6), R is calculated using

$$R = \int_A T_k \delta u_k dA + \int_V \rho_o F_k \delta u_k dV \tag{3.7}$$

The stresses S_{ij} and strains E_{ij}, which are unknown at time $t + \Delta t$, are decomposed as

$$S_{ij} = S^1_{ij} + S^0_{ij} \tag{3.8}$$

$$E_{ij} = E^1_{ij} + E^0_{ij} \tag{3.9}$$

where S^1_{ij} and E^1_{ij} are the known 2nd Piola–Kirchhoff stresses and Green–Lagrange strains in the configuration at time t, and S^0_{ij} and E^0_{ij} are the incremental components of the same quantities at time $t + \Delta t$. It follows from equation (3.9) that

$$E^0_{ij} = e^0_{ij} + \eta^0_{ij} \tag{3.10}$$

where

$$e^0_{ij} = \tfrac{1}{2}(\Delta u_{i,j} + \Delta u_{j,i} + U_{k,i}\Delta u_{k,j} + \Delta u_{k,i}U_{k,j}) \tag{3.11}$$

$$= \text{linear part of strain increment } E^0_{ij} \text{ (linear in } u_{i,j})$$

$$\eta^0_{ij} = \tfrac{1}{2}(\Delta u_{k,i}\Delta u_{k,j}) \tag{3.12}$$

$$= \text{nonlinear part of strain increment } E^0_{ij}$$

and

$$U_{i,j} = \frac{\partial U_i}{\partial X_j} \ , \ \Delta u_{k,i} = \frac{\partial \Delta u_k}{\partial X_i}$$

In the above formulation, the definition of the Green–Lagrange strain tensor was employed along with the following definition

$$u_i = U_i + \Delta u_i$$

where Δu_i is the incremental displacement and U_i is the displacement at time t.

The constitutive relationship for the incremental 2nd Piola–Kirchhoff stresses and incremental Green–Lagrange strains is assumed to be governed by the generalized Hooke's law,

$$S^0_{ij} = C_{ijrs} E^0_{rs} \tag{3.13}$$

where C_{ijrs} are components of the constitutive tensor. Substituting equations (3.8)–(3.13) into equation (3.6) it follows that

$$\int_V C_{ijrs} E^0_{rs} \delta E^0_{ij} dV + \int_V S^1_{ij} \delta \eta^0_{ij} dV = R - \int_V S^1_{ij} \delta e^0_{ij} dV \tag{3.14}$$

which represents a nonlinear equilibrium equation for the incremental displacements Δu_i.

3.3 Linearization of Incremental Equations of Motion

Since equation (3.14) is nonlinear in the incremental displacements and cannot be solved directly, approximate solutions are obtained by assuming

$E^0_{ij} = e^0_{ij}$ and $\delta E^0_{ij} = \delta e^0_{ij}$. The constitutive equation becomes

$$S^0_{ij} = C_{ijrs} e^0_{rs} \tag{3.15}$$

Making the above substitutions the approximate equation is now

$$\int_V C_{ijrs} e^0_{rs} \delta e^0_{ij} dV + \int_V S^1_{ij} \delta \eta^0_{ij} dV = R - \int_V S^1_{ij} \delta e^0_{ij} dV \tag{3.16}$$

Using Hamilton's principle, the effects of the inertial forces can be included. Employing similar procedures as before, we obtain the equations of motion of the moving body at time $t + \Delta t$ in the variational form as

$$\int_V \rho_0 \ddot{u}_i \delta u_i dV + \int_V C_{ijrs} e^0_{rs} \delta e^0_{ij} dV + \int_V S^1_{ij} \delta \eta^0_{ij} dV = R - \int_V S^1_{ij} \delta e^0_{ij} dV \tag{3.17}$$

Equation (3.17) forms the theoretical basis for the finite element model.

3.4 Finite Element Model

Using standard isoparametric interpolation, the final incremental equations of motion for an element are given by

$$[M^e]\{\ddot{\Delta}^e\} + ([K^e_L] + [K^e_{NL}])\{\Delta^e\} = \{R^e\} - \{F^e\} \tag{3.18}$$

where $\{\Delta^e\}$ is the vector of nodal incremental displacements from time t to

time t + Δt in an element, and $[M]\{\ddot{\Delta}\}$, $[K_L]\{\Delta\}$, $[K_{NL}]\{\Delta\}$, and $\{F\}$ are obtained, respectively, from the following integrals

$$\int_V \rho_o \ddot{u}_i \delta u_i dV \ , \ \int_V C_{ijrs} e^o_{rs} \delta e^o_{ij} dV$$

$$\int_V S^1_{ij} \delta \eta^o_{ij} dV \ , \text{ and } \int_V S^1_{ij} \delta e^o_{ij} dV$$

These integrals can be written in the standard matrix form as [86]

$$[K_L] = \int_V [B_L]^T [C][B_L] dV \tag{3.19}$$

$$[K_{NL}] = \int_V [B_{NL}][S][B_{NL}] dV \tag{3.20}$$

$$[M] = \int_V \rho_o [H]^T [H] dV \tag{3.21}$$

$$\{F\} = \int_V [B_L]^T \{\hat{S}\} dV \tag{3.22}$$

In equations (3.19)–(3.22), $[B_L]$ and $[B_{NL}]$ are linear and non–linear strain–displacement transformation matrices, [C] is the incremental stress–strain material property matrix, [S] is a matrix of 2nd Piola–Kirchhoff stress components, $\{\hat{S}\}$ is a vector of these stresses and [H] is the incremental displacement interpolation matrix. All matrix elements correspond to the

configuration at time t and are defined with respect to the configuration at time 0.

The finite element equations in (3.18) are second–order differential equations in time. Equation (3.18) must be further discretized in time to obtain algebraic equations, which can be assembled and solved after imposing initial and boundary conditions. Here the Newmark integration scheme is used to approximate the time derivatives. The resulting algebraic equations are given by (see Reddy [87])

$$[\hat{K}]\{\Delta\} = \{\hat{R}\} \tag{3.23}$$

where $\{\Delta\}$ is the vector of nodal incremental displacements at time t, and

$$[\hat{K}] = a_0[M] + [K_L] + [K_{NL}]$$

$$\{\hat{R}\} = \{R\} - \{F\} + [M](a_1\{\dot{\Delta}\} + a_2\{\ddot{\Delta}\}) \tag{3.24}$$

$$a_0 = \frac{1}{\beta(\Delta t)^2} \ , \ a_1 = a_0\Delta t \ , \ a_2 = \frac{1}{2\beta} - 1$$

where $\alpha = 1/2$, $\beta = 1/4$ for the constant average acceleration method and Δt is the time step. Once equation (3.23) is solved for $\{\Delta\}$ at time $t + \Delta t$, the acceleration and velocity vectors can be computed from

$$\{^2\ddot{\Delta}\} = a_0\{^2\Delta\} - a_1\{^1\dot{\Delta}\} - a_2\{^1\ddot{\Delta}\}$$

$$\{^2\dot{\Delta}\} = \{^1\dot{\Delta}\} + a_3\{^1\ddot{\Delta}\} + a_4\{^2\ddot{\Delta}\} \tag{3.25}$$

where the superscript 2 refers to time t + Δt and 1 refers to time t, and

$$a_3 = (1-\alpha)\Delta t \ , \ a_4 = \alpha\Delta t.$$

Equations (3.23) and (3.24) are only a linearized version of the actual governing equations of motion. Hence equation (3.23) should be solved iteratively for each time step until the actual equations of motion are satisfied to a required tolerance. Here the Newton–Raphson iteration technique is employed. In the Newton–Raphson method, the equation to be solved at the ith iteration for time step t + Δt has the form

$$(a_0[M] + [K_L] + [K_{NL}])^{(i-1)}(\{\Delta\}^{(i)} - \{\Delta\}^{(i-1)})$$

$$= \{R\} - [M](a_0\{\Delta\}^{(i-1)} - a_1\{\dot{\Delta}\} - a_2\{\ddot{\Delta}\}) - \{F\}^{(i-1)} \qquad (3.26)$$

where

$$\{F\}^{(i-1)} = \int_V [B_L^{(i-1)}]^T \{\hat{S}\}^{(i-1)} dV$$

After the ith iteration, the nodal displacement at time t + Δt is updated by

$$\{^2\Delta\}^{(i)} = \{^2\Delta\}^{(i-1)} + (\{\Delta\}^{(i)} - \{\Delta\}^{(i-1)})$$

in which

$$\{\Delta\}^{(0)} = \{0\}.$$

3.5 Degenerated Laminated 3–D Shell Element

The degenerated shell element developed by Chao and Reddy [88] for composite laminates will be utilized here. The shell element is degenerated

from the three–dimensional solid element by imposing two constraints: (1) straight lines normal to the midsurface before deformation remain straight but not normal after deformation; (2) the transverse normal components of strain and hence stress are ignored in the development. The resulting non–linear formulation allows arbitrarily large displacements and rotations of the shell element but small strains, since the thickness does not change and the normal does not distort.

As in [86,88], the 3–D solid element in Figure 3.1 is the starting point. The curvilinear coordinates in the middle surface of the shell are given by ξ, η, ζ, which are normalized such that they vary between –1 and 1. Here ζ denotes the thickness coordinate. The coordinates of a point are given by

$$X_i = \sum_{k=1}^{n} \phi_k(\xi,\eta)\left[\frac{1+\zeta}{2}(X_i^k)_{top} + \frac{1-\zeta}{2}(X_i^k)_{bottom}\right] \tag{3.27}$$

where n denotes the number of nodes per element, and $\phi_k(\xi,\eta)$ are the Lagrangian finite element interpolation functions. The normal vectors $\vec{V}_3^k$ connecting the upper and lower surfaces of the shell at node k are defined by their components as

$$V_{3i}^k = (X_i^k)_{top} - (X_i^k)_{bottom} \tag{3.28a}$$

$$e_{3i}^k = \vec{V}_3^k / |\vec{V}_3^k| \tag{3.28b}$$

Substituting these expressions into (3.27), we obtain

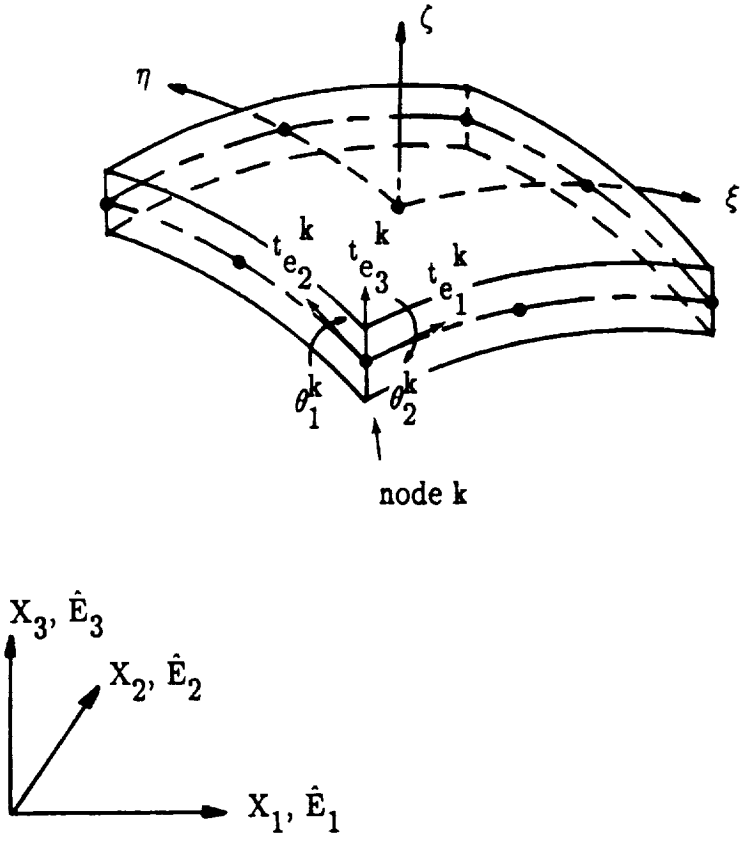

Figure 3.1 General 3–D solid geometry and resultant shell element.

$$X_i = \sum_{k=1}^{n} \phi_k(\xi,\eta)[(X_i^k)_{mid} + \frac{\zeta}{2} h_k e_{3i}^k] \tag{3.29}$$

where $h_k = |\vec{V}_3^k|$ is the thickness of the shell at node k. The displacement components become

$$U_i = {}^t x_i - X_i = \sum_{k=1}^{n} \phi_k(\xi,\eta)[U_i^k + \frac{\zeta}{2} h_k({}^t e_{3i}^k - {}^o e_{3i}^k)] \tag{3.30}$$

$$\Delta u_i = u_i - U_i = \sum_{k=1}^{n} \phi_k(\xi,\eta)[\Delta u_i^k + \frac{\zeta}{2} h_k({}^{t+\Delta t} e_{3i}^k - {}^t e_{3i}^k)] \tag{3.31}$$

where ${}^t x_i$ are the Cartesian coordinates at time t and ${}^t e_{3i}^k$ and ${}^o e_{3i}^k$ are the unit vectors at time t and 0, respectively. In order to update the vectors in (3.28) for small rotations, the rotation $d\vec{\Omega}$ is expressed as

$$d\vec{\Omega} = \theta_2^k \, {}^t e_1^k + \theta_1^k \, {}^t e_2^k + \theta_3^k \, {}^t e_3^k$$

The increment of ${}^t e_3^k$ can be written as

$$\Delta {}^t e_3^k = d\vec{\Omega} \times {}^t e_3^k = \theta_1^k \, {}^t e_1^k - \theta_2^k \, {}^t e_2^k \tag{3.32}$$

The equation (3.31) becomes finally

$$\Delta u_i = \sum_{k=1}^{n} \phi_k(\xi,\eta)[\Delta u_i^{\kappa} + \frac{\zeta}{2} h_k(\theta_1^k \, {}^t e_{1i}^k - \theta_2^k \, {}^t e_{2i}^k)] \qquad (3.33a)$$

where ${}^t e_1^k$ and ${}^t e_2^k$ are determined from

$${}^t e_1^k = \frac{\hat{E}_2 \times {}^t e_3^k}{|\hat{E}_2 \times {}^t e_3^k|}$$

$${}^t e_2^k = {}^t e_3^k \times {}^t e_1^k \qquad (3.33b)$$

$\hat{E}_i$ are the unit vectors of the stationary global coordinate system. Equation (3.33a) can be expressed in matrix form as

$$\{\Delta u\} = \{\Delta u_1 \; \Delta u_2 \; \Delta u_3\}^T = [H]\{\Delta^e\}$$

where

$$\{\Delta^e\} = \{\Delta u_1^k \; \Delta u_2^k \; \Delta u_3^k \; \theta_1^k \; \theta_2^k\}^T \quad (k = 1 \text{ to } n)$$

and [H] is the incremental displacement interpolation matrix, which can be found in [86].

Next, the linear strain increments $\{e^o\} = \{e_{11}^o \; e_{22}^o \; e_{33}^o \; 2e_{12}^o \; 2e_{13}^o \; 2e_{23}^o\}^T$ are written in matrix form

$$\{e^o\} = [A]\{\Delta \bar{u}\}$$

where

$$\{\Delta \bar{u}\} = \{\Delta u_{1,1} \; \Delta u_{1,2} \; \Delta u_{1,3} \; \Delta u_{2,1} \; \Delta u_{2,2} \; \Delta u_{2,3} \; \Delta u_{3,1} \; \Delta u_{3,2} \; \Delta u_{3,3}\}^T$$

and

$$u_{i,j} = \frac{\partial u_i}{\partial X_j}$$

The matrix [A] can be found in [86]. Denoting $\{\Delta\bar{u}\}$ by

$$\{\Delta\bar{u}\} = [N]\{\Delta u\} = [N][H]\{\Delta^e\}$$

with [N] being a matrix of differential operators, then $\{e^o\}$ becomes

$$\{e^o\} = [A]\{\Delta\bar{u}\} = [A][N][H]\{\Delta^e\} \equiv [B_L]\{\Delta^e\}$$

The usual Jacobian transformations are used to express $u_{i,j}$ in terms of the derivatives with respect to the global coordinates. Also in this work the integration is done in terms of the local curvilinear coordinate system (x_1', x_2', x_3'), as appropriate transformations are made.

The constitutive matrix [C′] for a lamina in the local coordinate system is given by

$$[C'] = \begin{bmatrix} C'_{11} & C'_{12} & C'_{13} & 0 & 0 \\ C'_{12} & C'_{22} & C'_{23} & 0 & 0 \\ C'_{13} & C'_{23} & C'_{33} & 0 & 0 \\ 0 & 0 & 0 & C'_{44} & C'_{45} \\ 0 & 0 & 0 & C'_{45} & C'_{55} \end{bmatrix} \tag{3.34}$$

where

$$C'_{11} = m^4 Q_{11} + 2m^2 n^2 (Q_{12} + 2Q_{33}) + n^4 Q_{22}$$

$$C'_{12} = m^2 n^2 (Q_{11} + Q_{22} - 4Q_{33}) + (m^4 + n^4) Q_{12}$$

$$C'_{13} = mn[m^2Q_{11} - n^2Q_{22} - (m^2 - n^2)(Q_{12} + 2Q_{33})]$$

$$C'_{22} = n^4Q_{11} + 2m^2n^2(Q_{12} + 2Q_{33}) + m^4Q_{22}$$

$$C'_{23} = mn[n^2Q_{11} - m^2Q_{22} + (m^2 - n^2)(Q_{12} + 2Q_{33})]$$

$$C'_{33} = m^2n^2(Q_{11} + Q_{22} - 2Q_{12}) + (m^2 - n^2)^2Q_{33}$$

$$C'_{44} = m^2Q_{44} + n^2Q_{55} \ , \quad C'_{45} = mn(Q_{44} - Q_{55})$$

$$C'_{55} = m^2Q_{55} + n^2Q_{44} \ , \quad m = \cos\theta \ , \quad n = \sin\theta$$

and Q_{ij} are the plane stress–reduced elastic coefficients in the material coordinates. By neglecting the normal stress in the thickness direction, the stiffnesses Q_{ij} for an orthotropic lamina are determined from the three–dimensional orthotropic stiffnesses, which can be expressed in terms of engineering constants as,

$$Q_{11} = \frac{E_{11}}{1 - \nu_{12}\nu_{21}} \ , \quad Q_{12} = \frac{\nu_{12}E_{22}}{1 - \nu_{12}\nu_{21}} \ , \quad Q_{22} = \frac{E_{22}}{1 - \nu_{12}\nu_{21}} \tag{3.35}$$

$$Q_{44} = (G_{13})K \ , \ Q_{55} = (G_{23})K \ , \ Q_{33} = G_{12}$$

where K is the shear correction coefficient taken to be 5/6.

In general, Gauss quadrature is used to integrate the element matrices. For laminated composite structures, the thickness direction integration could be done using Gauss quadrature, or the problem could be reduced to a 2–D one and hence explicit integration performed. In order to do this, the Jacobian matrix dependency on the thickness coordinate ζ is neglected. This is a valid assumption if the thickness to radius of the shell ratios are small. In this study we use the explicit integration for elastic behavior and numerical integration (quadrature) when elastic–plastic behavior is assumed.

From [86], the following symbolic representations of desired quantities are expressed explicitly in terms of ζ:

$$\{\Delta\bar{u}'\} = ([DH1] + \zeta[DH2])\{\Delta^e\}$$

$$[A'] = [SD] + \zeta[TD]$$

$$\begin{aligned}[B_L'] &= ([SD] + \zeta[TD])([DH1] + \zeta[DH2]) \\ &= [SD1] + \zeta[SD2] + \zeta^2[SD3]\end{aligned} \tag{3.36}$$

$$\{E_{ij}'\} = \{S_1\} + \zeta\{S2\} + \zeta^2\{S3\}$$

$$[B'_{NL}] = [DH1] + \zeta[DH2]$$

These representations can be used to perform explicit integration through the thickness.

In order to avoid locking behavior for thin shell structures, selective reduced or fully reduced integration is employed. Deformation dependent loading is also used and is described in [86].

4. MICROMECHANICS

4.1 Introduction

The Aboudi theory has been included in order to study the effect of using micromechanics constituent properties as random variables. In this section a review of Aboudi's theory is discussed, which is modeled after the development in [64].

4.2 The Aboudi Micromechanics Model

This theory involves the solution of a suitable boundary value problem whose domain is a typical representative volume V. The composite is modeled as an isotropic viscoplastic matrix reinforced by an elastic transversely isotropic fiber of rectangular cross section. The fibers extend in the x_1 direction and are arranged in a doubly periodic array in the x_2 and x_3 directions as shown in Figure 4.1a. The rectangular fiber has cross sectional dimensions h_1, ℓ_1 with h_2, ℓ_2 denoting the matrix spacing. Figure 4.1b shows the representative cell necessary for analysis due to the periodic arrangement. The cell is further divided into four subcells α, β = 1,2 each with a local coordinate system (x_1, $\bar{x}_2^{(\alpha)}$, $\bar{x}_3^{(\beta)}$).

The displacement field considered by Aboudi is a first–order expansion in each subcell, since only average behavior of the composite is sought. This displacement field of Aboudi is given by

$$u_i^{(\alpha\beta)} = w_i^{(\alpha\beta)} + \bar{x}_2^{(\alpha)}\phi_i^{(\alpha\beta)} + \bar{x}_3^{(\beta)}\psi_i^{(\alpha\beta)} \quad , \; i = 1,2,3 \tag{4.1}$$

where $w_i^{(\alpha\beta)}$ are the displacement components of the center of the subcell and

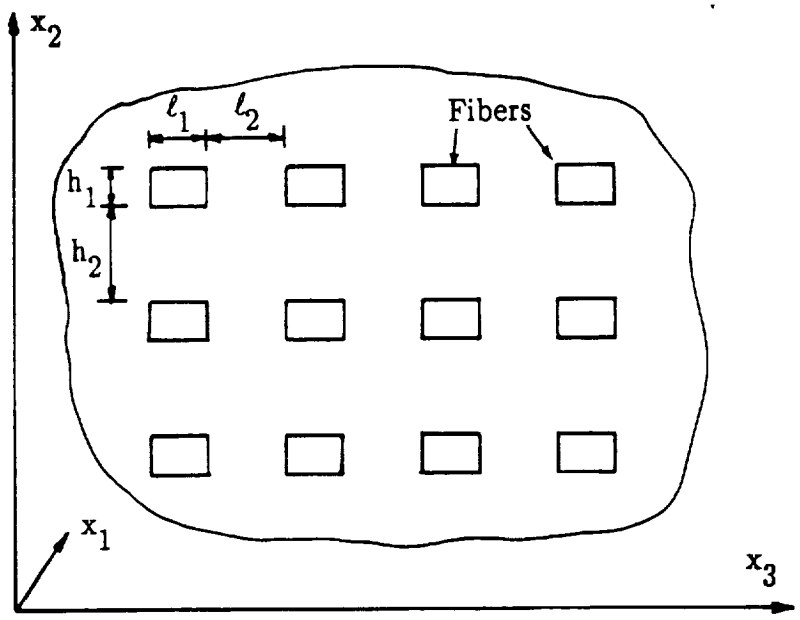

(a) Doubly periodic array of rectangular fibers extending in the x_1 direction.

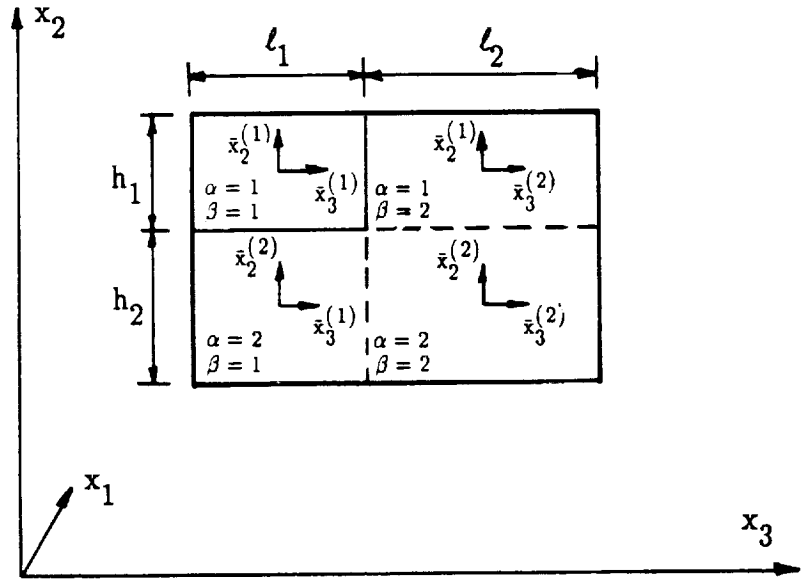

(b) The representative cell.

Figure 4.1 Micromechanics subcell geometry

$\phi_i^{(\alpha\beta)}$ and $\psi_i^{(\alpha\beta)}$ characterize the linear variations of the displacements within the subcell in the $\bar{x}_2^{(\alpha)}$ and $\bar{x}_3^{(\beta)}$ directions, respectively. In this section, repeated α and β do not imply summation.

Displacement continuity at the interfaces between the subcells are given by

$$w_i^{(11)} = w_i^{(12)} = w_i^{(21)} = w_i^{(22)} \equiv w_i \tag{4.2}$$

$$h_1\phi_i^{(1\beta)} + h_2\phi_i^{(2\beta)} = (h_1 + h_2)\frac{\partial w_i}{\partial x_2} \tag{4.3}$$

$$\ell_1\psi_i^{(\alpha 1)} + \ell_2\psi_i^{(\alpha 2)} = (\ell_1 + \ell_2)\frac{\partial w_i}{\partial x_3} \tag{4.4}$$

The average strain in the representative cell is given by

$$\bar{\epsilon}_{ij} = \frac{1}{V}\sum_{\alpha,\beta=1}^{2} v_{\alpha\beta}\epsilon_{ij}^{(\alpha\beta)} \tag{4.5}$$

where $v_{\alpha\beta} = h_\alpha \ell_\beta$ and $V = (h_1 + h_2)(\ell_1 + \ell_2)$ is the area of the representative cell. The infinitesimal strain tensor is

$$\epsilon_{ij}^{(\alpha\beta)} = \frac{1}{2}[\partial_i u_j^{(\alpha\beta)} + \partial_j u_i^{(\alpha\beta)}] \quad i,j = 1,2,3 \tag{4.6}$$

where

$$\partial_1 = \frac{\partial}{\partial x_1}\ ,\ \partial_2 = \frac{\partial}{\partial \bar{x}_2^{(\alpha)}}\ ,\ \partial_3 = \frac{\partial}{\partial \bar{x}_3^{(\beta)}}$$

Combining equations (4.3), (4.4), (4.6) then the following result is obtained

$$\bar{\epsilon}_{ij} = \frac{1}{2}\left(\frac{\partial w_i}{\partial x_j} + \frac{\partial w_j}{\partial x_i}\right) \tag{4.7}$$

The average stress in the composite cell is

$$\bar{\sigma}_{ij} = \frac{1}{V}\sum_{\alpha,\beta=1}^{2} v_{\alpha\beta} S_{ij}^{(\alpha\beta)} \tag{4.8}$$

where $S_{ij}^{(\alpha\beta)}$ is the average stress in the subcell. $S_{ij}^{(\alpha\beta)}$ is determined by

$$S_{ij}^{(\alpha\beta)} = \frac{1}{V}\int_{-h_{\alpha/2}}^{h_{\alpha/2}}\int_{-\ell_{\beta/2}}^{\ell_{\beta/2}} \sigma_{ij}^{(\alpha\beta)} d\bar{x}_2^{(\alpha)} d\bar{x}_3^{(\beta)} \tag{4.9}$$

Aboudi's theory is designed to allow both fiber and matrix constituents to be elasto–plastic materials. Thus the strain rate in the subcells are decomposed into elastic and plastic parts as

$$\dot{\epsilon}_{ij}^{(\alpha\beta)} = \dot{\epsilon}_{ij}^{E(\alpha\beta)} + \dot{\epsilon}_{ij}^{P(\alpha\beta)} \tag{4.10}$$

The constitutive equation for transversely isotropic constituents in the elastic range, with x_1 in the direction of anisotropy is

$$\{\sigma^{(\alpha\beta)}\} = [C^{(\alpha\beta)}]\{\epsilon^{E(\alpha\beta)}\} \tag{4.11}$$

where

$$\{\sigma^{(\alpha\beta)}\} = \{\sigma_{11}^{(\alpha\beta)}, \sigma_{22}^{(\alpha\beta)}, \sigma_{33}^{(\alpha\beta)}, \sigma_{12}^{(\alpha\beta)}, \sigma_{13}^{(\alpha\beta)}, \sigma_{23}^{(\alpha\beta)}\}^T$$

$$\{\epsilon^{E(\alpha\beta)}\} = \{\epsilon_{11}^{E(\alpha\beta)}, \epsilon_{22}^{E(\alpha\beta)}, \epsilon_{33}^{E(\alpha\beta)}, 2\epsilon_{12}^{E(\alpha\beta)}, 2\epsilon_{13}^{E(\alpha\beta)}, 2\epsilon_{23}^{E(\alpha\beta)}\}^T$$

and

$$[C^{(\alpha\beta)}] = \begin{bmatrix} C_{11}^{(\alpha\beta)} & C_{12}^{(\alpha\beta)} & C_{13}^{(\alpha\beta)} & 0 & 0 & 0 \\ & C_{22}^{(\alpha\beta)} & C_{23}^{(\alpha\beta)} & 0 & 0 & 0 \\ & & C_{33}^{(\alpha\beta)} & 0 & 0 & 0 \\ & & & C_{44}^{(\alpha\beta)} & 0 & 0 \\ & \text{sym.} & & & C_{55}^{(\alpha\beta)} & 0 \\ & & & & & C_{66}^{(\alpha\beta)} \end{bmatrix} \tag{4.12}$$

Appropriate elastic constants are substituted in (4.12) to represent either fiber or matrix subcells.

Combining (4.8), (4.9) and (4.10) the following relations for the average subcell stresses $S_{ij}^{(\alpha\beta)}$ are obtained

$$S_{11}^{(\alpha\beta)} = C_{11}^{(\alpha\beta)}\bar{\epsilon}_{11} + C_{12}^{(\alpha\beta)}(\phi_2^{(\alpha\beta)} + \psi_3^{(\alpha\beta)} - 2\mu_{\alpha\beta}L_{11}^{(\alpha\beta)}$$

$$S_{22}^{(\alpha\beta)} = C_{12}^{(\alpha\beta)}\bar{\epsilon}_{11} + C_{22}^{(\alpha\beta)}\phi_2^{(\alpha\beta)} + C_{23}^{(\alpha\beta)}\psi_3^{(\alpha\beta)} - 2\mu_{\alpha\beta}L_{22}^{(\alpha\beta)}$$

$$S_{33}^{(\alpha\beta)} = C_{12}^{(\alpha\beta)}\bar{\epsilon}_{11} + C_{23}^{(\alpha\beta)}\phi_2^{(\alpha\beta)} + C_{22}^{(\alpha\beta)}\psi_3^{(\alpha\beta)} - 2\mu_{\alpha\beta}L_{33}^{(\alpha\beta)}$$

$$S_{12}^{(\alpha\beta)} = C_{44}^{(\alpha\beta)}[\frac{\partial w_2}{\partial x_1} + \phi_1^{(\alpha\beta)}] - 2C_{44}^{(\alpha\beta)}L_{12}^{(\alpha\beta)} \tag{4.13}$$

$$S_{13}^{(\alpha\beta)} = C_{44}^{(\alpha\beta)}[\frac{\partial w_3}{\partial x_1} + \psi_1^{(\alpha\beta)}] - 2C_{44}^{(\alpha\beta)}L_{13}^{(\alpha\beta)}$$

$$S_{23}^{(\alpha\beta)} = C_{66}^{(\alpha\beta)}[\phi_3^{(\alpha\beta)} + \psi_2^{(\alpha\beta)}] - 2C_{66}^{(\alpha\beta)}L_{23}^{(\alpha\beta)}$$

In (4.13) above, $L_{ij}^{(\alpha\beta)}$ represents the average total subcell plastic strains, and $\mu_{\alpha\beta}$ is the isotropic constituents' elastic shear modulus.

If classical rate–independent plasticity theory is selected to describe the nonlinear material behavior, then the plastic strain rates are given by

$$\dot{\epsilon}_{ij}^{P(\alpha\beta)} = \dot{\Lambda}_{\alpha\beta}\hat{\sigma}_{ij}^{(\alpha\beta)} \tag{4.14}$$

which is the flow rule associated within the von Mises yield criterion, with $\hat{\sigma}_{ij} = \sigma_{ij} - \delta_{ij}\sigma_{kk}/3$ representing the deviatoric stresses (δ_{ij} is the Kronecker delta) and $\Lambda_{\alpha\beta}$ the flow rule function. The above leads to

$$\dot{L}_{ij}^{(\alpha\beta)} = \dot{\Lambda}_{\alpha\beta}\hat{S}_{ij}^{(\alpha\beta)} \tag{4.15}$$

where $\hat{S}_{ij}^{(\alpha\beta)}$ are the deviators of $S_{ij}^{(\alpha\beta)}$. Thus the plastic average strains $L_{ij}^{(\alpha\beta)}$ are determined by integrating the above flow rules.

The conditions of traction continuity along the interfaces of the subcells in the first order theory result in

$$S_{2i}^{(1\beta)} = S_{2i}^{(2\beta)}$$

$$S_{3i}^{(\alpha 1)} = S_{3i}^{(\alpha 2)} \tag{4.16}$$

By imposing the continuity conditions previously stated, the variables $\phi_i^{(\alpha\beta)}$ and $\psi_i^{(\alpha\beta)}$ can be eliminated. This leads to closed form solutions for the average subcell stress $S_{ij}^{(\alpha\beta)}$ in (4.13), and the average stress in the cell $\bar{\sigma}_{ij}$ in (4.8). Without listing the details (see [64]), the results are given here:

$$\begin{aligned}
\bar{\sigma}_{11} &= b_{11}\bar{\epsilon}_{11} + b_{12}\bar{\epsilon}_{22} + b_{13}\bar{\epsilon}_{33} - H_{11} \\
\bar{\sigma}_{22} &= b_{22}\bar{\epsilon}_{11} + b_{22}\bar{\epsilon}_{22} + b_{23}\bar{\epsilon}_{33} - H_{22} \\
\bar{\sigma}_{33} &= b_{13}\bar{\epsilon}_{11} + b_{23}\bar{\epsilon}_{22} + b_{33}\bar{\epsilon}_{33} - H_{33} \\
\bar{\sigma}_{12} &= 2b_{44}\bar{\epsilon}_{12} - H_{12} \\
\bar{\sigma}_{13} &= 2b_{55}\bar{\epsilon}_{13} - H_{13} \\
\bar{\sigma}_{23} &= 2b_{66}\bar{\epsilon}_{23} - H_{23}
\end{aligned} \tag{4.17}$$

where the b_{ij} are the effective elastic constants of the composite. The constants b_{ij} and H_{ij} are given in functional form as

$$b_{ij} = f(C_{ij}^{(\alpha\beta)}, v_{\alpha\beta}, h_{\alpha}, \ell_{\beta})$$

$$H_{ij} = g(L_{ij}^{(\alpha\beta)}, v_{\alpha\beta}, h_{\alpha}, \ell_{\beta}) \tag{4.18}$$

The resultant constitutive relations in (4.17) involve an overall elastic modulus matrix [B] consisting of 9 independent elastic constants b_{11}, b_{12}, b_{13}, b_{22}, b_{23}, b_{33}, b_{44}, b_{55}, b_{66} (thus orthotropic). For square fibers and equal spacing the number of independent elastic constants reduce to six since $b_{12} = b_{13}$, $b_{22} = b_{33}$, and $b_{44} = b_{55}$. If a transversely isotropic material representation is desired, in which only five independent effective elastic constants are needed, then a transversely isotropic averaging technique described in [64] can be implemented. The overall constitutive relationship is summarized by

$$\{\bar{\sigma}\} = [B](\{\bar{\epsilon}\} - \{\bar{\epsilon}^P\}) \tag{4.19a}$$

where

$$\{\bar{\epsilon}^P\} = [B]^{-1}\{H\} \tag{4.19b}$$

Equations (4.19) contain the average ply properties B_{ij} and the effects of applying plasticity at the subcell level, which are included in the term $\{\bar{\epsilon}^P\}$. This is the full development presented by Aboudi. For the present work, only the transversely isotropic version of the B_{ij} constants are of interest, as the plasticity is not implemented into the micromechanics theory. It is anticipated that this will be done in the future, and a systematic method for this implementation was developed by Arenburg [63]. In this study a macroscopic orthotropic plasticity development is included.

5. ORTHOTROPIC PLASTICITY FORMULATION

5.1 Introduction

In order to develop the capability of modeling orthotropic elastoplastic behavior from a macroscopic viewpoint, a yield function introduced by Sun et al. [74–77], which is quadratic in the stresses and employs the associative flow rule and isotropic hardening, was adopted. The plane stress radial return algorithm by Simo et al. [89,90] was modified to include this new yield function. This algorithm was chosen due to its accuracy, improved global convergence rates, and compatibility with the probabilistic finite element routines. In this chapter the basic governing plasticity equations will be stated, the radial return algorithm for their solution at each gauss point will be developed, and the solution of the finite element equilibrium equations along with the layerwise integration procedures will be discussed.

5.2 Governing Equations

According to Sun [76], the orthotropic yield function is given by

$$f = \frac{1}{2}(a_{11}\sigma_{11}^2 + a_{22}\sigma_{22}^2 + a_{33}\sigma_{33}^2 + 2a_{12}\sigma_{11}\sigma_{22} + 2a_{13}\sigma_{11}\sigma_{33} + 2a_{23}\sigma_{22}\sigma_{33}$$

$$+ 2a_{44}\sigma_{23}^2 + 2a_{55}\sigma_{13}^2 + 2a_{66}\sigma_{12}^2) = \bar{Y} \qquad (5.1)$$

where $\bar{Y}$ is a state variable and σ_{ij} are the stresses in principal material coordinates. The coefficients a_{ij} are constants, which are determined from experimental data and control the amount of anisotropy in the plasticity. This yield criterion does not include the assumption of incompressibility of plastic

strains or that hydrostatic stresses result in no yielding or plastic deformation. The function also reduces to the von Mises criterion or the Hill yield function for orthotropic materials [67,68] with appropriate selection of the a_{ij} values. For example, for the von Mises function the a_{ij} values are

$$a_{11} = a_{22} = a_{33} = 2/3 \qquad a_{12} = a_{13} = a_{23} = -1/3$$
$$a_{44} = a_{55} = a_{66} = 1$$

The associative flow rule is employed, which allows the incremental plastic strains to be stated as

$$d\epsilon^p_{ij} = d\gamma \frac{\partial f}{\partial \sigma_{ij}} \tag{5.2}$$

where $d\gamma$ is an incremental plastic load parameter, and index notation has been used. It is the practice in plasticity to define the effective stress in such a way that it is related to the yield function and in a manner that it reduces to the stress in a uniaxial tension test. With this in mind, and following the development of Sun [76], the effective stress is defined as

$$\bar{\sigma} = \sqrt{3f} \tag{5.3}$$

The effective plastic strain $\bar{\epsilon}^p$ must be related to the effective stress in such a way that plastic work considerations are consistent. Thus the quantity $\bar{\sigma} d\bar{\epsilon}^p$ must represent the increment of specific plastic work of deformation

$dW^p = \sigma_{ij} d\epsilon^p_{ij}$. Equating the two quantities of plastic work, we have

$$\bar{\sigma} d\bar{\epsilon}^p = \sigma_{ij} d\epsilon^p_{ij} \tag{5.4}$$

Substitution of (5.1) into (5.2) and the result into (5.4) gives

$$\sigma_{ij} d\epsilon^p_{ij} = 2f d\gamma$$

so that

$$d\bar{\epsilon}^p = \frac{2f d\gamma}{\bar{\sigma}} = \frac{2}{3} \bar{\sigma} d\gamma \tag{5.5}$$

It is also noted that $\bar{Y}$ becomes

$$\bar{Y} = \frac{2}{3} \bar{\sigma}^2 \tag{5.6}$$

The shell element used here is degenerated from 3–D elasticity using the kinematics of the first order shear deformation theory. In other words, transverse normals remain straight and inextensible, i.e., $\epsilon_{33} = 0$. Consequently, σ_{33} does not enter the strain energy of the shell.

Introducing vector notation, the stress and strain tensors become

$$\{\sigma\} = \{\sigma_{11} \ \sigma_{22} \ \sigma_{12} \ \sigma_{13} \ \sigma_{23}\}^T$$

and

$$\{\epsilon\} = \{\epsilon_{11}\ \epsilon_{22}\ 2\epsilon_{12}\ 2\epsilon_{13}\ 2\epsilon_{23}\}^T\ ,\ \{\epsilon^p\} = \{\epsilon^p_{11}\ \epsilon^p_{22}\ 2\epsilon^p_{12}\ 2\epsilon^p_{13}\ 2\epsilon^p_{23}\}^T$$

The components of the back stress q_{ij} (included to model kinematic hardening), and the relative stress $\eta_{ij} = \sigma_{ij} - q_{ij}$, are expressed in the vector form as

$$\{q\} = \{q_{11}\ q_{22}\ q_{12}\ q_{13}\ q_{23}\}^T\ ,\ \{\eta\} = \{\eta_{11}\ \eta_{22}\ \eta_{12}\ \eta_{13}\ \eta_{23}\}^T$$

Thus the governing elastoplastic equations in the nonincremental (time domain) vector form can be expressed as

$$\begin{aligned}
&\{\epsilon\} = \{\epsilon^e\} + \{\epsilon^p\} \\
&\{\sigma\} = [C]\,\{\epsilon^e\} \\
&\{\dot{\epsilon}^p\} = \dot{\gamma}\,\frac{\partial f}{\partial\{\eta\}} \quad \text{(associative flow rule)} \qquad (5.7) \\
&\{\dot{q}\} = \frac{2}{3}\,H'\,\{\dot{\epsilon}^p\} \\
f = \tfrac{1}{2}(a_{11}\eta_{11}^2 &+ a_{22}\eta_{22}^2 + 2a_{12}\eta_{11}\eta_{22} + 2a_{44}\eta_{23}^2 + 2a_{55}\eta_{13}^2 + 2a_{66}\eta_{12}^2) = \tfrac{1}{3}\,\bar{\sigma}^2 \\
&\dot{\alpha} = \frac{2}{3}\,\dot{\gamma}\,\bar{\sigma} \\
&\bar{\sigma} = \sqrt{3f}
\end{aligned}$$

where $\dot{\gamma}$ is the time derivative of the plastic load parameter, H' is the kinematic hardening modulus, and the symbol α denotes the equivalent plastic strain. The matrix [C] is the elastic constitutive matrix, adjusted for the constraint $\sigma_{33} = 0$.

When the flow rule in Equation $(5.7)_3$ is evaluated, the following result is obtained

$$\{\dot{\epsilon}^{p}\} = \dot{\gamma}[P]\{\eta\} \tag{5.8}$$

where the matrix [P] is given by

$$[P] = \begin{bmatrix} a_{11} & a_{12} & 0 & 0 & 0 \\ a_{12} & a_{22} & 0 & 0 & 0 \\ 0 & 0 & 2a_{66} & 0 & 0 \\ 0 & 0 & 0 & 2a_{55} & 0 \\ 0 & 0 & 0 & 0 & 2a_{44} \end{bmatrix}$$

The effective stress $\bar{\sigma}$ can be expressed as

$$\bar{\sigma} = \sqrt{\frac{3}{2}\ \{\eta\}^{T}[P]\{\eta\}}$$

Using the matrix [P], the governing equations (5.7) can be recast as

$$\begin{aligned} &\{\epsilon\} = \{\epsilon^{e}\} + \{\epsilon^{p}\} \\ &\{\sigma\} = [C]\ \{\epsilon^{e}\} \\ &\{\dot{\epsilon}^{p}\} = \dot{\gamma}\,[P]\{\eta\} \\ &\{\dot{q}\} = \dot{\gamma}\,\frac{2}{3}\,H'\ [P]\{\eta\} \\ &f = \frac{1}{2}\,\{\eta\}^{T}\,[P]\{\eta\} - \frac{1}{3}\,Y^{2}\,(\alpha) \leq 0 \\ &\dot{\alpha} = \dot{\gamma}\,[\frac{2}{3}\,\{\eta\}^{T}\,[P]\{\eta\}]^{1/2} \end{aligned} \tag{5.9}$$

where the parameter Y represents the hardening law in terms of the equivalent plastic strain α.

Loading and unloading conditions are stated in simple Kuhn–Tucker form [89] by requiring that

$$f \leq 0 \ , \ \dot{\gamma} \geq 0 \ , \ \dot{\gamma} f \equiv 0 \tag{5.10}$$

For an elastic process, $f < 0$ and $\gamma = 0$. For a plastic process $f = 0$ and $\gamma > 0$. These two conditions are generally valid, whether in the loading or unloading state.

5.3 Incremental Formulation

Employing a backward Euler difference scheme to integrate equations (5.9) over time $\{t_n, t_{n+1}\}$, and letting $\gamma_{n+1} = \dot{\gamma}_{n+1}\Delta t$ (the plastic load parameter) and $\bar{f} = \sqrt{\{\eta\}^T[P]\{\eta\}}$, the strain at t_{n+1} can be written in terms of the strain at t_n and the gradient of the incremental displacements,

$$\{\epsilon_{n+1}\} = \{\epsilon_n\} + \nabla\{\Delta u\} \tag{5.11}$$

where "∇" stands for the differential operator used in the definition of strains. A trial stress state is assumed by freezing plastic flow so that the entire step is purely elastic. The trial stress then becomes

$$\{\sigma_{n+1}^{trial}\} = [C](\{\epsilon_{n+1}\} - \{\epsilon_n^P\})$$

$$\{\eta_{n+1}^{trial}\} = \{\sigma_{n+1}^{trial}\} - \{q_n\}$$

$$\{\epsilon^{P}_{n+1}\} = \{\epsilon^{P}_{n}\} + \gamma_{n+1}[P]\{\eta_{n+1}\} \tag{5.12}$$

$$\{q_{n+1}\} = \{q_n\} + \gamma_{n+1}\frac{2}{3}H'[P]\{\eta_{n+1}\}$$

$$\alpha_{n+1} = \alpha_n + \sqrt{\frac{2}{3}}\,\gamma_{n+1}\bar{f}_{n+1}$$

Restating equation $(5.12)_1$ as

$$\{\sigma_{n+1}\} = \{\sigma^{trial}_{n+1}\} - [C]\{\Delta\epsilon^{P}_{n+1}\}, \tag{5.13}$$

substituting $\{\Delta\epsilon^{P}_{n+1}\} = \gamma_{n+1}[P]\{\eta_{n+1}\}$ and $\{\eta_{n+1}\} = \{\sigma_{n+1}\} - \{q_{n+1}\}$, and rearranging the terms, the following relations are obtained:

$$\{\eta_{n+1}\} = \frac{1}{1 + \frac{2}{3}H'\gamma_{n+1}}[\Xi][C]^{-1}\{\eta^{trial}_{n+1}\} \tag{5.14}$$

where

$$[\Xi] \equiv \left[[C]^{-1} + \left[\frac{\gamma_{n+1}}{1 + \frac{2}{3}H'\gamma_{n+1}}\right][P]\right]^{-1}$$

In order to perform the incremental updates required in equations (5.12) the plastic load parameter (Lagrange multiplier) γ must be determined. It is found by enforcing the consistency condition at time t_{n+1}, i.e.,

$$f^2(\gamma_{n+1}) \equiv \frac{1}{2}\bar{t}^2_{n+1} - \frac{1}{3}[Y(\alpha_n + \sqrt{\frac{2}{3}}\,\gamma_{n+1}\bar{t}_{n+1})]^2 = 0 \tag{5.15}$$

The actual hardening functions used in the program are those recommended by Simo and Hughes [89]

$$Y(\alpha) = \beta\bar{H}\alpha + \sigma_Y + (K_\infty - \sigma_Y)[1 - \exp(-\lambda\alpha)] \tag{5.16}$$

and by Sun [76],

$$Y(\alpha) = \bar{H}\left[\alpha + \left[\frac{\sigma_Y}{\bar{H}}\right]^{\lambda}\right]^{1/\lambda} \tag{5.17}$$

where $\bar{H}$ is the hardening modulus, σ_Y the uniaxial yield stress, K_∞ and λ are other input parameters, and

$$H(\alpha) = (1-\beta)\bar{H}\alpha$$

Here β denotes the fraction of kinematic and isotropic hardening desired, i.e. $\beta = 1$ denotes purely isotropic hardening, and $\beta = 0$ denotes purely kinematic hardening. Equation (5.15) is solved at each gauss point in the structure for γ by a local Newton iteration procedure, as it is generally a nonlinear scalar equation.

The global equilibrium is obtained by using Newton–Raphson iteration. This requires that the tangent moduli be known in the form

$$[C^{eP}]|_{n+1} = \frac{\{d\sigma\}}{\{d\epsilon\}}|_{n+1} \tag{5.18}$$

Simo and Hughes developed tangent moduli, which are consistent with the integration algorithm previously discussed. For finite values of load step size,

they showed that the consistent elastoplastic tangent moduli preserved the quadratic rate of asymptotic convergence that is characteristic of Newton's method. Use of the continuum tangent moduli derived independent of the algorithm loses this convergence rate. Differentiating the following incremental equations

$$\{\sigma_{n+1}\} = [C](\{\epsilon_{n+1}\} - \{\epsilon^{P}_{n+1}\})$$

$$\alpha_{n+1} = \alpha_n + \sqrt{\frac{2}{3}}\,\gamma_{n+1}\bar{f}_{n+1} \tag{5.19}$$

$$\{q_{n+1}\} = \{q_n\} + \gamma_{n+1}\frac{2}{3}H'[P]\{\eta_{n+1}\}$$

and substituting equation $(5.12)_3$ and $\{\eta_{n+1}\} = \{\sigma_{n+1}\} - \{q_{n+1}\}$, we obtain

$$\{d\sigma_{n+1}\} = [C][\{d\epsilon_{n+1}\} - d\gamma_{n+1}[P]\{\eta_{n+1}\} - \gamma_{n+1}[P](\{d\sigma_{n+1}\} - \{dq_{n+1}\})]$$

$$d\alpha_{n+1} = \sqrt{\frac{2}{3}}(\bar{f}_{n+1}d\gamma_{n+1} + \gamma_{n+1}d\bar{f}_{n+1}) \tag{5.20}$$

$$\{dq_{n+1}\} = \frac{\frac{2}{3}H'}{1 + \frac{2}{3}H'\gamma_{n+1}}(d\gamma_{n+1}\{\eta_{n+1}\} + \gamma_{n+1}\{d\sigma_{n+1}\})]$$

By regrouping equations $(5.19)_1$ and $(5.19)_3$ it can be shown that

$$\{d\sigma_{n+1}\} = [\Xi]\left[\{d\epsilon_{n+1}\} - \frac{d\gamma_{n+1}}{1 + \frac{2}{3} H' \gamma_{n+1}} [P]\{\eta_{n+1}\}\right] \qquad (5.21)$$

$$\{d\eta_{n+1}\} = \frac{1}{1 + \frac{2}{3} H' \gamma_{n+1}} \left[\{d\sigma_{n+1}\} - \frac{2}{3} H' d\gamma_{n+1}\{\eta_{n+1}\}\right]$$

Differentiation of the consistency condition (5.15) and use of the definition of $\bar{f}_{n+1}$ results in the expression

$$(1 - \frac{2}{3} Y' \gamma_{n+1})\{\eta_{n+1}\}^T[P]\{d\eta_{n+1}\} - \frac{2}{3} Y' \bar{f}^2_{n+1} d\gamma_{n+1} = 0 \qquad (5.22)$$

Substituting equations $(5.20)_3$ and (5.21) into equation (5.22) and solving it for $d\gamma_{n+1}$ we obtain

$$d\gamma_{n+1} = \frac{\theta_1\{\eta_{n+1}\}^T [P][\Xi]\{d\epsilon_{n+1}\}}{(1+\beta_{n+1})\{\eta_{n+1}\}^T[P][\Xi][P]\{\eta_{n+1}\}} \qquad (5.23)$$

where

$$\theta_1 = 1 + \frac{2}{3} H' \gamma_{n+1}$$

$$\theta_2 = 1 - \frac{2}{3} Y' \gamma_{n+1}$$

$$\beta_{n+1} = \frac{2}{3}\frac{\theta_1}{\theta_2}\bar{f}^2_{n+1}\frac{[Y'\theta_1 + H'\theta_2]}{\{\eta_{n+1}\}^T[P][\Xi][P]\{\eta_{n+1}\}}$$

Substituting (5.23) into $(5.20)_1$ and using the definition of $[\Xi]$, the consistent elastoplastic tangent moduli can be expressed as

$$[C^{ep}] = \frac{\{d\sigma_{n+1}\}}{\{d\epsilon_{n+1}\}} = [\Xi] - \frac{([\Xi][P]\{\eta_{n+1}\})([\Xi][P]\{\eta_{n+1}\})^T}{(1+\beta_{n+1})\{\eta_{n+1}\}^T[P][\Xi][P]\{\eta_{n+1}\}} \tag{5.24}$$

5.4 Computer Implementation

For the general case of orthotropic plasticity, the constitutive matrix [C] is given by

$$[C] = \begin{bmatrix} \frac{E_{11}}{D} & \frac{\nu_{12}E_{22}}{D} & 0 & 0 & 0 \\ \frac{\nu_{12}E_{22}}{D} & \frac{E_{22}}{D} & 0 & 0 & 0 \\ 0 & 0 & G_{12} & 0 & 0 \\ 0 & 0 & 0 & KG_{13} & 0 \\ 0 & 0 & 0 & 0 & KG_{23} \end{bmatrix} \tag{5.25}$$

where $D = 1 - \nu_{12}\nu_{21}$ and K is the shear correction factor taken to be 5/6. If yielding occurs, it becomes necessary to solve the scalar consistency condition of equation (5.15) for the load parameter γ_{n+1}. A Newton iteration is used here due to the general nonlinearity of (5.15). Thus, if the variable F is used to represent the consistency condition, then the Newton iteration is performed by employing

$$\gamma_{i+1} = \gamma_i - \frac{F(\gamma_i)}{F'(\gamma_i)} \tag{5.26}$$

at each yielded gauss point. Using the chain rule of differentiation, the necessary derivatives of (5.15) can be obtained in a straightforward manner for the general case of orthotropic plasticity.

For the special case of isotropic (von Mises) plasticity, Simo and Hughes [89] have developed a simplified form of the consistency condition that is a direct function of the load parameter γ_{n+1}. This extra work results in an effective reduction of the number of computations required in the Newton iteration. Recall that for isotropic elasticity, the matrix [C] is modified by $E_{11} = E_{22} = E$, $\nu_{12} = \nu_{21} = \nu$, and $G_{12} = G_{13} = G_{23} = G$, and the matrix [P] is modified due to the von Mises values for the coefficients a_{ij} previously mentioned. Thus the isotropic matrices [C] and [P] can be simultaneously diagonalized using the following spectral decomposition

$$[P] = [Q][\Lambda_p][Q]^T \text{ and } [C] = [Q][\Lambda_c][Q]^T \tag{5.27}$$

where

$$[Q] = \frac{1}{\sqrt{2}} \begin{bmatrix} 1 & -1 & 0 & 0 & 0 \\ 1 & 1 & 0 & 0 & 0 \\ 0 & 0 & \sqrt{2} & 0 & 0 \\ 0 & 0 & 0 & \sqrt{2} & 0 \\ 0 & 0 & 0 & 0 & \sqrt{2} \end{bmatrix}$$

$$[\Lambda_p] = \begin{bmatrix} 1/3 & 0 & 0 & 0 & 0 \\ 0 & 1 & 0 & 0 & 0 \\ 0 & 0 & 2 & 0 & 0 \\ 0 & 0 & 0 & 2 & 0 \\ 0 & 0 & 0 & 0 & 2 \end{bmatrix}$$

$$[\Lambda_c] = \begin{bmatrix} \frac{E}{1-\nu} & 0 & 0 & 0 & 0 \\ 0 & 2G & 0 & 0 & 0 \\ 0 & 0 & G & 0 & 0 \\ 0 & 0 & 0 & GK & 0 \\ 0 & 0 & 0 & 0 & GK \end{bmatrix}$$

Using the matrix [Q], the following transformation is introduced

$$\{\xi\} = [Q]^T\{\eta\} = \begin{Bmatrix} (\eta_{11} + \eta_{22})/\sqrt{2} \\ (-\eta_{11} + \eta_{22})/\sqrt{2} \\ \eta_{12} \\ \eta_{13} \\ \eta_{23} \end{Bmatrix}$$

The mapped trial state in terms of the elastic trial state defined in equations $(5.12)_{1,2}$ can also be transformed as

$$\{\xi_{n+1}^{trial}\} = [Q]^T \{\eta_{n+1}^{trial}\} \tag{5.28}$$

Substituting relations (5.27) in (5.14) the diagonalized update equations can be expressed as

$$\{\xi_{n+1}\} =$$

$$\begin{bmatrix} \frac{1}{\theta_1 + \frac{E\gamma}{3(1-\nu)}} & 0 & 0 & 0 & 0 \\ 0 & \frac{1}{\theta_1 + 2G\gamma} & 0 & 0 & 0 \\ 0 & 0 & \frac{1}{\theta_1 + 2G\gamma} & 0 & 0 \\ 0 & 0 & 0 & \frac{1}{\theta_1 + 2GK\gamma} & 0 \\ 0 & 0 & 0 & 0 & \frac{1}{\theta_1 + 2GK\gamma} \end{bmatrix} \cdot \{q_{n+1}^{trial}\} \tag{5.29}$$

Transforming the consistency equation into $\{\xi\}$ variables, and utilizing equation (5.29), we have

$$f^2(\gamma_{n+1}) = \frac{1}{2}\left[\frac{1}{6}\frac{(\eta_{11}^{trial}+\eta_{22}^{trial})^2}{(\theta_1+\frac{E\gamma}{3(1-\nu)})^2} + \frac{1}{2}\frac{(\eta_{22}^{trial}-\eta_{11}^{trial})^2}{(\theta_1+2G\gamma)^2} + \frac{(\eta_{12}^{trial})^2}{(\theta_1+2G\gamma)^2}\right.$$

$$\left. + \frac{(\eta_{13}^{trial})^2}{(\theta_1+2GK\gamma)^2} + \frac{(\eta_{23}^{trial})^2}{(\theta_1+2GK\gamma)^2}\right] - \frac{1}{3}Y^2(\alpha_{n+1}) = 0 \qquad (5.30)$$

This is the form of the consistency equation that is used in the scalar Newton iteration at each gauss point to solve for γ_{n+1} for the case of isotropic von Mises plasticity.

The radial return algorithm for the constrained $\sigma_{33} = 0$ state of stress can be summarized as follows:

1. Update the total strain using (5.11) and compute the trial elastic stresses from $(5.12)_{1,2}$.
2. Compute f_{n+1}^{trial} from (5.15) or (5.30). Exit if $f_{n+1}^{trial} < 0$; otherwise solve consistency equation (5.15 or 5.30) for γ_{n+1} using Newton iteration.
3. Compute the algorithmic moduli matrix $[\Xi]$ from equation $(5.14)_2$.
4. Update relative stress, back stress, actual stress, plastic strain, and equivalent strain from $(5.14)_1$, $(5.12)_4$, $\{\sigma_{n+1}\} = \{\eta_{n+1}\} + \{q_{n+1}\}$, $(5.12)_3$, and $(5.12)_5$, respectively.
5. Compute consistent elastoplastic tangent moduli from (5.24).

6. Update ϵ_{33} using, if desired,

$$\epsilon_{33_{n+1}} = -\left[\frac{\nu_{13}}{E_{11}}\sigma_{11_{n+1}} + \frac{\nu_{23}}{E_{22}}\sigma_{22_{n+1}}\right] - \left[\epsilon^{P}_{11_{n+1}} + \epsilon^{P}_{22_{n+1}}\right]$$

5.5 Layerwise Integration Procedure

Recall equations (3.19), (3.20) and (3.22):

$$[K_L] = \int_V [B_L]^T [C][B_L] dV \tag{3.19}$$

$$[K_{NL}] = \int_V [B_{NL}][S][B_{NL}] dV \tag{3.20}$$

$$\{F\} = \int_V [B_L]^T \{\hat{S}\} dV \tag{3.22}$$

From equations (3.19) and (3.36) $[K_L]$ can be written explicitly in terms of the thickness coordinate ζ as

$$[K_L] = \int_V ([SD1] + \zeta[SD2] + \zeta^2[SD3])^T [C'] ([SD1] + \zeta[SD2] + \zeta^2[SD3]) dV \tag{5.31}$$

Gauss quadrature is used to perform the numerical integration. In Gauss quadrature an integral over the interval [–1,1] is replaced by the weighted sum of function values at selected points and weights:

$$\int_{-1}^{1} f(\xi)d\xi \cong \sum_{i=1}^{N} w_i f(\xi_i) \tag{5.32}$$

where w_i are weights and ξ_i are the base points. Equation (5.31) is evaluated using gauss quadrature:

$$[K_L] = \sum_{k=1}^{P} \sum_{\xi=1}^{3} \sum_{\eta=1}^{3} \sum_{\zeta=1}^{2} [B_L']^T [C']_{(k)} [B_L'] w_\xi w_\eta w_\zeta {}^{o}|J| \frac{h_k}{h} \tag{5.33}$$

where $[B_L']$ denotes the expression in the parenthesis of equation (5.31), and

P = total number of layers in the laminate

h_k = the thickness of the kth layer

h = total thickness of the shell

${}^{o}|J|$ = determinant of the Jacobian matrix

For elastic structures, the problem is reduced to a 2–D one by performing explicit integration through the thickness. The Jacobian matrix, in general, is a function of ξ, η, and ζ; the ζ terms in the Jacobian matrix may be neglected if the thickness to radius of the shell ratio is small. If the Jacobian ${}^{o}|J|$ is independent of ζ, explicit integration can be used. In addition, we neglect the ζ^2 terms in $[B_L']$. With these assumptions, $[K_L]$ in equation (5.31) can be written as

$$[K_L] = \sum_{r=1}^{3}\sum_{s=1}^{3}\Big\{[SD1]^T[A1][SD1] + [SD2]^T[A2][SD1]$$

$$+ [SD1]^T[A2][SD2] + [SD2]^T[A3][SD2]\Big\}^{o}|J|w_{\xi_r}w_{\eta_s} \qquad (5.34)$$

where

$$[A1] = \sum_{k=1}^{P}\int_{\zeta_k}^{\zeta_{k+1}}[C']d\zeta$$

$$[A2] = \sum_{k=1}^{P}\int_{\zeta_k}^{\zeta_{k+1}}\zeta[C']d\zeta \qquad (5.35)$$

$$[A3] = \sum_{k=1}^{P}\int_{\zeta_k}^{\zeta_{k+1}}\zeta^2[C']d\zeta$$

It is important to note that the upper limit on the number of quadrature points is set to the value 3, which implies full integration. Reduced integration implies a value of 2. For elastic structures, $[C']$ is constant within each layer and thus (5.35) can be integrated explicitly. For elastic–plastic structures, some locations through the thickness become plastic, so that $[C']$ must be replaced by $[C^{ep}]$, the elastoplastic tangent moduli. Thus, when plasticity is included, numerical integration must be used through the thickness as well. Gauss quadrature will also be used in the thickness direction with the thickness

coordinate given as

$$\zeta = \zeta_k + \frac{h_k}{h}(1 + z_i) \tag{5.36}$$

Here z_i is the base point, and $-1 < z < 1$ for each layer. Substituting equation (5.36) into (5.35), then [A1], [A2], and [A3] take the form

$$[A1] = \sum_{k=1}^{P} \sum_{i=1}^{N} [\bar{C}] \frac{h_k}{h} w_i$$

$$[A2] = \sum_{k=1}^{P} \sum_{i=1}^{N} (\zeta_k + \frac{h_k}{h}(1 + z_i))[\bar{C}] \frac{h_k}{h} w_i \tag{5.37}$$

$$[A3] = \sum_{k=1}^{P} \sum_{i=1}^{N} (\zeta_k + \frac{h_k}{h}(1 + z_i))^2[\bar{C}] \frac{h_k}{h} w_i$$

where

$[\bar{C}] = [C']$ for an elastic gauss point, or $[C^{eP}]$ for a plastic gauss point

N = number of gauss points per layer

Next we consider the matrix $[K_{NL}]$ from equations (3.20) and (3.36), which can be rewritten as

$$[K_{NL}] = \sum_{r=1}^{3} \sum_{s=1}^{3} \left\{ [DH1]^T \left[\sum_{k=1}^{P} \int_{\zeta_k}^{\zeta_{k+1}} [S'] d\zeta \right] [DH1] \right.$$

$$+ [DH1]^T \left[\sum_{k=1}^{P} \int_{\zeta_k}^{\zeta_{k+1}} \zeta [S'] d\zeta \right] [DH2]$$

$$+ [DH2]^T \left[\sum_{k=1}^{P} \int_{\zeta_k}^{\zeta_{k+1}} \zeta [S'] d\zeta \right] [DH1]$$

$$+ [DH2]^T \left[\sum_{k=1}^{P} \int_{\zeta_k}^{\zeta_{k+1}} \zeta^2 [S'] d\zeta \right] [DH2] \Big\}^o |J| w_{\xi_r} w_{\eta_s} \tag{5.38}$$

The stresses $[S']$ are calculated from either the elastic constitutive relations or the radial return algorithm when the gauss point yields. The integrals

$$[N] = \sum_{k=1}^{P} \int_{\zeta_k}^{\zeta_{k+1}} [S'] d\zeta \ , \quad [M] = \sum_{k=1}^{P} \int_{\zeta_k}^{\zeta_{k+1}} \zeta [S'] d\zeta, \text{ and}$$

$$[M2] = \sum_{k=1}^{P} \int_{\zeta_k}^{\zeta_{k+1}} \zeta^2 [S'] d\zeta \tag{5.39}$$

must be evaluated using gauss quadrature as in (5.37) when plasticity occurs.

The load vector $\{F\}$ from equations (3.22) and (3.36) can be written as

$$\{F\} = \int_V \left\{ [SD1]^T + \zeta [SD2]^T + \zeta^2 [SD3]^T \right\} \{S'\} dV \tag{5.40}$$

Regrouping the terms and neglecting ζ^2, we can write

$$\{F\} = \sum_{r=1}^{3}\sum_{s=1}^{3}\left\{[SD1]^T\left[\sum_{k=1}^{P}\int_{\zeta_k}^{\zeta_{k+1}}[S']d\zeta\right]\right.$$

$$\left. + [SD2]^T\left[\sum_{k=1}^{P}\int_{\zeta_k}^{\zeta_{k+1}}\zeta\{S'\}d\zeta\right]\right\}^{o}|J|w_{\xi_r}w_{\eta_s} \qquad (5.41)$$

The thickness direction integrals are evaluated numerically when plasticity occurs:

$$\{N\} = \sum_{k=1}^{P}\int_{\zeta_k}^{\zeta_{k+1}}\{S'\}d\zeta$$

$$\{M\} = \sum_{k=1}^{P}\int_{\zeta_k}^{\zeta_{k+1}}\zeta\{S'\}d\zeta \qquad (5.42)$$

This numerical integration through the thickness for plasticity greatly increases the computational expense.

5.6 Solution of Equilibrium Equations with Plasticity

At each load step, the plastic strain $\{\epsilon_n^P\}$ and the back stress $\{q_n\}$ are "frozen" for the next (n+1) load step and are not updated until convergence is achieved. This is important so that inaccurate iterative plastic strain and back stress increments are not used.

The Newton Raphson method described for the geometric nonlinear case is also used here to solve for global equilibrium. When a gauss point yields, the elastoplastic tangent moduli are substituted. Two convergence criteria have been installed: 1) a displacement norm, and 2) a force residual norm. Convergence is achieved if the specified norm is within a preassigned tolerance ϵ, usually selected to be .001 or less. The displacement norm is defined as

$$\left[\sum_{j=1}^{NEQ} (\Delta_j^{(i)} - \Delta_j^{(i-1)})^2 / \sum_{j=1}^{NEQ} (\Delta_j^{(i)})^2\right]^{1/2} \leq \epsilon$$

where NEQ is the total number of equations (or degrees of freedom) in the model. The force residual norm is given by

$$\left[\sum_{j=1}^{NEQ} \left[R_j^{(i)} - F_j^{(i)}\right]^2 / \sum_{j=1}^{NEQ} (R_j)^2\right]^{1/2} \leq \epsilon$$

where R_j is the jth component of the external load vector $\{R\}$, F_j is the jth component of the internal force vector $\{F\}$, and the superscript (i) denotes the iteration number.

6. SECOND–MOMENT PROBABILISTIC FINITE ELEMENT METHOD

6.1 Introduction

In this chapter, the second–moment probabilistic theory for linear, geometrical nonlinear, and material nonlinear analysis are developed for time independent behavior. The selection of random variables are discussed, along with methods for computing the necessary derivatives. Computational savings techniques are presented, and various correlation assumptions discussed. The theoretical developments given are as applied to the degenerated 3–D shell element discussed in Chapter 3.

6.2 Second–Moment Probabilistic Method

In Chapter 3, the finite element incremental equations were cast as

$$[\hat{K}]\{\Delta\} = \{\hat{R}\} \tag{6.1}$$

which is applicable to both linear and nonlinear analysis. Following the development of Liu et al. [33–40], equation (6.1) can be rewritten as

$$\{F(\{\Delta\},\{b\})\} = \{R(\{b\})\} \tag{6.2}$$

where $\{F\}$ is the internal force vector, $\{\Delta\}$ is the displacement vector, $\{R\}$ is the external force, and $\{b\}$ is a discretized vector of the random function $b(x)$, where x is a spatial coordinate $\{x\}$. As in typical finite element analysis, the random function $b(x)$ is expanded using shape functions $\psi_i(x)$

$$b(x) = \sum_{i=1}^{n} \psi_i(x) b_i \tag{6.3}$$

where b_i are the nodal values of b(x). Generally the random quantity b can be a material property, geometric dimension, or a load.

The second–moment probabilistic method can be mathematically viewed as a perturbation method, in which only up to second–order terms are retained. Following the typical perturbation procedure, the matrices in equation (6.2) are expanded in Taylor series about the mean value of the random quantity of interest b. After substituting the Taylor series into (6.2) and equating similar order terms, one obtains equations involving various order derivatives of the displacements with respect to b. These displacement derivatives can be used to determine the statistical mean and covariances of both the displacement and element stress.

In order to describe the probabilistic distribution of the input random function b(x), two statistical moments are required as input. In addition, if spatial correlation is used, this functional dependence must be described as well. Using the notation in [33], the expectation $\bar{b}(x)$, denoted by E[b(x)], coefficient of variation α, and autocorrelation coefficient function $A(b(x_i), b(x_j))$ must be defined. These quantities are known inputs to the model. Typical representations for the autocorrelation coefficient function are of the form,

$$A(b(x_i), b(x_j)) = \exp(-|x_i - x_j|/\lambda) \tag{6.4}$$

where λ is the known correlation length of the random field. The covariance $\mathrm{cov}(b_i,b_j)$ is given by

$$\mathrm{cov}(b_i,b_j) = [\mathrm{var}(b(x_i))\mathrm{var}(b(x_j))]^{1/2} A(b(x_i),b(x_j)) \tag{6.5a}$$

where

$$\text{var}(b(x_i)) = \alpha^2 E[b(x_i)]^2 \tag{6.5b}$$

The definitions of autocorrelation and the actual functions used are discussed in more detail in the sequel.

The vectors $\{\Delta\}$, $\{R\}$, and $\{F\}$ are expanded about the mean of the random function b using the Taylor series:

$$\{\Delta\} = \{\bar{\Delta}\} + \sum_{i=1}^{n} \{\bar{\Delta}\}_{b_i} db_i + \frac{1}{2} \sum_{i,j=1}^{n} \{\bar{\Delta}\}_{b_i b_j} db_i db_j \tag{6.6}$$

$$\{R\} = \{\bar{R}\} + \sum_{i=1}^{n} \{\bar{R}\}_{b_i} db_i + \frac{1}{2} \sum_{i,j=1}^{n} \{\bar{R}\}_{b_i b_j} db_i db_j \tag{6.7}$$

$$\{F\} = \{\bar{F}\} + \sum_{i=1}^{n} \left[\{\bar{F}\}_{b_i} + [\bar{K}^T]\{\bar{\Delta}\}_{b_i}\right] db_i$$

$$+ \sum_{i,j=1}^{n} \left[\frac{1}{2}\{\bar{F}\}_{b_i b_j} + \frac{1}{2}[\bar{K}^T]\{\bar{\Delta}\}_{b_i b_j} + [\bar{K}^T]_{b_i}\{\bar{\Delta}\}_{b_i}\right] db_i db_j \tag{6.8}$$

In the above equations the following notation is used:

$\bar{b}(x) = E[b(x)]$ – for mean value or expected value of b

$db_i = \epsilon(b_i - \bar{b}_i)$ – first order variation of b_i about $\bar{b}_i$

$\bar{g}_{b_i} = \frac{\partial g}{\partial b_i}$ – partial derivative of a function g with respect to b_i and evaluated at $\bar{b}_i$

Also $[K^T]$ is defined to be the tangent stiffness matrix,

$$[K^T] = \frac{\{\partial F\}}{\{\partial \Delta\}} \tag{6.9}$$

Use of the above approximations in equation (6.2) results in the following perturbation equations:

Zeroth–order equation

$$\{\bar{F}\} = \{\bar{R}\} \tag{6.10}$$

First–order equations

$$[\bar{K}^T]\{\bar{\Delta}\}_{b_i} = \{\bar{R}\}_{b_i} - \{\bar{F}\}_{b_i} \quad , \; i = 1,\ldots,n \tag{6.11}$$

Second–order equations

$$[\bar{K}^T]\{\bar{\Delta}_2\} = \{\bar{R}_2\} \tag{6.12a}$$

where

$$\{\bar{\Delta}_2\} = \frac{1}{2} \sum_{i,j=1}^{n} \{\bar{\Delta}\}_{b_i b_j} \mathrm{cov}(b_i, b_j) \tag{6.12b}$$

and

$$\{\bar{R}_2\} = \sum_{i,j=1}^{n} [\frac{1}{2}\{\bar{R}\}_{b_i b_j} - \frac{1}{2}\{\bar{F}\}_{b_i b_j} - [\bar{K}^T]_{b_i}\{\bar{\Delta}\}_{b_j}]\mathrm{cov}(b_i, b_j) \tag{6.12c}$$

Once $\{\bar{\Delta}\}$, $\{\bar{\Delta}\}_{b_i}$, and $\{\bar{\Delta}_2\}$ are obtained by solving equations (6.10)–(6.12), the mean and autocovariance matrices for the nodal displacements can be determined. These are formally defined as

$$E[\{\Delta\}] = \int_{-\infty}^{\infty} \{\Delta(\{b\})\} f(\{b\}) d\{b\} \tag{6.13}$$

and

$$\mathrm{cov}(\Delta^r, \Delta^s) = \int_{-\infty}^{\infty} (\Delta^r - \bar{\Delta}^r)(\Delta^s - \bar{\Delta}^s) f(\{b\}) d\{b\} \tag{6.14}$$

respectively. Here f denotes the joint probability density function, Δ^i is the ith degree of freedom of $\{\Delta\}$, and $\{b\}$ is the random variable vector. By substituting the Taylor series expansion of $\{\Delta\}$ from equation (6.6) into (6.13), the second–order estimate of the mean value of $\{\Delta\}$ is obtained (see [23]),

$$E[\{\Delta\}] = \{\bar{\Delta}\} + \frac{1}{2} \{ \sum_{i,j=1}^{n} \{\bar{\Delta}\}_{b_i b_j} \mathrm{cov}(b_i, b_j) \} \tag{6.15}$$

Similarly, the first–order $\mathrm{cov}(\Delta^i, \Delta^j)$, which is consistent with a second–order analysis, is given by

$$\mathrm{cov}(\Delta^r, \Delta^s) = \sum_{i,j=1}^{n} \bar{\Delta}^r_{b_i} \bar{\Delta}^s_{b_j} \mathrm{cov}(b_i, b_j) \tag{6.16}$$

Recall that the stress vector in an element is given by

$$\{\sigma\} = [C]\{\epsilon\} = [C][B]\{\Delta\} \tag{6.17}$$

The functional dependence of $\{\sigma\}$ on $\{b\}$ is through the constitutive matrix,

$$[C] = [C(x,b)]$$

and [B] is the linear or nonlinear strain–displacement matrix. The Taylor series expansion of [C] is

$$[C] = [\bar{C}] + \sum_{i=1}^{n} \{\bar{C}\}_{b_i} db_i + \frac{1}{2} \sum_{i,j=1}^{n} \{\bar{C}\}_{b_i b_j} db_i db_j \tag{6.18}$$

Substituting (6.18) and (6.6) into the definition of $E[\sigma]$ (similar to equation (6.13)), the second–order mean stress can be written as

$$E[\{\sigma\}] = [\bar{C}]E[\{\epsilon\}] + \left\{ \sum_{i,j=1}^{n} \left[[\bar{C}]_{b_i} ([B]\{\bar{\Delta}\})_{b_j} + \frac{1}{2}[\bar{C}]_{b_i b_j} [B]\{\bar{\Delta}\} \right] \mathrm{cov}(b_i, b_j) \right\} \tag{6.19a}$$

where

$$E[\{\epsilon\}] = [B]\{\bar{\Delta}\} + \frac{1}{2} \left\{ \sum_{i,j=1}^{n} ([B]\{\bar{\Delta}\})_{b_i b_j} \mathrm{cov}(b_i, b_j) \right\} \tag{6.19b}$$

The autocovariance of stress can be expressed as

$$\mathrm{cov}(\{\sigma_e\},\{\sigma_f\}) = \sum_{i,j=1}^{n} \{\sigma_e\}_{b_i} \{\sigma_f\}_{b_j} \mathrm{cov}(b_i,b_j) \tag{6.20}$$

where $\{\sigma_e\}$ represents the stress vector for element e. The vector $\{\sigma_e\}_{b_i}$ is obtained from (6.17) as

$$\{\sigma_e\}_{b_i} = [\bar{C}_e]_{b_i}[B_e]\{\bar{\Delta}_e\} + [\bar{C}_e]([B_e]\{\bar{\Delta}_e\})_{b_i} \tag{6.21}$$

Thus (6.20) can be evaluated using (6.21).

6.3 Composite Random Variables

Sources of randomness can be material properties, geometric dimensions, or loads. For the present study, the only geometric dimensions selected as random variables are the ply thickness and ply angle. The loading is considered to be deterministic throughout this study. All material properties are treated as random variables, either from the point of view of the ply level or the micro level (when a micromechanics constitutive theory is incorporated). At the ply level, material variables could be any of the engineering material properties E_{11}, E_{22}, ν_{12}, G_{12}, G_{13}, G_{23}. Recall that these properties along with the ply angle θ define the coefficients of the constitutive matrix $[C']$ in equations (3.34) and (3.35). At the micromechanics level, the material variables could be the fiber and matrix properties: E_{f11}, E_{f22}, G_{f12}, ν_{f12}, ν_{f23}, E_m, ν_m, FVR, where "f" denotes fiber property, "m" denotes matrix property, and FVR is the fiber volume ratio. These micro–variables are used in the Aboudi micromechanics equations to determine the engineering (ply level) material properties. In this

section, detailed discussions of the technical assumptions and subtleties of incorporating these random variables are presented.

6.3.1 Ply Thickness

The total thickness of a laminate is determined by summing the individual ply thicknesses, which for a composite made of one material type, are assumed to be a constant for every ply. Here it is assumed that the thickness of all layers fluctuate, but that the total thickness of the laminate (shell) remains unchanged. This is the assumption made by Nakagiri et al. [26] for eigenvalue analysis of composite plates. In [26] only ply thickness and orientation angle were selected as random variables. Since the total thickness is assumed to be constant, the ζ coordinates of the upper and lower surfaces of the shell are deterministic. The through–the–thickness integration, as described in equations (5.35), involves the ply thickness coordinates as follows:

$$[A1] = \sum_{k=1}^{P} \int_{\zeta_k}^{\zeta_{k+1}} [C']d\zeta$$

$$[A2] = \sum_{k=1}^{P} \int_{\zeta_k}^{\zeta_{k+1}} \zeta[C']d\zeta$$

$$[A3] = \sum_{k=1}^{P} \int_{\zeta_k}^{\zeta_{k+1}} \zeta^2[C']d\zeta$$

For elastic structures, these integrations are carried out explicitly,

$$[A1] = \sum_{k=1}^{P} [C']_k(\zeta_{k+1} - \zeta_k)$$

$$[A2] = \frac{1}{2} \sum_{k=1}^{P} [C']_k(\zeta_{k+1}^2 - \zeta_k^2) \tag{6.22}$$

$$[A3] = \frac{1}{3} \sum_{k=1}^{P} [C']_k(\zeta_{k+1}^3 - \zeta_k^3)$$

where ζ_k is the lower coordinate of the kth layer. For elastic–plastic structures, the integrals must be numerically evaluated. For a two–layer composite, for example, the previous assumption results in only the upper coordinate ζ_2 of layer 1 being random. In general, ζ_{k+1} is the random variable for the kth layer, unless k is equal to P, the last layer.

The random variable ζ_{k+1} is also interpolated using the finite element interpolation functions $\psi_i(x)$:

$$\zeta_{k+1} = \sum_{i=1}^{n} \psi_i(x)(\zeta_{k+1})_i \tag{6.23}$$

Substituting (6.23) into (6.22), the perturbation derivatives $\{\bar{F}\}_{b_i}$ required in equations (6.11) can be evaluated for the thickness random variable. For the kth layer, assuming again an elastic constitutive law, the results are

$$\frac{\partial[A1]}{\partial(\zeta_{k+1})_i} = ([C']_k - [C']_{k+1})\psi_i$$

$$\frac{\partial[A2]}{\partial(\zeta_{k+1})_i} = ([C']_k - [C']_{k+1})\zeta_{k+1}\psi_i \qquad (6.24)$$

$$\frac{\partial[A3]}{\partial(\zeta_{k+1})_i} = ([C']_k - [C']_{k+1})\zeta_{k+1}^2\psi_i \qquad i = 1,n$$

Since the matrices [A1], [A2], and [A3] contain the only dependence on the random variable ζ_{k+1}, equations (6.24) are used directly to assemble the resulting $\{\bar{F}\}_{b_i}$.

6.3.2 Ply Angle

The only dependence on the ply angle θ exists in the constitutive matrix $[C']$ (see equation (3.54)). Therefore, in order to evaluate $\{\bar{F}\}_{b_i}$, where b is the ply angle, it is necessary only to determine the derivative matrix $\frac{\partial[C']}{\partial\theta_i}$ for each layer. This differentiation is done explicitly and is straight–forward, so the details are not presented here.

6.3.3 Ply–Level Material Properties

The only dependence on the ply–level engineering constants E_{11}, E_{22}, ν_{12}, G_{12}, G_{13}, G_{23} is in equations (3.34) and (3.35). The derivatives $\frac{\partial[C']}{\partial b_i}$,

where b is any of these properties for a particular layer, are explicitly differentiated here as well.

6.3.4 Micro–Level Material Properties

The micro–level random variables E_{f11}, E_{f22}, G_{f12}, ν_{f12}, ν_{f23}, E_m, ν_m and FVR are specified inputs to the Aboudi micromechanics equations with the output being the ply–level engineering constants. These engineering constants are used to calculate the [A1], [A2], and [A3] matrix stiffnesses in equation (5.35). It should be noted that when the micromechanics model is used, only linear or geometrical nonlinear behavior is allowed. Thus, in order to evaluate the $\{\bar{F}\}_{b_i}$ matrices needed in equations (6.11), equations (6.22) must be differentiated in terms of the micro–level random variables. Referring to equation $(6.22)_1$, the chain rule of differentiation is performed

$$\frac{d[A1]}{dFVR} = \frac{d[A1]}{dE_{11}}\frac{dE_{11}}{dFVR} + \frac{d[A1]}{dE_{22}}\frac{dE_{22}}{dFVR} + \frac{d[A1]}{d\nu_{12}}\frac{d\nu_{12}}{dFVR}$$

$$+ \frac{d[A1]}{dG_{12}}\frac{dG_{12}}{dFVR} + \frac{d[A1]}{dG_{13}}\frac{dG_{13}}{dFVR} + \frac{d[A1]}{dG_{23}}\frac{dG_{23}}{dFVR} \quad (6.25)$$

where the selected micro random variable is FVR. Note that the terms $\frac{d[A1]}{dE_{11}}$, $\frac{d[A1]}{dE_{22}}$ etc. are already known explicitly from the discussion in section 6.3.3, so that only the terms $\frac{dE_{11}}{dFVR}$, $\frac{dE_{22}}{dFVR}$, etc. must be computed.

The relationship between E_{11} and FVR is given in terms of the micromechanics equations. Hence, these equations must be differentiated in order to determine $\frac{dE_{11}}{dFVR}$. Since the Aboudi model is rather complex, the finite difference technique is used. The derivatives are calculated as follows:

$$FVR^{+} = (1 + Delta)FVR$$
$$FVR^{-} = (1 - Delta)FVR \tag{6.26}$$

$$\frac{dE_{11}}{dFVR} = \frac{E_{11}^{+} - E_{11}^{-}}{2(Delta)FVR}$$

where E_{11}^{+} is evaluated using FVR^{+} and E_{11}^{-} is evaluated using FVR^{-}, and Delta is a small number, usually set to .05 or less. In this way the perturbation derivatives $\{\bar{F}\}_{b_i}$ for micro random variables are successfully calculated for linear elastic or geometrical nonlinear elastic structures.

6.4 Linear and Geometric Nonlinear Elastic Problems

In this problem group, all of the necessary perturbation derivatives at the ply level are determined by exact differentiation of the stiffness matrices in equations (6.22), due to the elastic behavior. Finite difference derivatives in (6.26) are still used for micro–level random variables. For linear elastic problems, the vector $\{\bar{F}\}$ in equation (6.10) is represented by $[\bar{K}]\{\Delta\}$ (as in (3.23)) and the derivative matrix $\{\bar{F}\}_{b_i}$ by $[\bar{K}]_{b_i}\{\Delta\}$. For geometric nonlinear elastic problems, $\{\bar{F}\}$ is given by:

$$\{\bar{F}\} = \int_V [B_L]^T \{\hat{S}\} dV$$

Therefore $\{\bar{F}\}_{b_i}$ becomes

$$\{\bar{F}\}_{b_i} = \int_V [B_L]^T \{\hat{S}\}_{b_i} dV \tag{6.27}$$

The solution procedure involves a consecutive solution of equations (6.10) through (6.12). After the deterministic zeroth–order equation (6.10) is solved, either once for the linear case or iteratively at each load step in the nonlinear case, the generalized displacement vector $\{\bar{\Delta}\}$ is used to perform the perturbation solutions in equations (6.11)–(6.12). In (6.11), there are as many solutions for $\{\Delta\}_{b_i}$ as there are number of nodes in the model, and in (6.12) one solution for $\{\bar{\Delta}_2\}$. In addition, the computations in equations (6.11) and (6.12) must be performed for each layer in the model, as a particular random function is assumed to be independent from layer to layer. If there are n nodes and P layers in the model, (n + 1)P more matrix solutions are required at each load step for each random variable. This is not as expensive as it seems, because the stiffness matrix $[\bar{K}^T]$ is inverted once and used in equations (6.11)–(6.12).

The next step is to determine the mean and variance of the response. This is done using equations (6.15)–(6.16) for displacement and (6.19)–(6.20) for stress. Note that the derivatives of the term $[B]\{\bar{\Delta}\}$ are required in equation (6.19) and for the stress derivatives in equation (6.21). For linear

structures this becomes

$$([B_L]\{\bar{\Delta}\})_{b_i} = [B_L]_{b_i}\{\bar{\Delta}\} + [B_L]\{\bar{\Delta}\}_{b_i} \tag{6.28}$$

and for geometric nonlinear elastic problems it is

$$([B_{NL}]\{\bar{\Delta}\})_{b_i} = [B_{NL}]_{b_i}\{\bar{\Delta}\} + [B_{NL}]\{\bar{\Delta}\}_{b_i} \tag{6.29}$$

which implies that the left hand side of the equations are functions of both $\{\bar{\Delta}\}$ and $\{\bar{\Delta}\}_{b_i}$.

6.5 Material Nonlinear Problems

As in the geometric nonlinear problem, the residual vector is given by $\{\bar{F}\}$. Therefore, the derivatives are the same as in equation (6.27). Recalling equation (6.2), $\{F\}$ is functionally represented in the form

$$\{F\} = \{F(\{\Delta\},\{b\})\} \tag{6.30}$$

Temporarily dropping the vector braces, and differentiating F with respect to b

$$\frac{dF}{db} = \frac{\partial F}{\partial b} + \frac{\partial F}{\partial \Delta}\frac{\partial \Delta}{\partial b} \tag{6.31}$$

The first term on the right hand side involves the explicit derivative of F with respect to b. This is the result required in equation (6.27), in which the derivative of F is expressed in terms of explicit derivatives of the stress vector $\hat{S}$. As stated in the last section, all these derivatives can be expressed exactly when elastic behavior exists. However, when material nonlinear behavior is

present, finite difference derivatives are used once again due to the complex nonlinear relationship between stress and strain. Since orthotropic plasticity is present in certain layers, the radial return algorithm discussed previously is considered to be very good for this purpose [38,40]. This is true since at a particular load step, the plastic strain and effective plastic strain are "frozen" and only updated after equilibrium conversion is achieved. This update can be done after the finite difference calculations are made, so that the true effect of perturbing the random variable about its mean is measured. Other advantages of the radial return method are the increased accuracy involved in the stress recovery routine and the algorithmic compatible tangent moduli which results in a more accurate tangent stiffness matrix. This accuracy is important in computing the perturbation derivatives (e.g., $\{\bar{\Delta}\}_{b_i}$ in equations (6.9)–(6.12)).

The evaluation of $\{\bar{F}\}_{b_i}$ involves the explicit differentiation of $\{\hat{S}\}$, which is achieved using the finite difference formulas in (6.26), as recommended in [38,40]. Define

$$b_i^+ = (1 + \text{Delta})b$$

$$b_i^- = (1 - \text{Delta})b$$

$$\hat{S}^+ = \hat{S}(b_i^+) \text{ and } \hat{S}^- = \hat{S}(b_i^-) \tag{6.32}$$

so that

$$\frac{\partial \hat{S}}{\partial b_i} \cong \frac{\hat{S}^+ - \hat{S}^-}{2(\text{Delta})b_i} \qquad i = 1...,n$$

It should be noticed in equations (6.32) that the perturbations on b are made at

a particular nodal location i to evaluate $\frac{\partial \hat{S}}{\partial b_i}$, while for all other locations the derivative is zero. In this manner the applicable random variable derivatives can be evaluated. These include the ply level stiffnesses (E_{11}, E_{22}, ν_{12}, G_{13}, G_{23}, G_{12}), ply thickness, and any plastic parameters desired. The plastic random variables selected are the uniaxial yield stress σ_Y and the hardening modulus $\bar{H}$.

In order to evaluate the autocovariance of stress, equation (6.20) is used as usual in conjunction with the total derivatives of $\hat{S}$:

$$\frac{d\hat{S}}{db_i} = \frac{\partial \hat{S}}{\partial b_i} + \frac{\partial \hat{S}}{\partial \Delta}\frac{\partial \Delta}{\partial b_i}$$

or

$$\frac{d\hat{S}}{db_i} = \frac{\partial \hat{S}}{\partial b_i} + \frac{\partial \hat{S}}{\partial \epsilon}\frac{\partial \epsilon}{\partial b_i} \tag{6.33}$$

The first term on the right hand side of $(6.33)_2$ is the explicit derivative already evaluated using finite differences. The second term $\frac{\partial \hat{S}}{\partial \epsilon}$ is simply the tangent moduli matrix given by equation (5.18), and (bringing back the vector braces notation) $\{\epsilon\}$ is represented from (6.17) as

$$\{\epsilon\} = [B]\{\Delta\} \tag{6.34}$$

These derivatives are the same as expressed in equations (6.28) and (6.29) for geometrically linear and nonlinear structures, respectively. Substituting the results into (6.33), we obtain

$$\{\hat{S}\}_{b_i} = \frac{\partial\{\hat{S}\}}{\partial b_i} + [C^{eP}](\{B\}\{\Delta\})_{b_i} \tag{6.35}$$

which is used to evaluate the autocovariance in equation (6.20).

When combined geometric and material nonlinear behavior exists, the previously mentioned methods of differentiation are used for the appropriate plies. That is, exact differentiation is used for general elastic layers, and finite difference for elastic–plastic layers. The finite difference method is also used for the micro–level random variables, which are not applicable to the elastic–plastic layers.

Up to this point the second–order equations have been developed. It turns out that for layered composite materials, independent random fields have been modeled for each layer. This greatly increases the cost of both assembly of the perturbation derivatives and of the solution of the first and second–order equations. Due to the immense assembly and storage requirements as well as computational effort required for the second–order equations when multiple layers exist, the analysis has been limited to the first–order equations. It can be observed that the second–order term results only in a small correction to the mean displacement and stress response, and it is assumed negligible when weighed against the cost of obtaining it.

6.6 Spatial Correlation

The probabilistic finite element procedure developed herein has the ability to model the correlation involved in spatial fields. Consider the random variable vector $\{b(x)\}$, which can be a general random field, e.g., a family of related random variables such as Young's modulus which can vary in the spatial coordinate x. The autocorrelation coefficient function of the discrete random field $\{b(x)\}$ is thus defined similar to equation (6.14) as

$$A(b(x_i),b(x_j)) = \frac{\int_{-\infty}^{\infty} (b_i - \bar{b}_i)(b_j - \bar{b}_j) f(\{b\}) d\{b\}}{[\mathrm{var}(b(x_i))\ \mathrm{var}(b(x_j))]^{1/2}} \tag{6.36}$$

The term "auto" here refers to the fact that we are dealing with the same random field $\{b\}$, and are concerned with its correlation in space. In order to determine the autocovariance of the response such as displacement and stress, $A(b_i,b_j)$ must be a known input characteristic of the input random field b. A typical representation for the autocorrelation was given in equation (6.3), but this case was for isotropic spatial correlation. Extending this to an orthotropic ply and referring to Figures 6.1 and 6.2, we assume an orthotropic autocorrelation coefficient function in the following form

$$A(b_i,b_j) = \exp\left[-\left[\frac{\xi_i' - \xi_j'}{\lambda_{\xi'}}\right]^2\right]\exp\left[-\left[\frac{\eta_i' - \eta_j'}{\lambda_{\eta'}}\right]^2\right] \quad i,j = 1\ldots,n \tag{6.37}$$

In Figure 6.1, ξ and η are the curvilinear coordinates of the shell which are aligned with the body coordinates, ξ' and η' are the curvilinear coordinates in

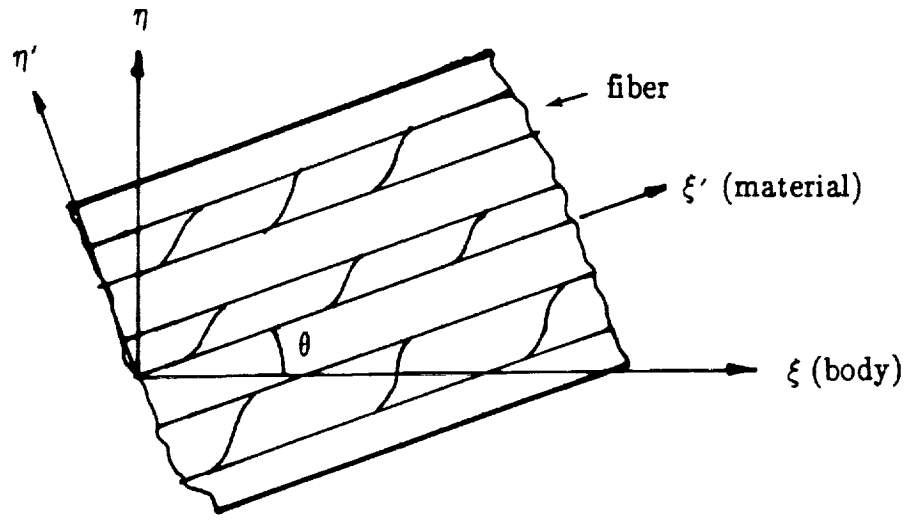

Figure 6.1 Local coordinate systems for body and material coordinates.

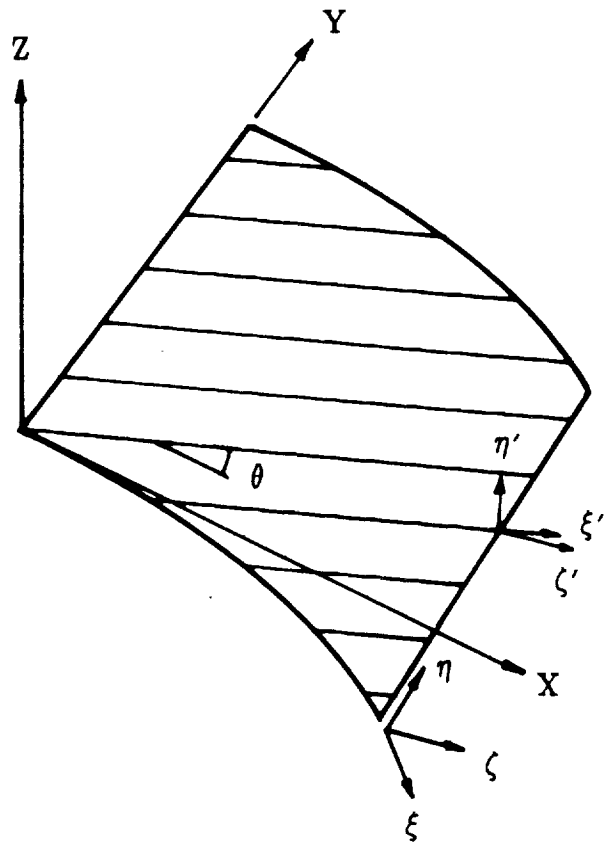

Figure 6.2 Body and material coordinates in the shell curvilinear plane.

the principal material coordinate system, aligned with the fibers, and $\lambda_{\xi'}$, $\lambda_{\eta'}$ are input correlation lengths. Transforming ξ and η to the principal material coordinates ξ' and η', we obtain

$$\begin{Bmatrix}(\xi_i' - \xi_j')\\(\eta_i' - \eta_j')\end{Bmatrix} = \begin{bmatrix}\cos\theta & \sin\theta\\-\sin\theta & \cos\theta\end{bmatrix}\begin{Bmatrix}(\xi_i - \xi_j)\\(\eta_i - \eta_j)\end{Bmatrix} \tag{6.38}$$

The formulation for the autocorrelation allows ply random variables to be correlated in the plane of the shell aligned with the material coordinates. For the case of material properties, we assume that they will have correlation trends which are parallel and perpendicular to the fiber directions.

An underlying assumption in equation (6.37) is that $A(b_i,b_j)$ is not a function of the shell thickness coordinate ζ. This leads to independent random fields from ply to ply (uncorrelated). This assumption is not a requirement, and correlation could be assumed in the ζ direction, but for all of the examples given in this work all layers have been chosen to be independent.

If the form of equation (6.37) is studied in relation to the correlation lengths $\lambda_{\xi'}$ and $\lambda_{\eta'}$, one discovers that for small $\lambda_{\xi'}$ and $\lambda_{\eta'}$ (say 1% of the length of the shell) that very little correlation $A(b_i,b_j)$ exists from node i to j and corresponds to almost independent random variables. On the other hand, for large $\lambda_{\xi'}$ and $\lambda_{\eta'}$ (say greater than four times the length of the shell) the correlation becomes almost constant from node to node. As will be shown in the next chapter, this is equivalent to assuming a "uniform variance" field in which the fluctuation due to each random field is uniform over the entire shell layer. Basically this random field is fully correlated, and is equivalent to

assuming a single random variable for that ply. This is the same assumption made by Nakagiri [26], and it considerably simplifies the computations. Whereas previously the first–order equations (6.11) must be solved for all n nodes and for each of the P independent layers, the uniform variance assumption requires (6.11) to only be solved for each layer. This greatly reduces the number of computations required in (6.11), (6.16) and (6.20) as the loops extend only to P layers as opposed to P layers times n nodes. Thus if the random field is highly correlated so that the variance is essentially the same from node to node, then the random field can be dropped and a uniform variance field assumed to reduce the cost of the analysis.

6.7 Computational Saving Techniques

Three methods are utilized in this work to reduce the computational effort involved when a nonuniform correlated field is assumed. Liu et al. [33–40] discussed a method for diagonalizing the covariance matrix, and a technique for computing only the kth component of the displacement derivatives, which they called the adjoint method. Both of these are incorporated here, as well as a way to reduce the assembly time for stiffness and residual force derivatives by using the chain rule of differentiation. All three of these techniques will be discussed in this section.

6.7.1 Diagonalization of Covariance Matrix

In order to compute the covariance of the displacement and stress response, the multiplications involved in the double summations on i and j in equations (6.16) and (6.20) must be performed. As mentioned in [33], the

number of multiplications is proportional to $n(n + 1)/2$, and is expensive. However, if the double loops on i and j could be reduced to a single loop, then substantial savings would result (the number of multiplications is reduced to n). This is accomplished by transforming the covariance matrix $\text{cov}(b_i,b_j)$ to a diagonal variance matrix $\text{var}(c_i,c_j)$ so that the following conditions hold

$$\text{var}(c_i,c_j) = 0 \qquad \text{for } i \neq j$$

and

$$\text{var}(c_i,c_j) = \text{var}(c_i) \quad \text{for } i = j \tag{6.39}$$

The transformation is performed by solving the following eigenproblem

$$[G][\phi] = [\phi][\Lambda] \tag{6.40}$$

where [G] and $[\Lambda]$ represent $\text{cov}(b_i,b_j)$ and $\text{var}(c_i,c_j)$, respectively, $[\phi]$ is the matrix of eigenvectors normalized according to

$$[\phi][\phi]^T = [I]$$

$$[\Lambda] = [\phi]^T[G][\phi] \tag{6.41}$$

and [I] is the identity matrix. The random variable vector {b} is transformed to the new random variable vector {c} according to

$$\{c\} = [\phi]^T\{b\}$$

or

$$\{b\} = [\phi]\{c\} \tag{6.42}$$

The perturbation equations (6.10) and (6.11) to be solved take the form (only dealing with first–order)

Zeroth–order

$$\{\bar{F}\} = \{\bar{R}\} \tag{6.43}$$

First–order

$$[\bar{K}^T]\{\Delta\}_{c_i} = \{\bar{R}\}_{c_i} - \{\bar{F}\}_{c_i} \quad , \quad i = 1,\ldots n \tag{6.44}$$

and the covariance solutions in equations (6.16) and (6.20) become

$$\mathrm{cov}(\Delta^r,\Delta^s) = \sum_{j=1}^{n} \bar{\Delta}^r_{c_j} \bar{\Delta}^s_{c_j} \mathrm{var}(c_j) \tag{6.45}$$

$$\mathrm{cov}(\{\sigma_r\},\{\sigma_s\}) = \sum_{j=1}^{n} \{\sigma_r\}_{c_j}\{\sigma_s\}_{c_j} \mathrm{var}(c_j) \tag{6.46}$$

Here $\mathrm{var}(c_j)$ is obtained from the diagonal terms of $[\Lambda]$.

In order to solve equation (6.44), the derivatives $\{\bar{R}\}_{c_i}$ and $\{\bar{F}\}_{c_i}$ must be found. Considering $\{\bar{F}\}_{c_i}$, for example, the transformation is achieved by using the chain rule of differentiation,

$$\{\bar{F}\}_{c_i} = \sum_{k=1}^{n} \{\bar{F}\}_{b_k} \frac{\partial b_k}{\partial c_i} \tag{6.47}$$

Since the random variable vector $\{b\}$ is given by

$$\{b\} = [\phi]\{c\}$$

we have

$$\frac{\partial b_k}{\partial c_i} = \phi_{ki}$$

Hence, equation (6.47) becomes

$$\{\bar{F}\}_{c_i} = \sum_{k=1}^{n} \{\bar{F}\}_{b_k} \phi_{ki} \tag{6.48}$$

Thus, prior to computing $\{\bar{F}\}_{c_i}$ from equation (6.48), all n vectors $\{\bar{F}\}_{b_k}$ must be assembled and stored.

It has been found that this diagonalization technique is highly beneficial when nonlinear computations are performed, since the eigenproblem in (6.40) can be solved once at the beginning and the result can be used for each load step. Thus, the double summations are reduced to single summations for each load step, without having to resolve the eigenproblem each time.

6.7.2 Adjoint Method

A distinct advantage in this first–order probabilistic finite element method is its ability to preselect certain displacement and stress responses of interest and thereby save computational effort by not calculating covariance response of others. Since the assumption has been made here that the random variables are independent from layer to layer, then the perturbation equations (6.43)–(6.46) must be solved for each layer as well. This could become expensive as the number of layers become large, therefore it would be nice to separate the computations from a dependency on the number of layers as much as possible.

Liu et al. [34,40] introduced an adjoint method which, when used properly, partially achieves this goal. The method is used to calculate the displacement derivatives of the kth component of the generalized displacements

$\{\Delta\}$. Using the chain rule of differentiation on $\{\Delta\}$, we obtain

$$\Delta^k_{e_i} \equiv \frac{d\Delta^k}{dc_i} = \frac{\partial\Delta^k}{\partial c_i} + \frac{\partial\Delta^k}{\partial\{\Delta\}}\frac{\partial\{\Delta\}}{\partial c_i} \equiv 0 + \{D^k\}\{\Delta\}_{c_i} \tag{6.49}$$

where

$$\{D^k\} = \partial\Delta^k/\partial\{\Delta\}$$

We can calculate $\{\Delta\}_{c_i}$ from Eq. (6.44)

$$\{\Delta\}_{c_i} = [K^T]^{-1}(\{R\}_{c_i} - \{F\}_{c_i}) \equiv [K^T]^{-1}\{f\}_{c_i} \tag{6.50}$$

Substituting (6.50) into (6.49) (note that the explicit derivative term $\frac{\partial\Delta^k}{\partial c_i}$ is zero), we obtain

$$\Delta^k_{c_i} = \{D^k\}[K^T]^{-1}\{f\}_{c_i} \tag{6.51}$$

The adjoint problem is defined by

$$[K^T]\{\lambda^k\} = \{D^k\} \tag{6.52}$$

Substituting (6.52) into (6.51), we arrive at the result

$$\Delta^k_{c_i} = [K^T]\{\lambda^k\}[K^T]^{-1}\{f\}_{c_i}$$

or, finally, we obtain

$$\Delta^{k}_{c_i} = \{\lambda^{k}\}^{T}\{f\}_{c_i} \tag{6.53}$$

The result in equation (6.53) expresses the desired displacement derivative component $\Delta^{k}_{c_i}$ in terms of the known force derivatives $\{f\}_{c_i}$ and the solution to the adjoint problem $\{\lambda^{k}\}^{T}$. In solving the adjoint problem in equation (6.52), we note that the right hand side $\{D^{k}\}$ simply becomes a Boolean vector, with unit value at the kth component. With this method, we simply select m displacement degrees of freedom (k = 1,...m) of interest (usually only those necessary to calculate the stresses of interest), and solve equation (6.52) m times. Once m solutions are available, then equation (6.53) can be used to determine all ply level derivatives of random variables. Since the number of random variables is a function of the number of layers, equation (6.53) gives the derivatives for each ply without having to solve a structural level problem as in (6.44) for each set of random variables in each ply. Thus, we have succeeded in separating the solution of equation (6.44) from dependency on the number of layers in the model. Moreover, if the need to solve for a preselected m degrees of freedom exists, and m is much smaller than the number of nodal random variables times the number of layers, then substantial savings can result. One can easily see that for a large number of layers in the composite the adjoint method is very beneficial.

6.7.3 Assembly Savings Technique

After gaining experience with the probabilistic methods in the shell program, it was discovered that considerable computational time is used in assembling the necessary residual force derivatives $\{\bar{F}\}_{b_i}$ in equation (6.11). This expense is due to the fact that $\{\bar{F}\}_{b_i}$ must be assembled independently for each "i" node in the model and for each of the P layers, or i*P assemblies for the solutions of equation (6.11). Recalling equation (5.41) for the residual force vector {F}, and substituting (5.42) we can express the integration of $\{F\}_{b_i}$ as

$$\{F\}_{b_i} = \sum_{r=1}^{3}\sum_{s=1}^{3}\left\{[SD1]^T\{N\}_{b_i} + [SD2]^T\{M\}_{b_i}\right\}^{o}|J|w_{\xi_r}w_{\eta_s} \tag{6.54}$$

For the example of elastic materials, $\{N\}_{b_i}$ and $\{M\}_{b_i}$ become

$$\{N\}_{b_i} = [A1]_{b_i}\{S1\} + [A2]_{b_i}\{S2\}$$

$$\{M\}_{b_i} = [A2]_{b_i}\{S1\} + [A3]_{b_i}\{S2\} \tag{6.55}$$

where the general Green–Lagrange strains have been expressed as

$$\{\epsilon\} = \{S1\} + \zeta\{S2\} + \zeta^2\{S3\} \tag{6.56}$$

and terms with higher degrees than ζ^2 have been ignored. Equations (6.24) contain the derivatives $[A1]_{b_i}$, $[A2]_{b_i}$, $[A3]_{b_i}$ for the case in which the ply thickness is a random variable. Each of these equations are in the form

$$[A]_{b_i} = [D(\zeta)]\psi_i \tag{6.57}$$

where $[D(\zeta)]$ is some general function of ζ and ψ_i is the interpolation function used in the expansion $b(x) = \sum_{i=1}^{n} \psi_i(x) b_i$. In symbolic form the integration of $\{F\}_{b_i}$ involves terms of the form

$$\{F\}_{b_i} = \sum_{r=1}^{3} \sum_{s=1}^{3} \left\{ [SD1]^T [D(\zeta)](\psi_i)\{S1\} \right\}^o |J| w_{\xi_r} w_{\eta_s} \tag{6.58}$$

for each random variable b_i at the ith node. Applying the chain rule of differentiation to $\{F\}_{b_i}$, we obtain

$$\{F\}_{b_i} = \{F\}_b \frac{\partial b}{\partial b_i} = \{F\}_b \psi_i \tag{6.59}$$

The result in (6.59) allows us to express (6.58) as

$$\{F\}_{b_i} = \left[\sum_{r=1}^{3} \sum_{s=1}^{3} \left\{ [SD1]^T [D(\zeta)]\{S1\} \right\}^o |J| w_{\xi_r} w_{\eta_s} \right] \psi_i = \{F\}_b \psi_i \tag{6.60}$$

In summary, the new approach is to assemble $\{F\}_b$ once for each layer, independent of the nodal random variable quantities b_i, and then determine $\{F\}_{b_i}$ after assembly for each node i by the use of equation (6.60). Even though $\{F\}_b$ must still be assembled for each layer, the separate assemblies for each node are now successfully eliminated with considerable savings.

7. APPLICATIONS

7.1 Introduction

A number of problems have been solved to demonstrate various aspects and capabilities of the formulation developed in the present study. Verification of the accuracy of the first–order second–moment probabilistic finite element method (FOSM–PFEM) for all linear and nonlinear problems is carried out by comparison with Monte Carlo simulation results (for a description of the Monte Carlo method see Appendix B). Examples of linear problems are presented first to demonstrate modeling refinement requirements, sensitivities of the solution to various random variables, and effects of different levels of spatial correlation and input variance. Graphite–epoxy and metal matrix composite properties are compared as well. Geometric nonlinear examples involving postbuckling of plates and shells are presented next, with sensitivity to individual random variables demonstrated throughout the load range. Finally, combined elastoplastic and geometric nonlinear examples are given for a tension specimen with a hole for both ARALL and Boron/Aluminum composites. Experimental comparisons are given whenever possible.

7.2 Linear Analyses

The problem chosen as a comparison base for all examples in this section is a shallow spherical shell with simply supported boundary conditions and uniform external pressure. The problem description is given in Figure 7.1, and all input material properties, variances and levels of spatial correlation are given in Table 7.1. The coefficient of variation (COV) is defined as the ratio of the standard deviation to the mean for a given random variable. All examples

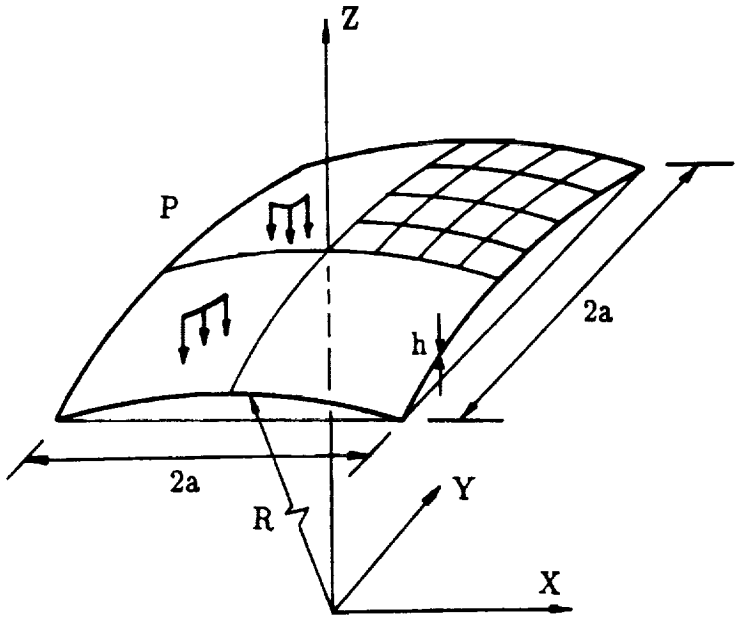

Two layer (0/90)

R = 1000 in a = 50 in h = 1 in

BC's (Simply Supported)

$u = w = \theta_2 = 0$ at $x = a/2$

$v = w = \theta_1 = 0$ at $y = a/2$

$v = \theta_2 = 0$ at $y = 0$ $u = \theta_1 = 0$ at $x = 0$

Figure 7.1 Spherical shell under external pressure; out–of–plane displacement w measured at the center; σ_{xx} stress measured at gauss point nearest center in 0 degree ply.

Table 7.1

Material Properties and Statistics for Graphite–Epoxy Spherical Shell Problem

Random Variable	Mean	Standard Deviation	Coefficient of Variation	$\lambda_{\xi'}$	$\lambda_{\eta'}$
E_{11}	15.75×10^{6}	7.8750×10^{5}	0.05	25	15
E_{22}	0.9091×10^{6}	4.5454×10^{4}	0.05	15	25
G_{12}	0.4475×10^{6}	2.2376×10^{4}	0.05	20	20
ν_{12}	0.2223	1.1116×10^{-2}	0.05	20	20
G_{13}	0.4475×10^{6}	2.2376×10^{4}	0.05	20	20
G_{23}	0.3497×10^{6}	1.7487×10^{4}	0.05	20	20
E_{f11}	31.0×10^{6}	1.55×10^{6}	0.05	25	15
E_{f22}	2.0×10^{6}	1.0×10^{5}	0.05	15	25
G_{f12}	2.0×10^{6}	1.0×10^{5}	0.05	20	20
ν_{f12}	0.2	1.0×10^{-2}	0.05	20	20
ν_{f23}	0.25	1.25×10^{-2}	0.05	20	20
E_{m}	0.5×10^{6}	2.5×10^{4}	0.05	25	25
ν_{m}	0.25	1.25×10^{-2}	0.05	25	25
FVR	0.5	2.5×10^{-2}	0.05	20	20
θ^{*}	0°,90°	2°	–	25	25
δ^{*}	0.5	.025	0.05	25	25

* θ indicates fiber orientation angle and δ indicates ply thickness.

The subscripts f and m stand for fiber and matrix; absence of a letter subscript indicates a ply–level property. The units are psi and inches where appropriate.

in this study used a COV of .05 except for the case of ply orientation angle, where the standard deviation was chosen to be 2 degrees. When spatial correlation was used, typical correlation lengths were around one half of the domain of the problem for each principal material direction. Only one quadrant of the shell was modeled in the interest of computational savings, even though the spatial correlation assumptions may not be symmetric across the shell. Of course, this is not a limitation of the procedures or computational model developed herein.

7.2.1 Graphite–Epoxy Composite Shell

The first example in this section involved the base line shell problem modeled with graphite–epoxy ply–level properties. The intent here is to illustrate both the agreement of the first–order second–moment probabilistic finite element method results with the Monte Carlo results, and to show the mesh refinement requirements in relation to the random field. Figures 7.2 through 7.5 contain plots of out–of–plane displacement and stress for both mean and variance along the x–axis. A 2x2 mesh of nine–node Lagrange elements was used here with fully reduced (2x2) integration. The Monte Carlo solution is one that fully converged at 1500 simulations. While the agreement for the mean plots is good, the variance results are less satisfactory. Refining the mesh to a 4x4 nine–node element mesh, quite good results for the variances as well as the mean values were obtained (see Figures 7.6 through 7.9). This can be attributed to the fact that even though the 2x2 mesh was a reasonable one to discretize the deterministic equilibrium field equations, it was not refined enough to discretize the chosen random field. Thus the analyst must be

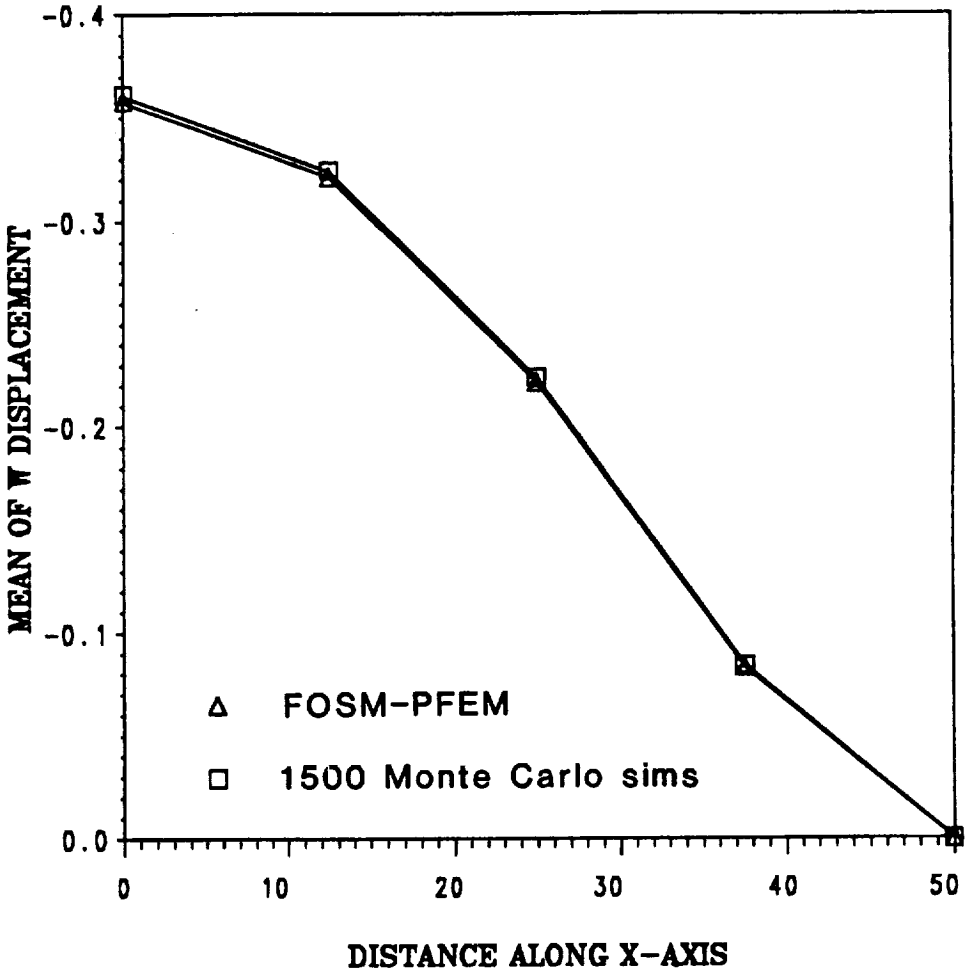

Figure 7.2 Mean center diplacement w along x–axis of spherical shell using all ply–level random variables and a 2x2 nine–node element mesh.

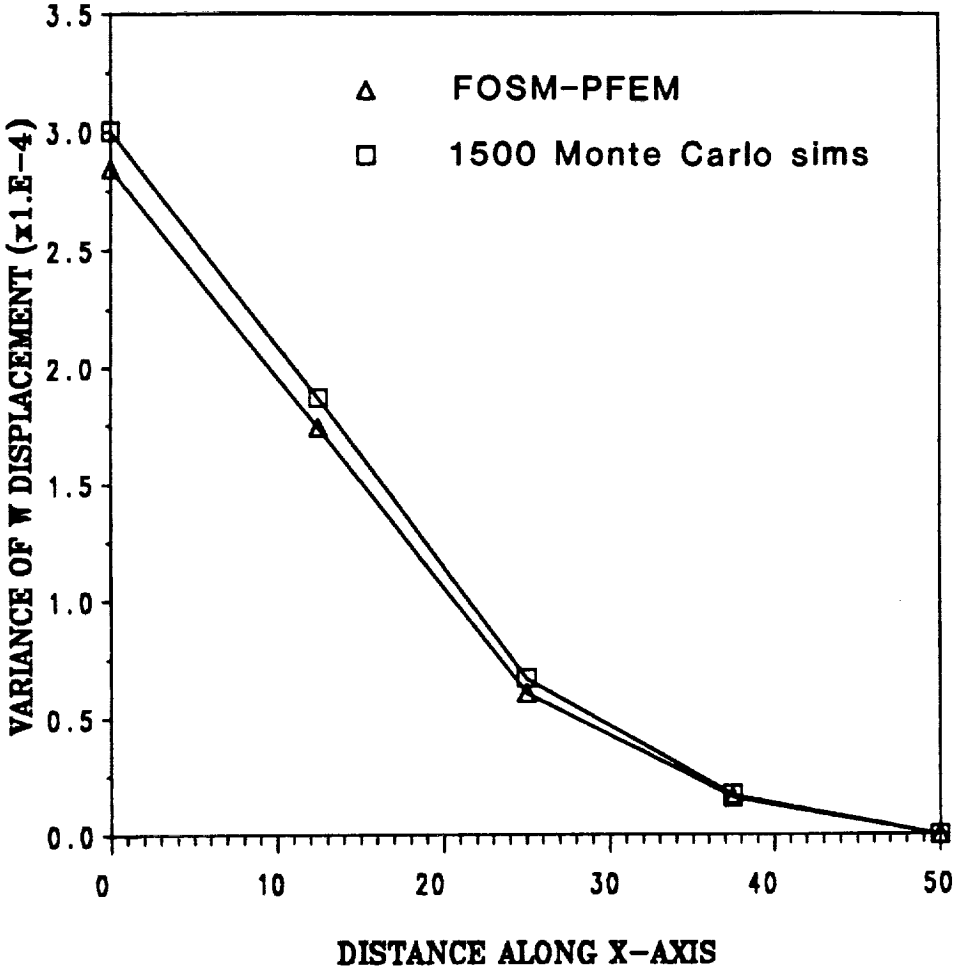

Figure 7.3 Variance of center displacement w along x–axis of spherical shell using all ply–level random variables and a 2x2 nine–node element mesh.

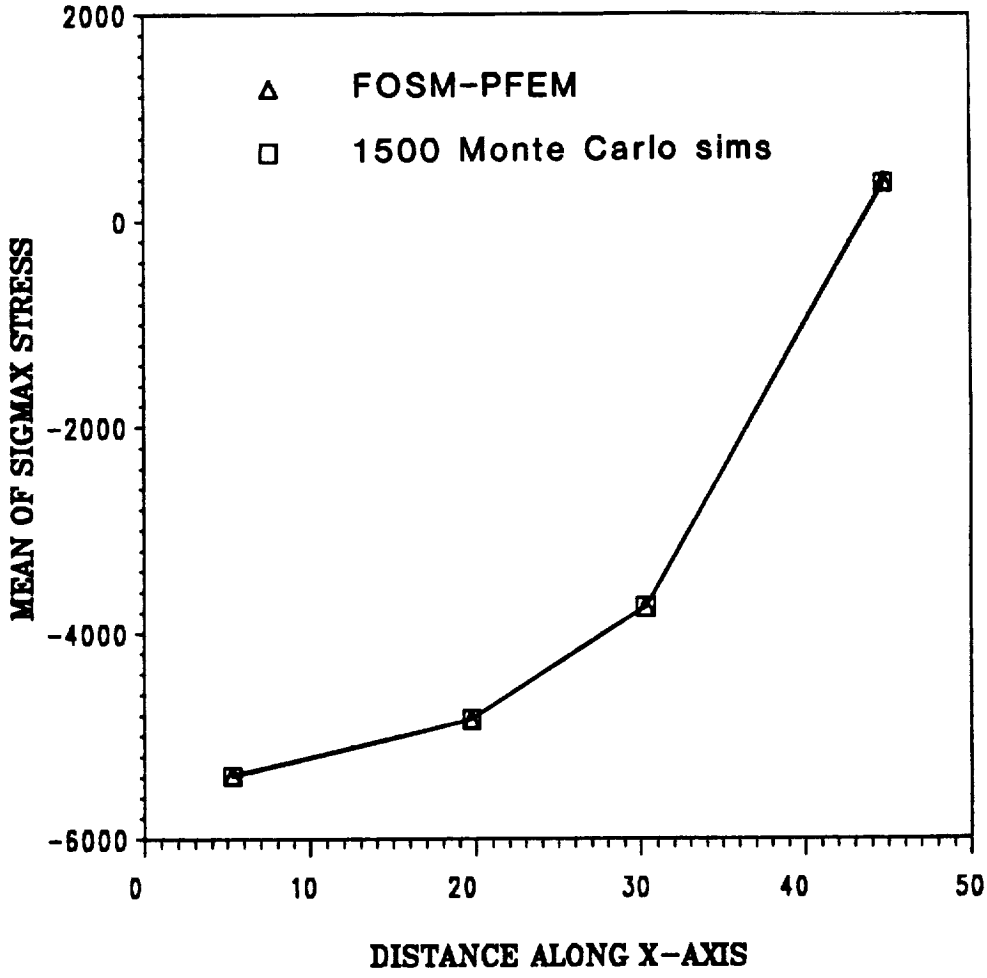

Figure 7.4 Mean σ_{xx} stress along x–axis of spherical shell using all ply–level random variables and a 2x2 nine–node element mesh.

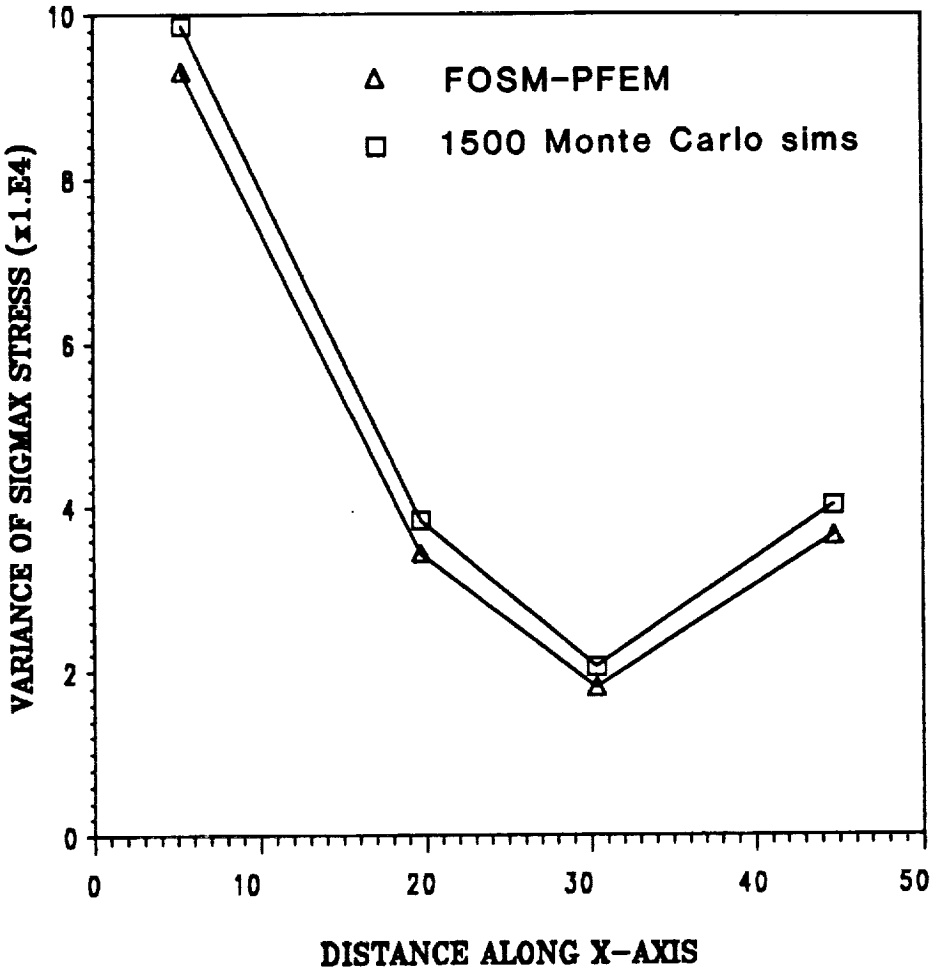

Figure 7.5 Variance of σ_{xx} stress along x–axis of spherical shell using all ply–level random variables and a 2x2 nine–node element mesh.

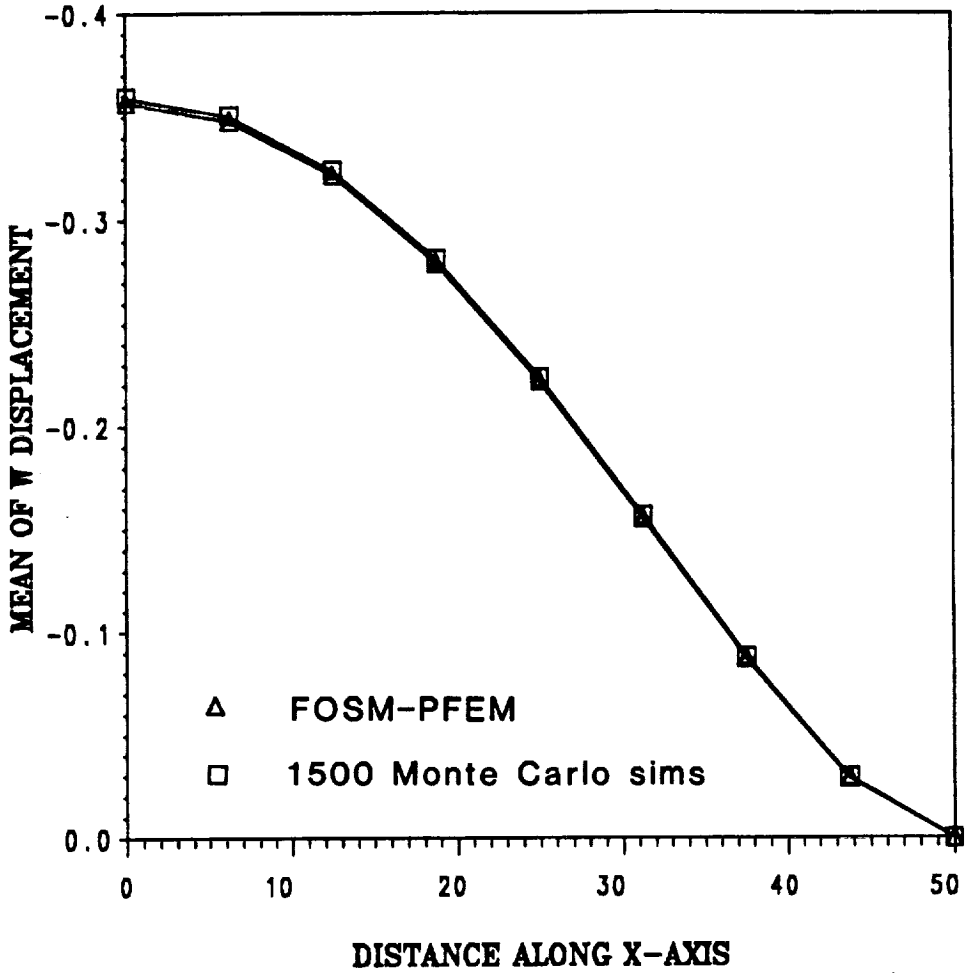

Figure 7.6 Mean center displacement w along x–axis of spherical shell using all ply–level random variables and a 4x4 nine–node element mesh.

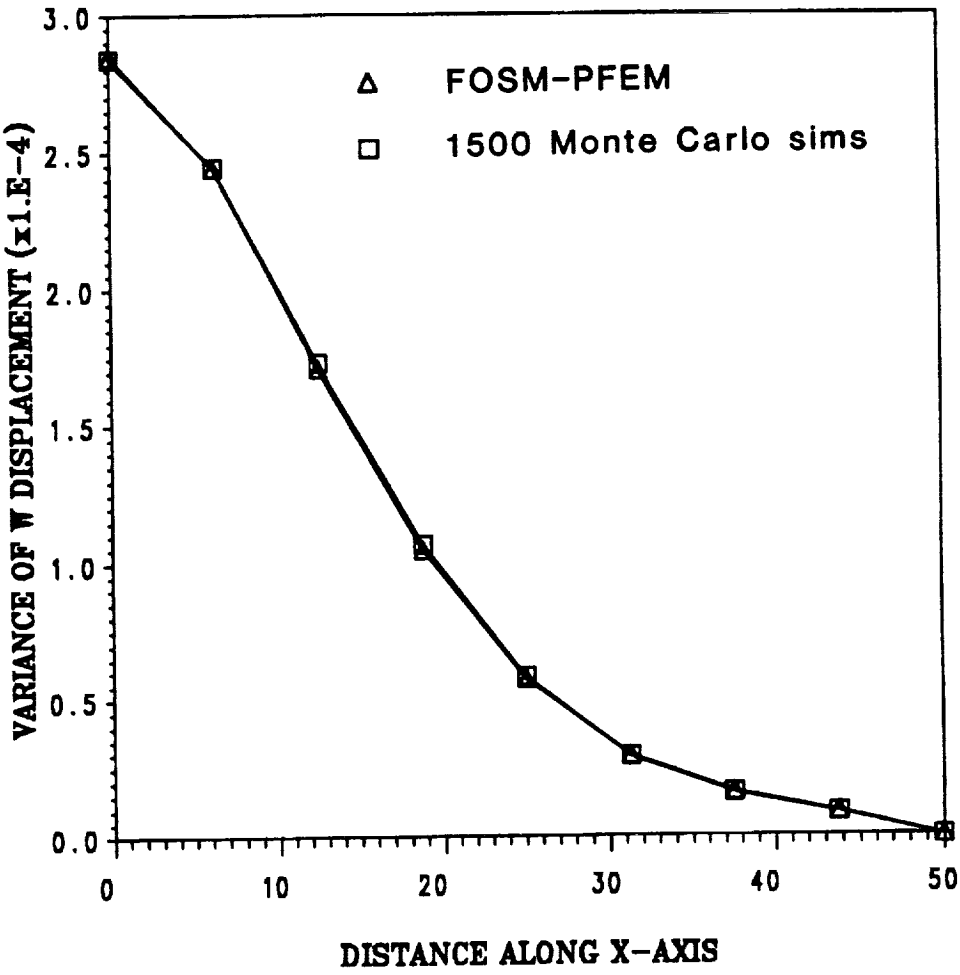

Figure 7.7 Variance of center displacement w along x–axis of spherical shell using all ply–level random variables and a 4x4 nine–node element mesh.

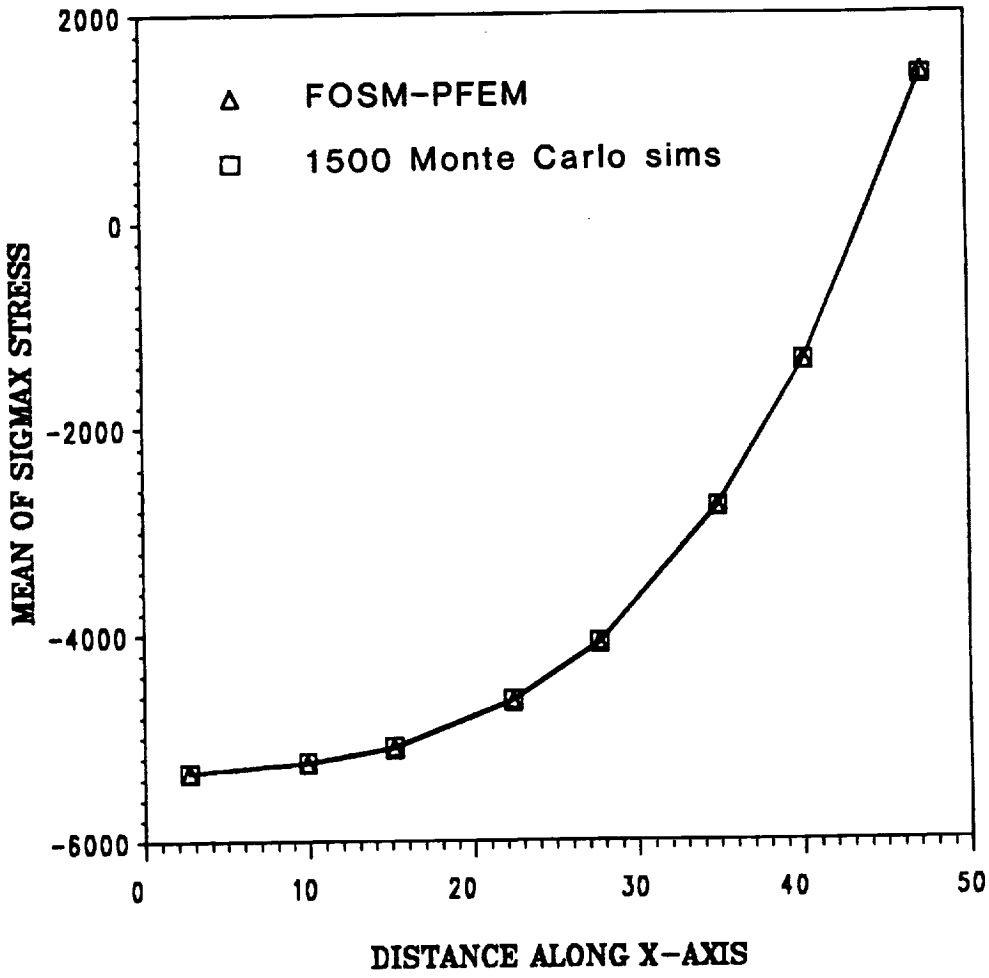

Figure 7.8 Mean σ_{xx} stress along x–axis of spherical shell using all ply–level random variables and a 4x4 nine–node element mesh.

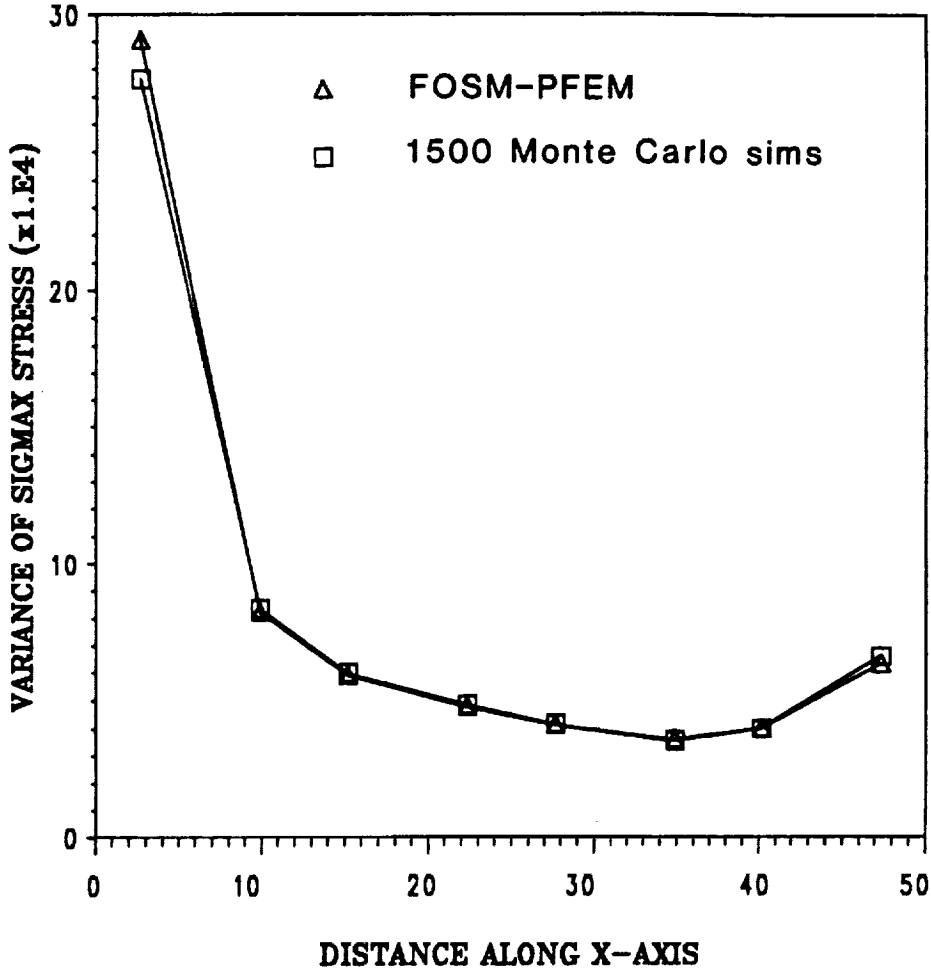

Figure 7.9 Variance of σ_{xx} stress along x–axis of spherical shell using all ply–level random variables and a 4x4 nine–node element mesh.

sensitive to both of these requirements when deciding whether a mesh is sufficiently refined. Generally, as the correlation lengths are increased, the effect on mesh requirements is that a coarser mesh can be used. For the rest of the spherical shell examples, this 4x4 nine–node mesh was selected.

In Chapter 6 it was indicated that as the correlation lengths become larger, eventually the random field becomes fully correlated and equivalent to assuming a single random variable for that layer. This was called the "uniform variance" assumption, and the solution technique that results from this assumption involves considerably less computational expense. It is desirable to know when this method can be used versus the random field approach. Figures 7.10 and 7.11 contain plots of displacement and stress variance versus the $\lambda_{\xi'}$ correlation length normalized by the x–direction dimension of the shell. The $\lambda_{\eta'}$ correlation length was selected to be five times the y–dimension of the shell and was held constant. The horizontal line in each figure is the uniform variance solution. From these results it is apparent that once both correlation lengths $\lambda_{\xi'}$ and $\lambda_{\eta'}$ are greater than four times their respective domain dimensions, the uniform variance solution can be used with equivalent results and considerably less expense.

In all examples presented so far, a COV of .05 was used. A legitimate question remains as to how large the input variance (COV) can become before this first–order probabilistic method becomes inaccurate. Figures 7.12 and 7.13 contain plots of the percentage difference of the first–order second–moment and Monte Carlo solutions versus the standard deviation for the ply angle and ply modulus E_{11} random variables, respectively. From these results it can be concluded that for this problem if the ply angle standard deviation is less than 5

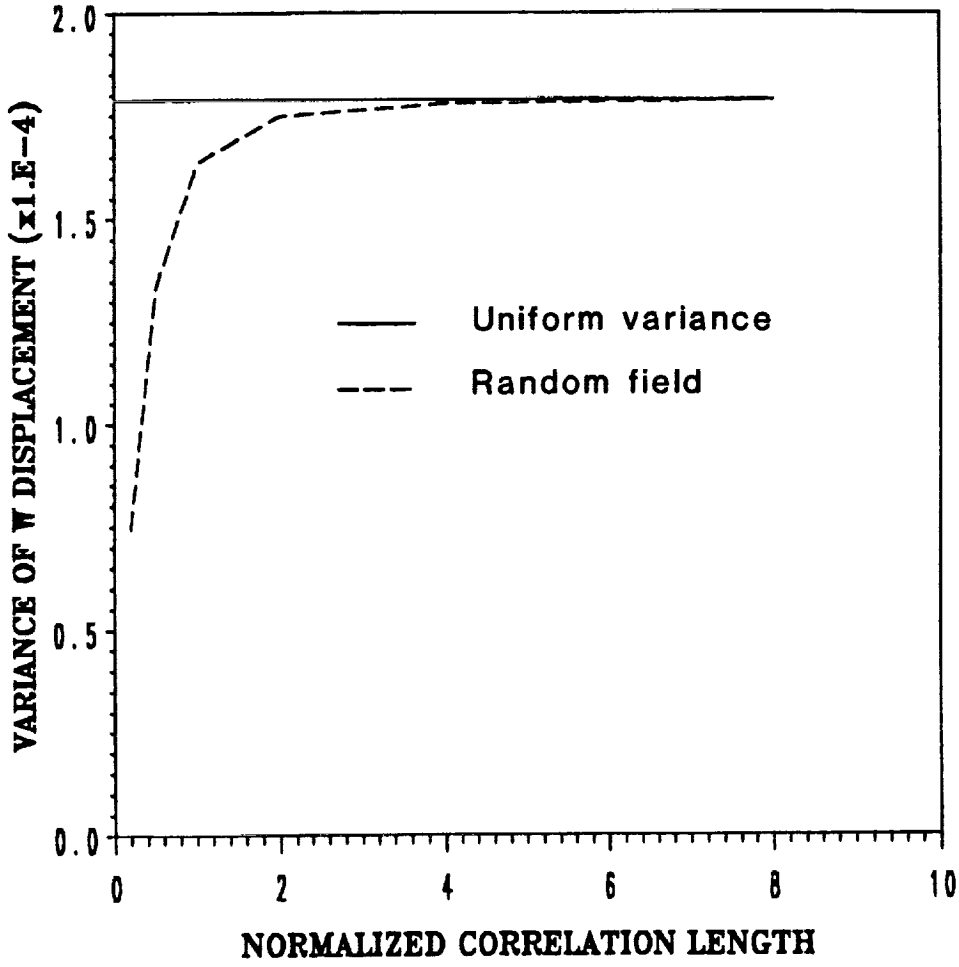

Figure 7.10 Variance of center displacement w versus correlation length for spherical shell problem; comparison of uniform variance and random field results.

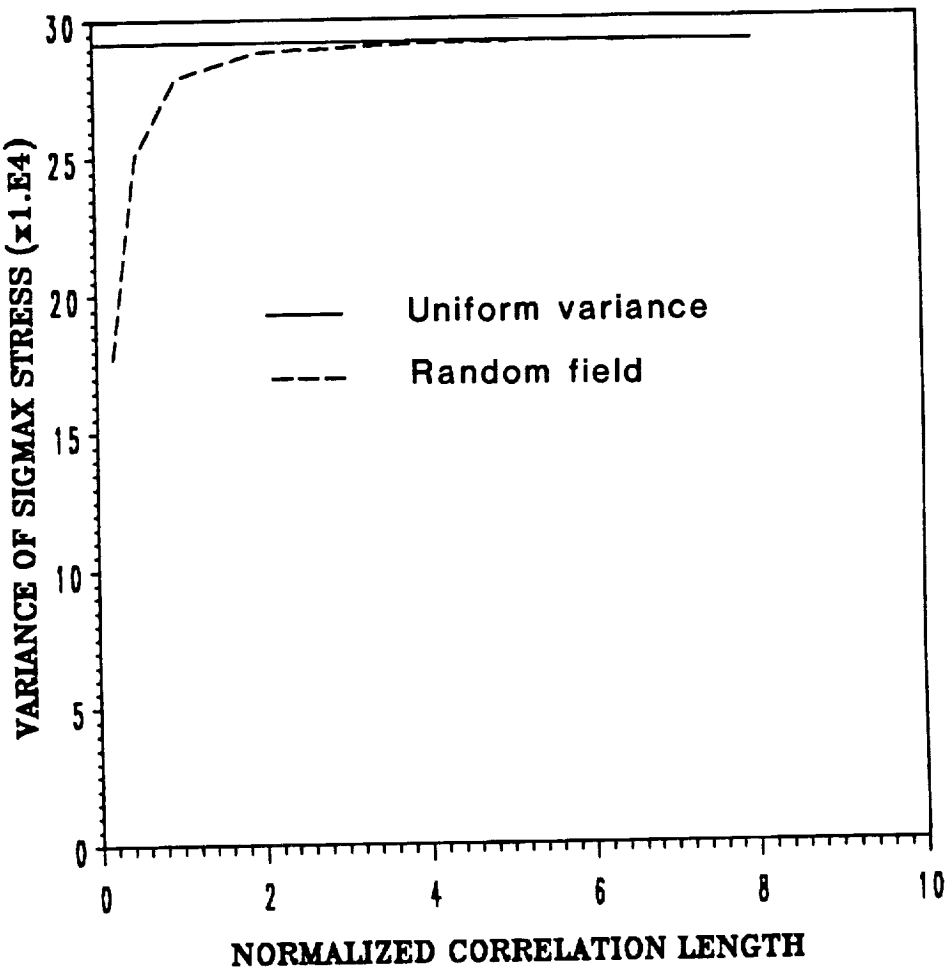

Figure 7.11 Variance of σ_{xx} stress versus correlation length for spherical shell problem; comparison of uniform variance and random field results.

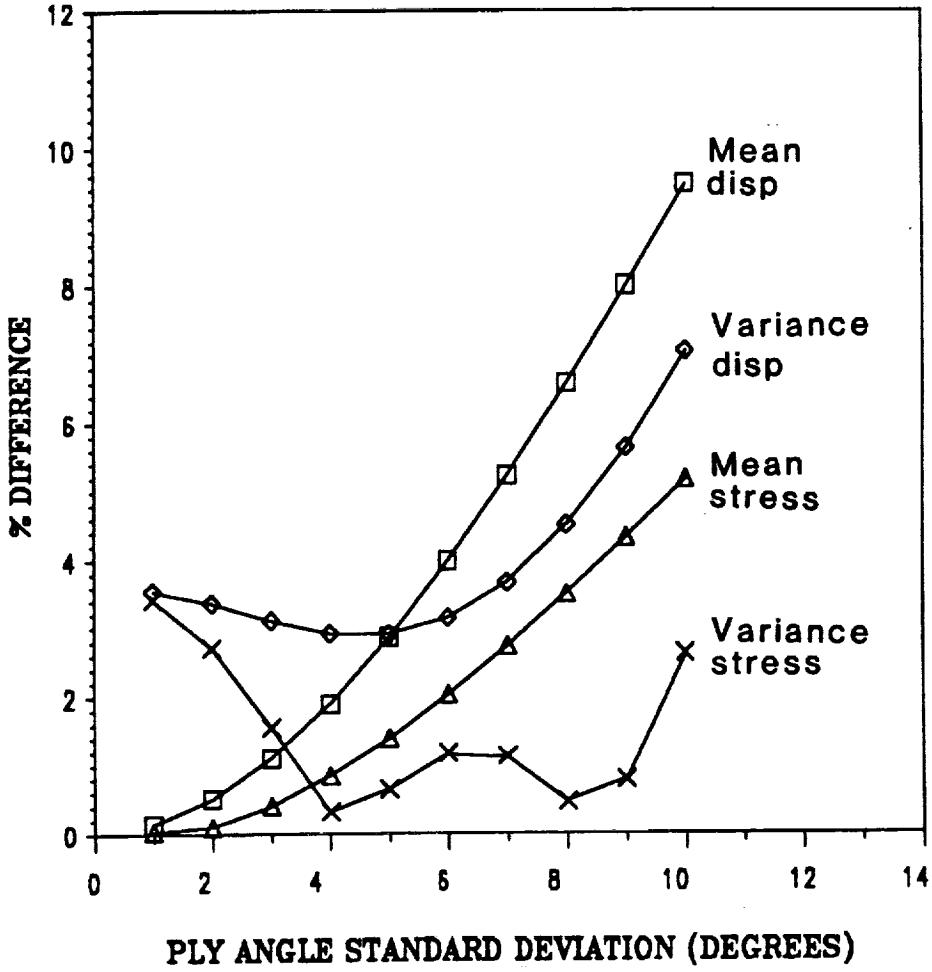

Figure 7.12 Percent difference between first–order second–moment method and Monte Carlo method for various standard deviations of the fiber orientation angle random variable.

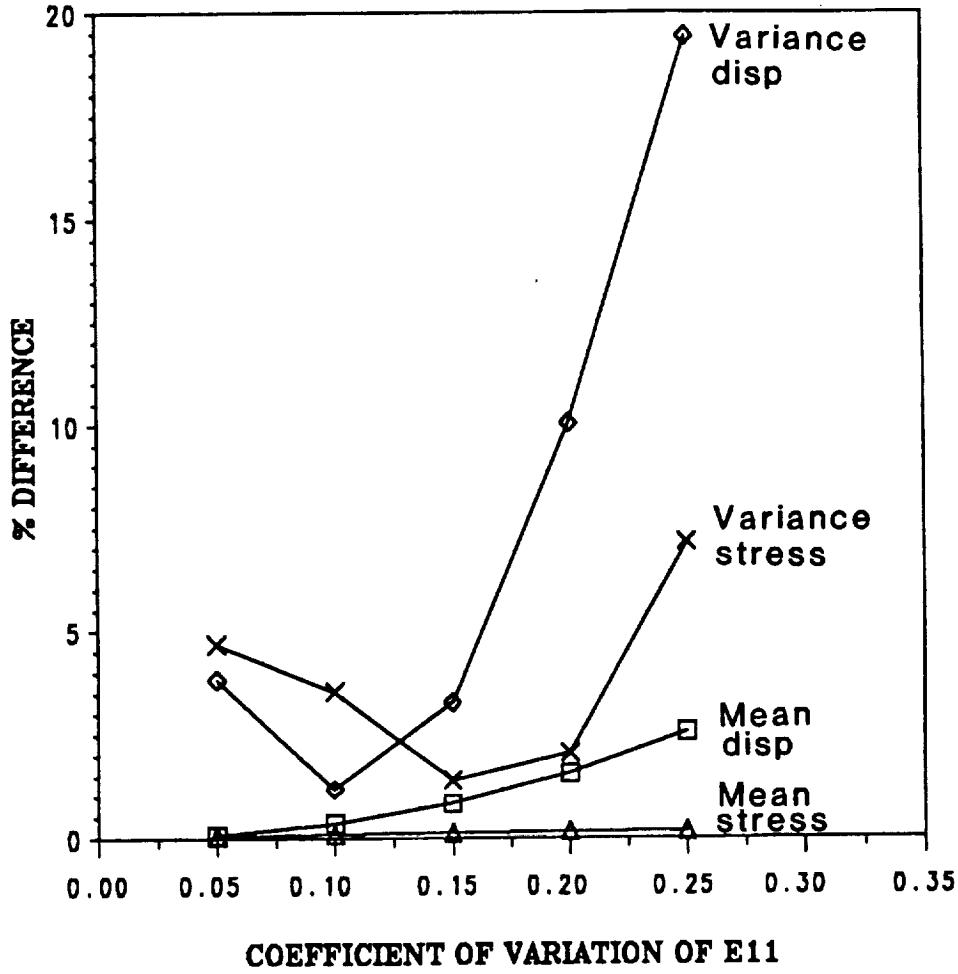

Figure 7.13 Percent difference between first–order second–moment method and Monte Carlo method for various COV levels of E_{11} random variable.

degrees, and the E_{11} COV is less than .15, the percentage difference in the first–order second–moment and Monte Carlo solutions is less than 5%. This is reasonable, considering the fact that a 5 degree standard deviation for ply angle or a COV of .15 for E_{11} is quite large for most composite (or isotropic for that matter) material variations. This is in agreement with Ang [23] and Liu et al. [33–40], who stated that accuracy is maintained for a COV of .10 or less. Note that the first–order mean values here are nothing but the deterministic values, and that the agreement here is good without including the second–order perturbation effect.

One very important benefit of the probabilistic finite element method is the ability to quantify the variations in the structural response caused by individual random variables. In the present study these random variables can include ply–level material stiffnesses or micro–level material stiffnesses, the latter evaluated with the aid of the Aboudi micromechanics model [64]. Figures 7.14 and 7.15 illustrate both the combined and individual variances for displacement and stress response. It is interesting to note that for this particular shell problem, the w–displacement response is most affected by the ply thickness, ply angle, and E_{11} variables, while the stress (σ_{xx} in the 0 degree layer) is primarily influenced by the ply angle, with E_{11} and ply thickness variables much less significant. In Figures 7.16 and 7.17, micromechanics–level random variables were chosen. For the w–displacement variance, once again ply thickness and ply angle were important, along with FVR and E_{f11} micro–variables. As for the stress, ply angle is still very dominant with E_{f11}, FVR, and ply thickness secondary. It has been found that for these shell problems with graphite–epoxy materials, generally the dominant random

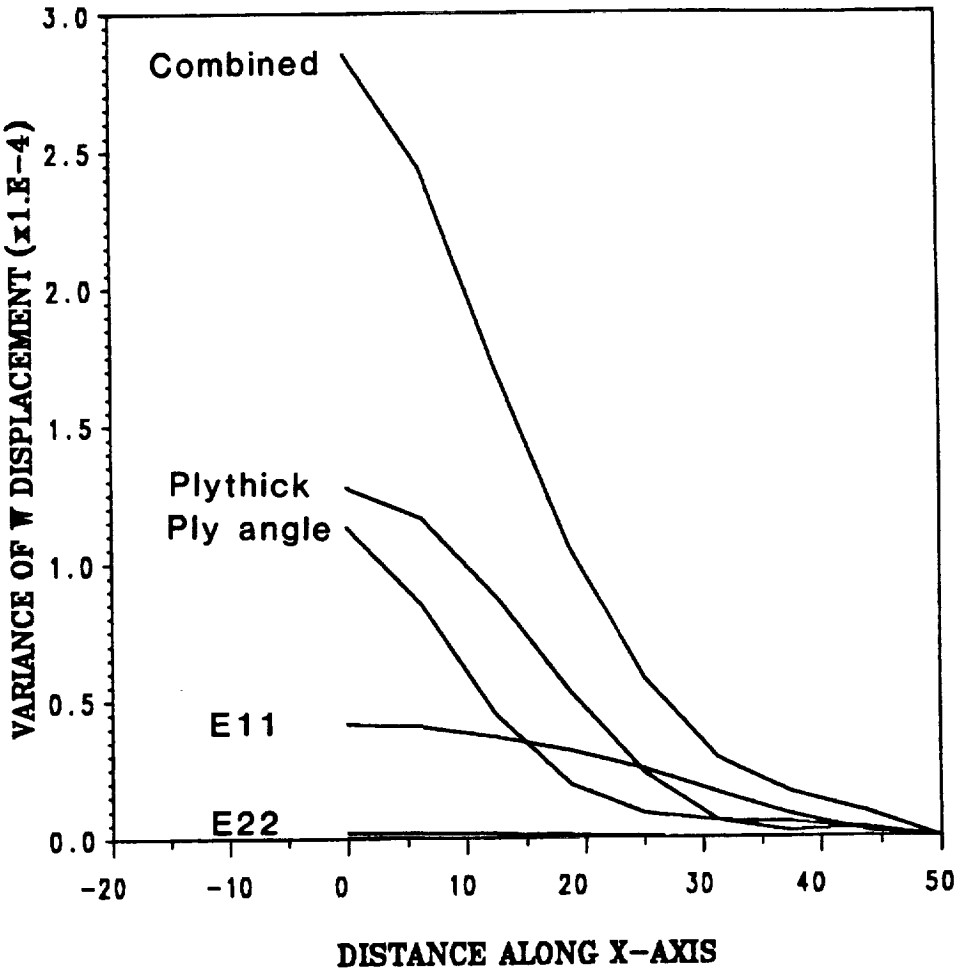

Figure 7.14 Variance of center displacement w along x–axis of spherical shell showing the combined and individual effects of the ply–level graphite–epoxy random variables.

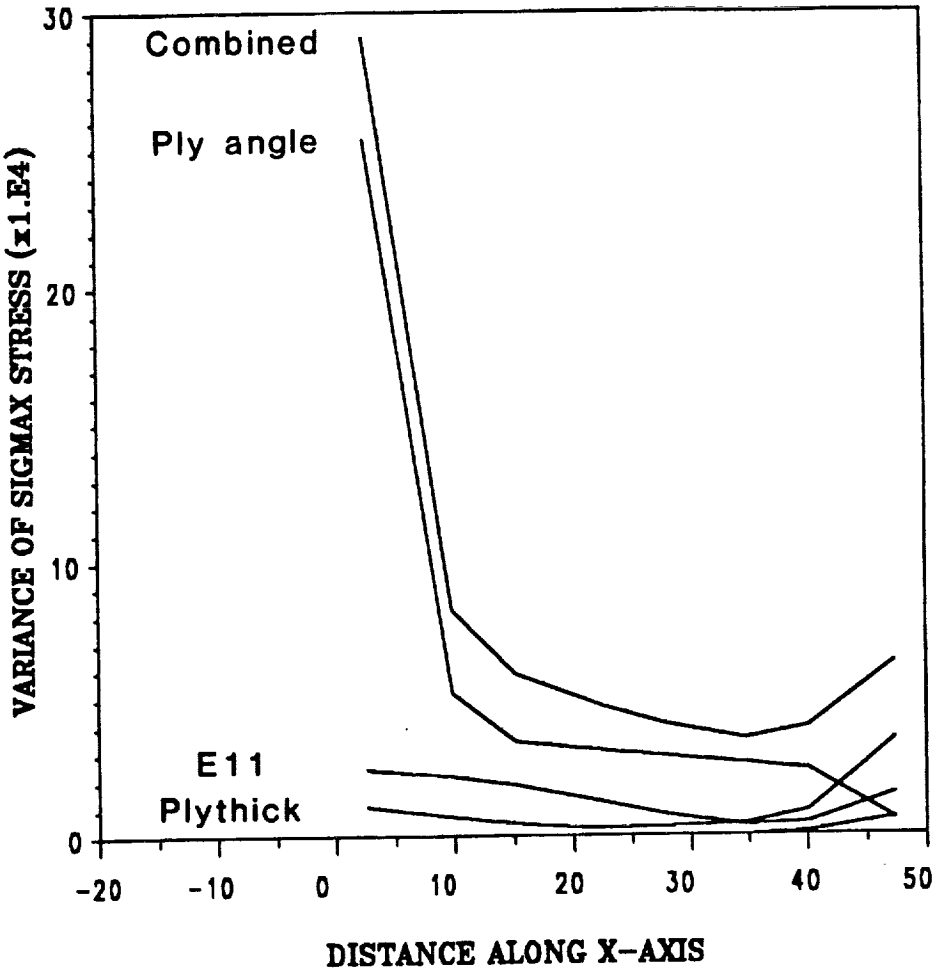

Figure 7.15 Variance of σ_{xx} stress along x–axis of spherical shell showing the combined and individual effects of the ply–level graphite–epoxy random variables.

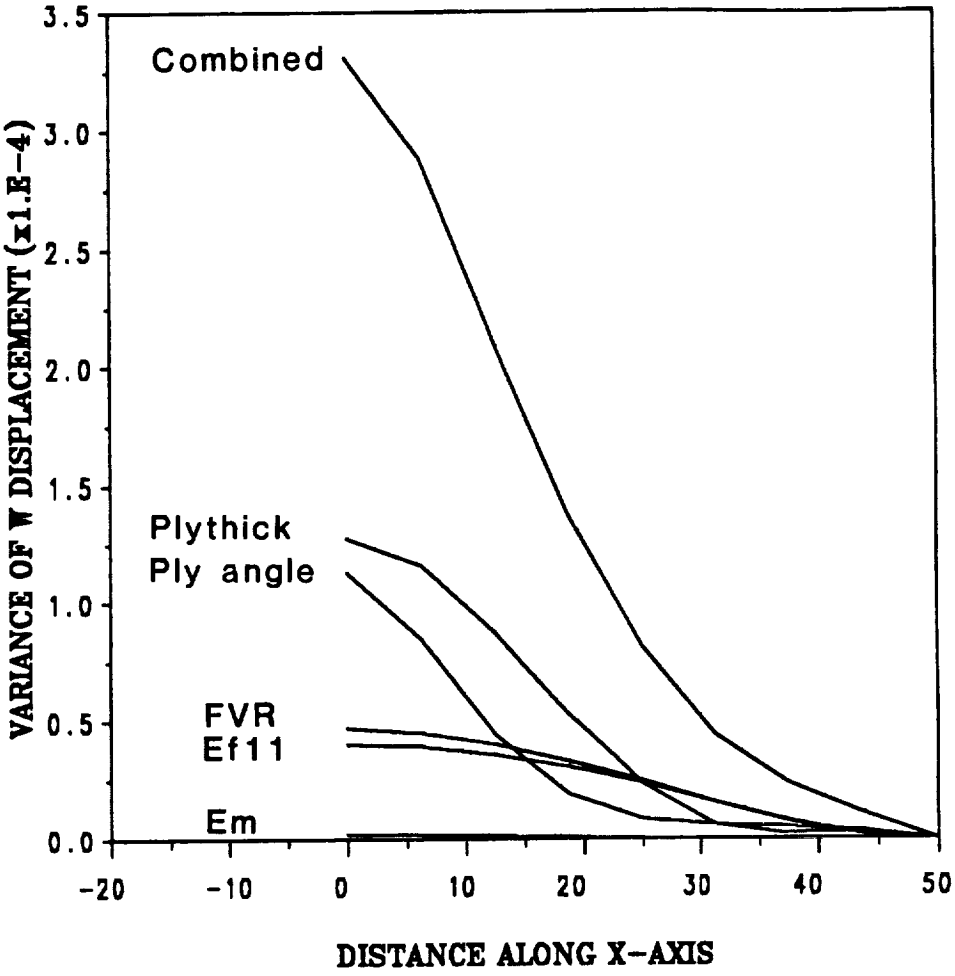

Figure 7.16 Variance of center displacement w along x–axis of spherical shell showing the combined and individual effects of the micro–level graphite–epoxy random variables.

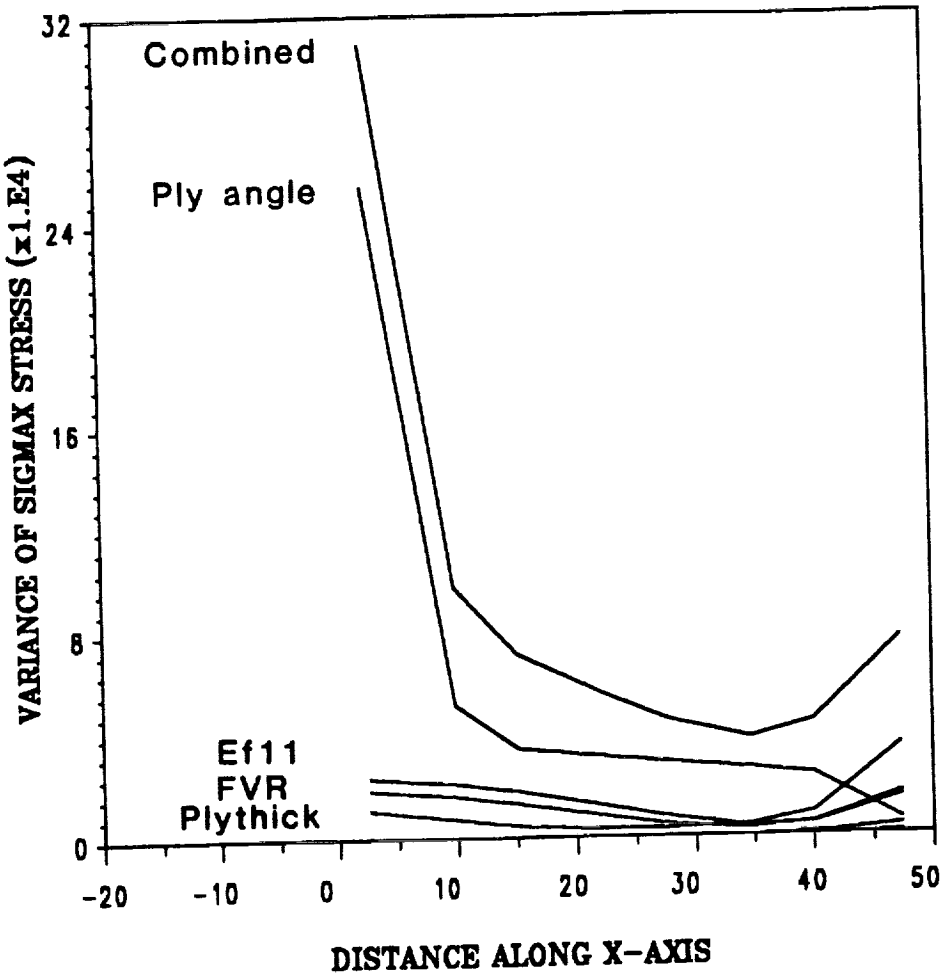

Figure 7.17 Variance of σ_{xx} stress along x–axis of spherical shell showing the combined and individual effects of the micro–level graphite–epoxy random variables.

variable is the ply angle, as would be expected due to the low stiffness of the matrix in comparison with the fibers.

7.2.2 Metal Matrix Composite Shell

To illustrate the differences in response when using metal matrix composite properties, the same shell was modeled using Silicon Carbide fibers in a Titanium Aluminide matrix. The input properties and statistical parameters used are listed in Table 7.2. Figures 7.18 and 7.19 illustrate the combined and individual variances for displacement and stress response with micro–level random variables. Now with the metal matrix properties, the w–displacement response is most affected by the matrix modulus E_m and fiber volume ratio (FVR). This may be due to the fact that the mean FVR was selected to be .35, so if a higher mean FVR is input, fiber properties may dominate. As for the σ_{xx} stress, the longitudinal fiber modulus E_{f11} and FVR were the most important. Figures 7.20 and 7.21 contain the corresponding results but using ply–level random variables. Similar to the previous results, the E_{22} and E_{11} moduli dominate the variance for the w–displacement response, and for the σ_{xx} stress E_{11} is by far the most influential.

7.3 Geometric Nonlinear Analyses

Two problem types are discussed in this section. First, the graphite–epoxy spherical shell used in the previous section is analyzed deep into the postbuckling range, and second, the postbuckling of a flat non–stiffened graphite–epoxy panel with uniaxial compression is investigated. Experimental comparisons are made for the second example.

Table 7.2

Material Properties and Statistics for Silicon Carbide Titanium Aluminide Spherical Shell Problem

Random Variable	Mean	Standard Deviation	Coefficient of Variation	$\lambda_{\xi'}$	$\lambda_{\eta'}$
E_{11}	25.783×10^{6}	1.2892×10^{6}	0.05	25	15
E_{22}	18.683×10^{6}	9.3415×10^{5}	0.05	15	25
G_{12}	7.028×10^{6}	3.5140×10^{5}	0.05	25	25
ν_{12}	0.2706	1.3528×10^{-2}	0.05	25	25
G_{13}	7.028×10^{6}	3.5140×10^{5}	0.05	25	25
G_{23}	6.955×10^{6}	3.4774×10^{5}	0.05	25	25
E_{f11}	50.7×10^{6}	2.535×10^{6}	0.05	25	15
E_{f22}	50.7×10^{6}	2.535×10^{6}	0.05	15	25
G_{f12}	21.3×10^{6}	1.065×10^{6}	0.05	25	25
ν_{f12}	0.19	9.5×10^{-3}	0.05	25	25
ν_{f23}	0.19	9.5×10^{-3}	0.05	25	25
E_{m}	12.3×10^{6}	6.15×10^{5}	0.05	25	25
ν_{m}	0.32	1.6×10^{-2}	0.05	25	25
FVR	0.35	1.75×10^{-2}	0.05	25	25
θ^{*}	0°,90°	2°	–	25	25
δ^{*}	0.5	2.5×10^{-2}	0.05	25	25

* θ indicates fiber orientation angle and δ indicates ply thickness.

The subscripts f and m stand for fiber and matrix; absence of a letter subscript indicates a ply–level property. The units are psi and inches where appropriate.

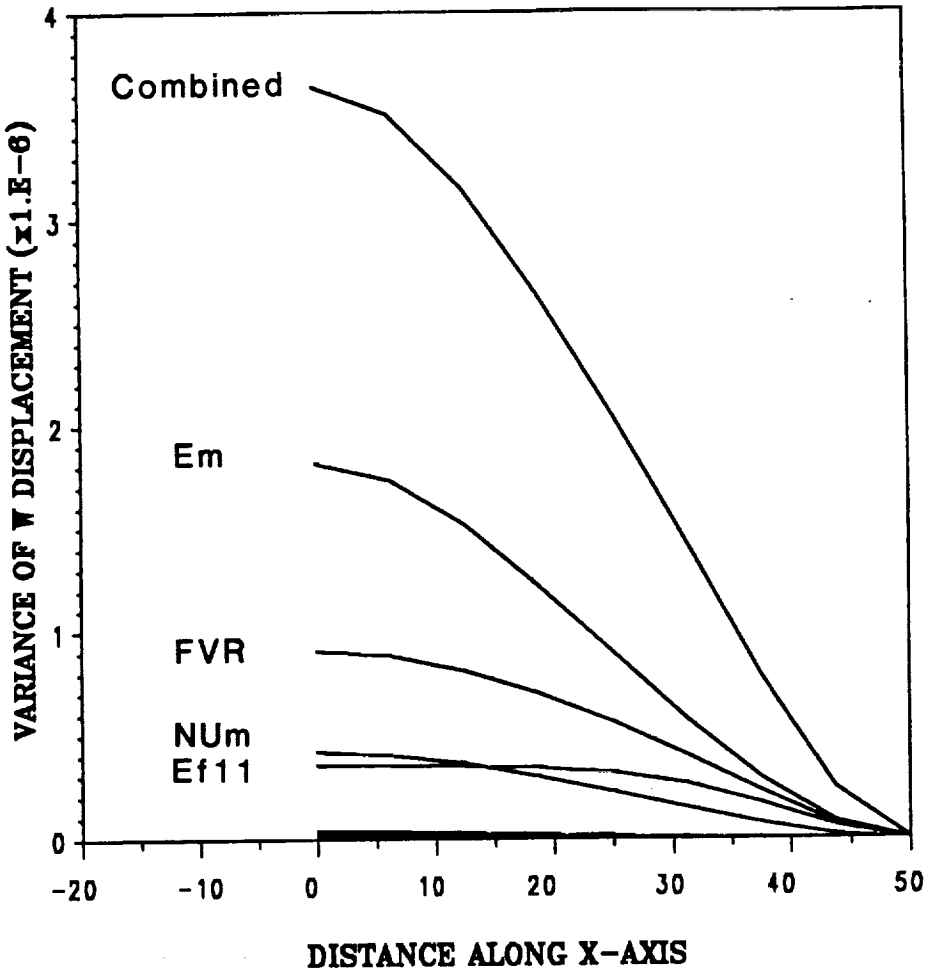

Figure 7.18 Variance of center displacement w along x–axis of spherical shell showing the combined and individual effects of the micro–level Silicon Carbide Titanium Aluminide random variables.

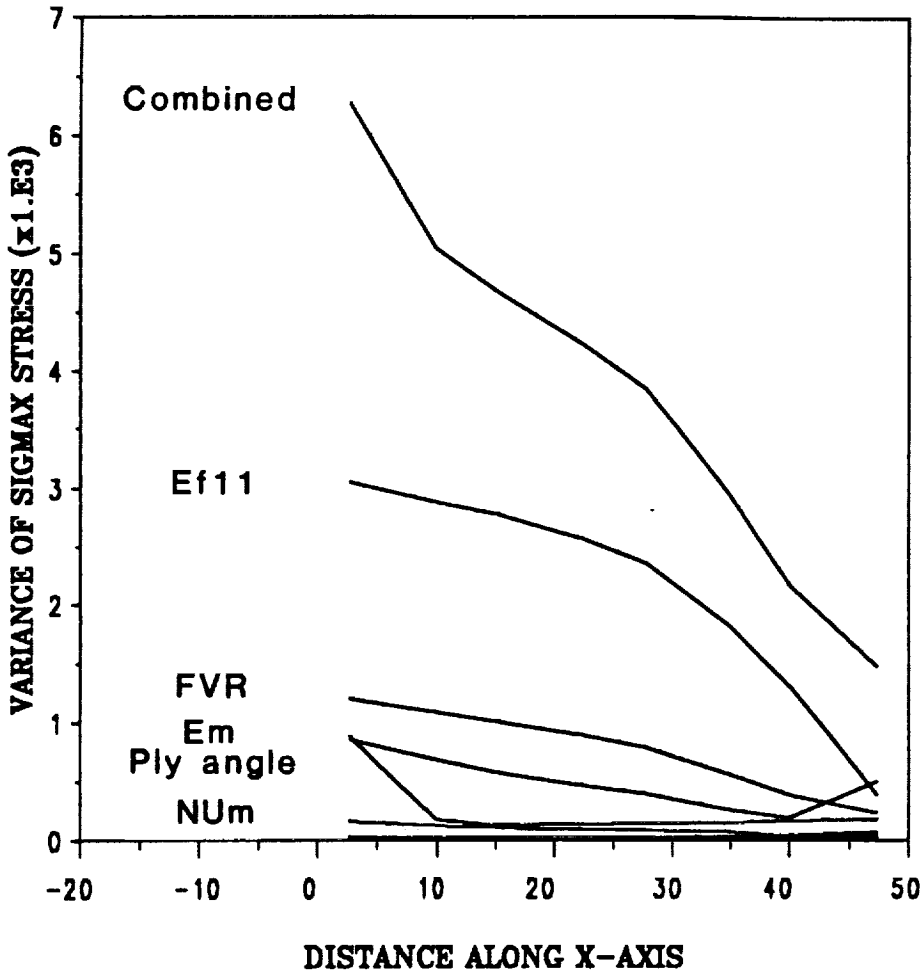

Figure 7.19 Variance of σ_{xx} stress along x–axis of spherical shell showing the combined and individual effects of the micro–level Silicon Carbide Titanium Aluminide random variables.

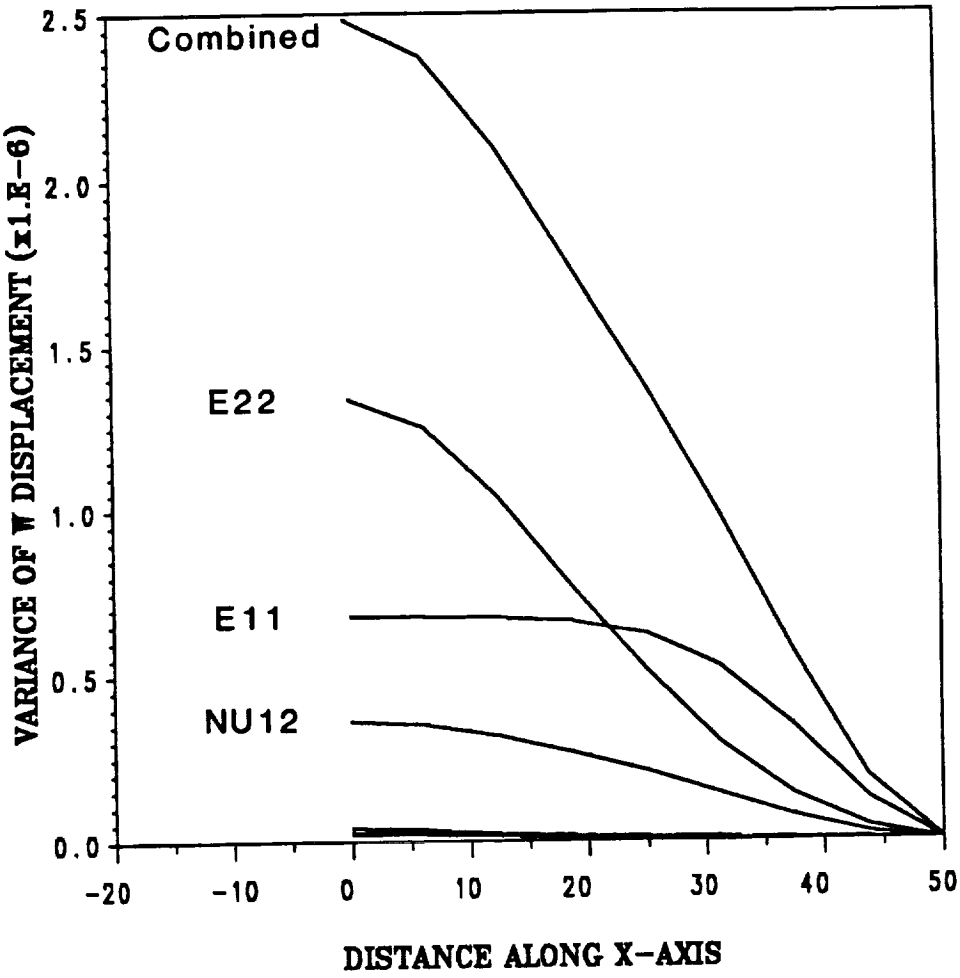

Figure 7.20 Variance of center displacement w along x–axis of spherical shell showing the combined and individual effects of the ply–level Silicon Carbide Titanium Aluminide random variables.

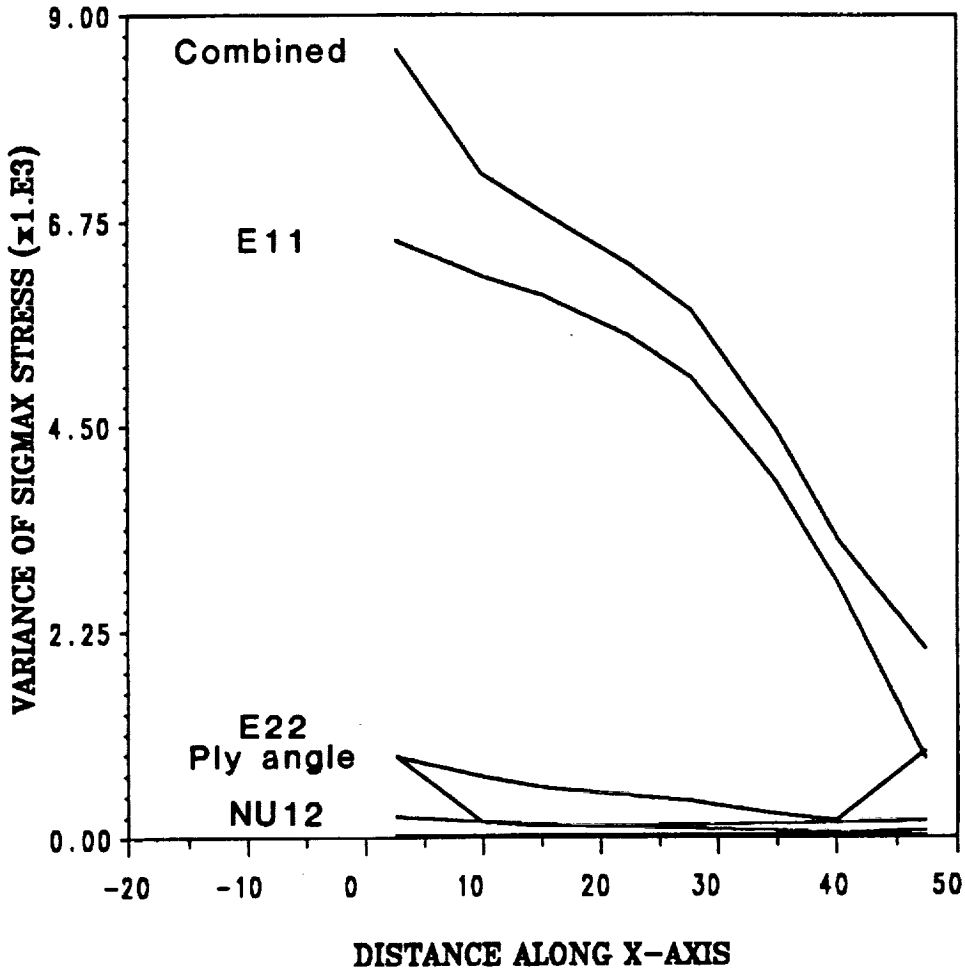

Figure 7.21 Variance of σ_{xx} stress along x–axis of spherical shell showing the combined and individual effects of the ply–level Silicon Carbide Titanium Aluminide random variables.

7.3.1 Postbuckling of Spherical Shell

All input properties and statistical parameters are the same as in section 7.2.1 for the graphite–epoxy spherical shell. The difference here is that a geometric nonlinear solution is included, one that follows the nonlinear path past the snap through point (or limit point) and into the postbuckling range. The modified–Riks method [86,91] is used, as the regular Newton–Raphson method with load step control cannot trace this type of postbuckling curve.

Once again, the Monte Carlo method is utilized to verify the first–order second–moment probabilistic results. Since the Monte Carlo method solves the nonlinear problem completely for each sample (or simulation) of the random variables, if the modified–Riks method is used in conjunction with the Monte Carlo method, each sample would result in a different set of load step sizes due to the self adjusting mechanism of the Riks method. The statistics used to estimate the mean and variance from the simulation results at each load step rely on all the variable responses residing at the same load value. For this reason the modified–Riks method was not used with Monte Carlo to verify the geometric nonlinear results. Instead, the Newton–Raphson method with constant load step size was used during this verification stage. Since the Newton–Raphson method could not pass the first limit point (zero–slope), then the solution was stopped there. Figures 7.22 through 7.25 contain the comparisons of the Monte Carlo and first–order second–moment solutions for mean and variance displacement and stress responses, and the agreement is very good.

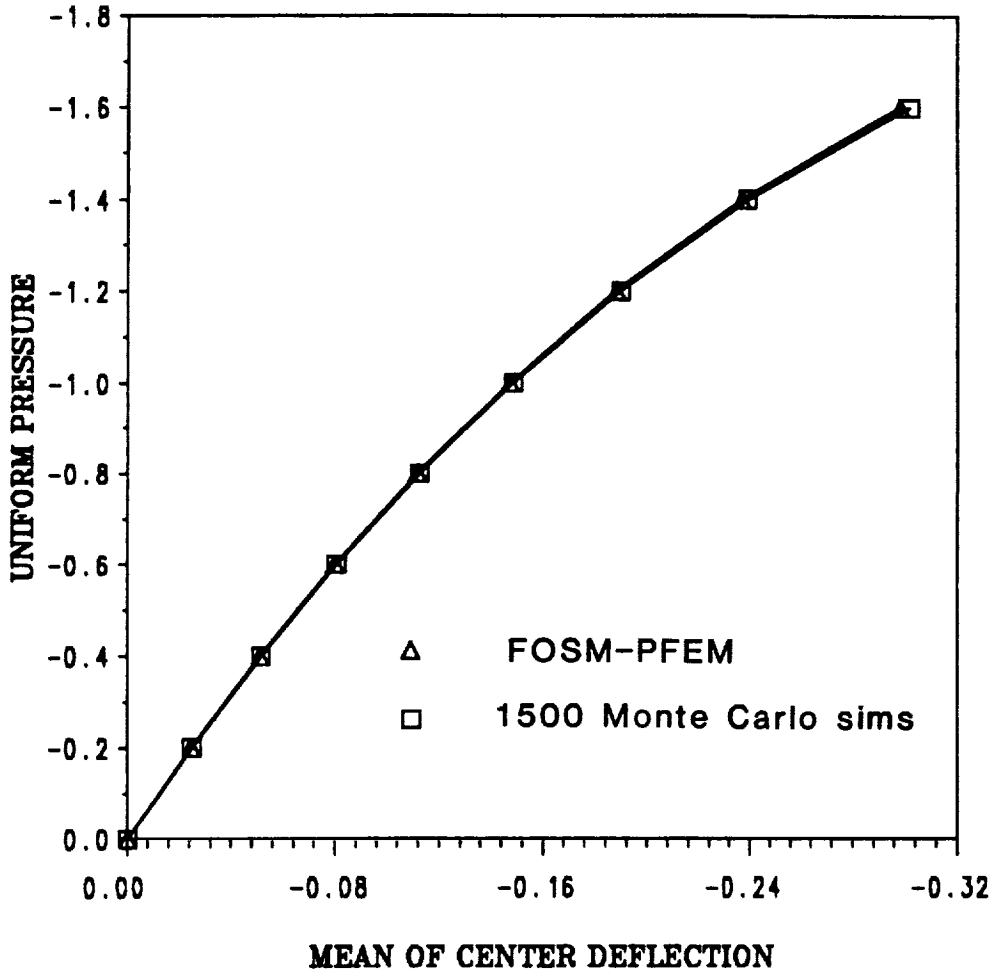

Figure 7.22 Mean center displacement w versus load for spherical shell using all ply–level graphite–epoxy random variables.

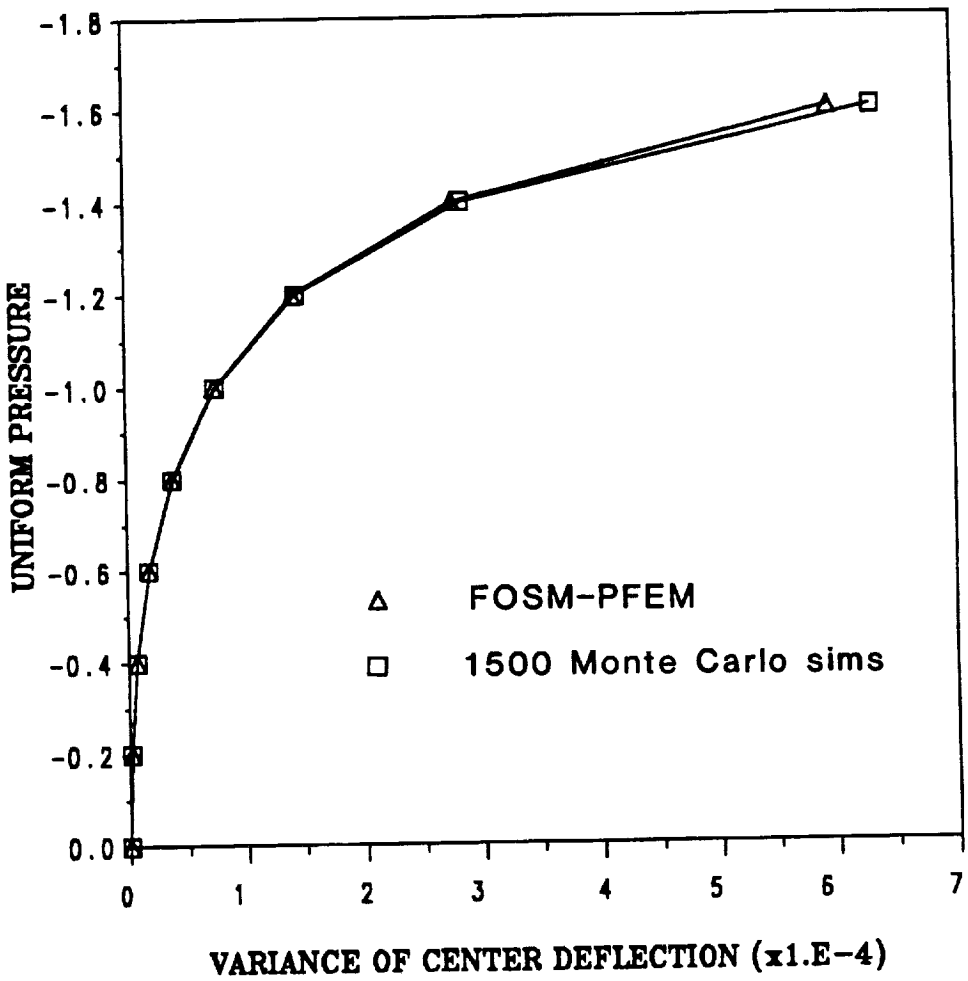

Figure 7.23 Variance of center displacement w versus load for spherical shell using all ply–level graphite–epoxy random variables.

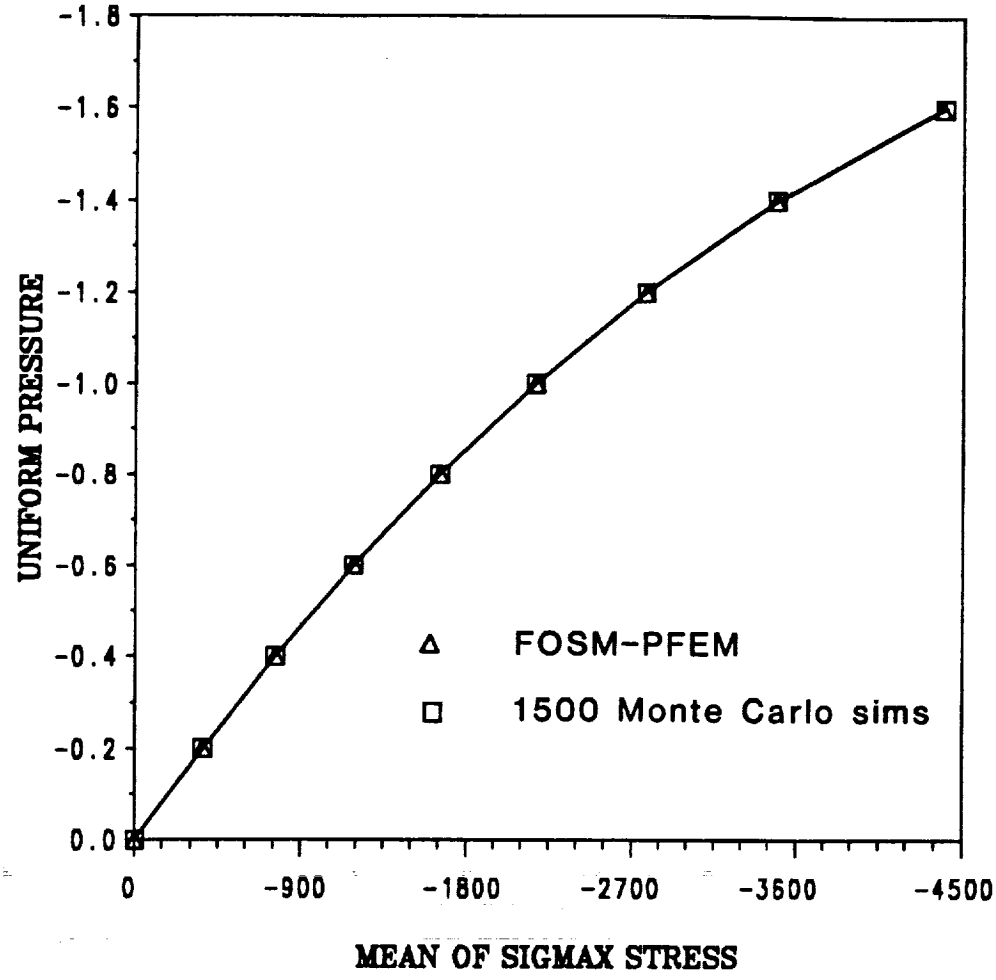

Figure 7.24 Mean of σ_{xx} stress versus load for spherical shell using all ply–level graphite–epoxy random variables.

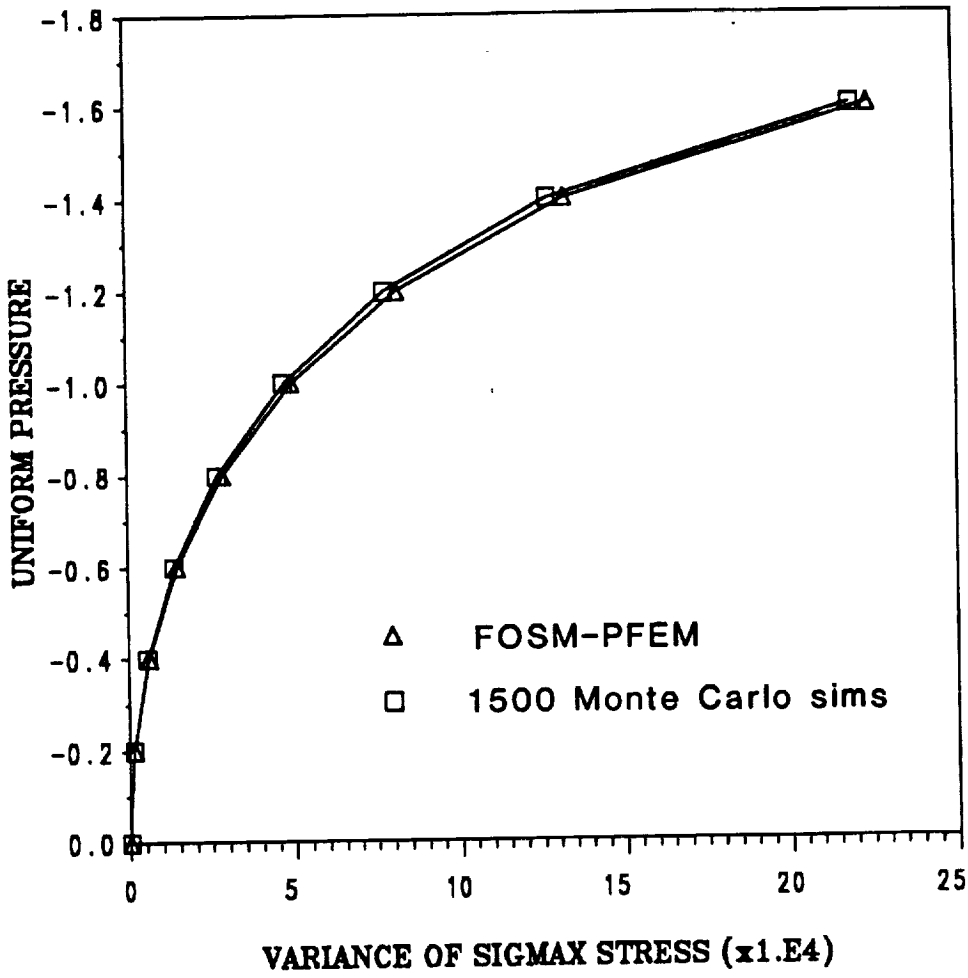

Figure 7.25 Variance of σ_{xx} stress versus load for spherical shell using all ply–level graphite–epoxy random variables.

Next, using the first–order second–moment method combined with the modified–Riks technique, the responses throughout the postbuckling range, including the limit points, are calculated and presented in Figures 7.26 and 7.27. Figures 7.26a and b exhibit the w–displacement mean and COV. It is evident that at the limit points the COV is very large, almost 0.5. Figures 7.27a and b contain the σ_{xx} stress mean and COV. Again near a zero slope point on the stress curve the COV was quite large, almost 0.5. Figures 7.28 and 7.29 illustrate the results in a different format. Here the squares indicate mean response while the stars are the mean plus or minus one standard deviation (one sigma) points. The influence of the limit points is more apparent in this format.

The increase in variance at the limit points occurs since the buckling behavior of the structure is more sensitive to any changes in stiffness or load at these points. It should be noted that while the displacement COV begins at about .05 before the limit points, it becomes quite small after the limit points, settling to a value of about .01. As for the stress, the initial COV is .10, and after the limit points is still quite large, in the range of .07 to 1.6.

7.3.2 Postbuckling of Flat Panel Under Axial Compression

The problem under consideration here is a flat, rectangular graphite–epoxy panel loaded in axial compression. An experimental study was performed on a series of these panels by Starnes and Rouse [92]. Figure 7.30 shows a typical panel with fixture and the resulting failure mode. The loaded ends of the panels were clamped by fixtures and the unloaded edges were simply supported by knife–edge restraints to prevent the panels from buckling as wide

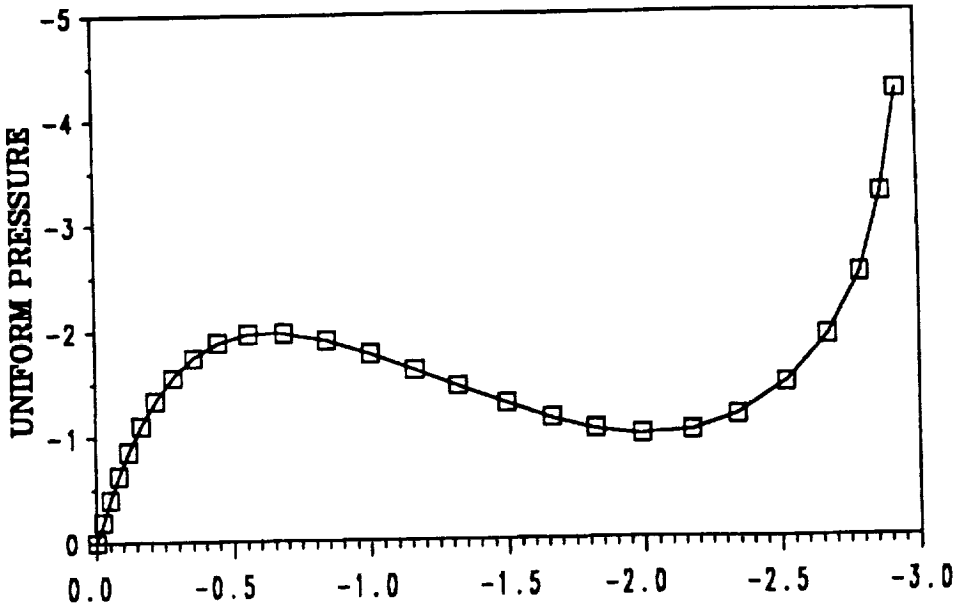

(a) **MEAN OF CENTER DEFLECTION**

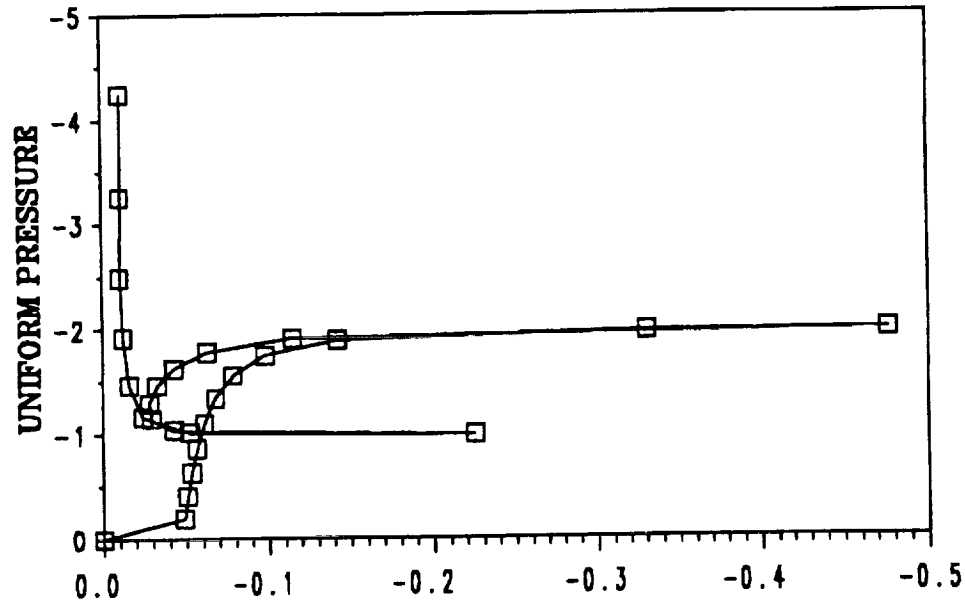

(b) **COV OF CENTER DEFLECTION**

Figure 7.26 Displacement postbuckling response of spherical shell using all ply–level graphite–epoxy random variables.

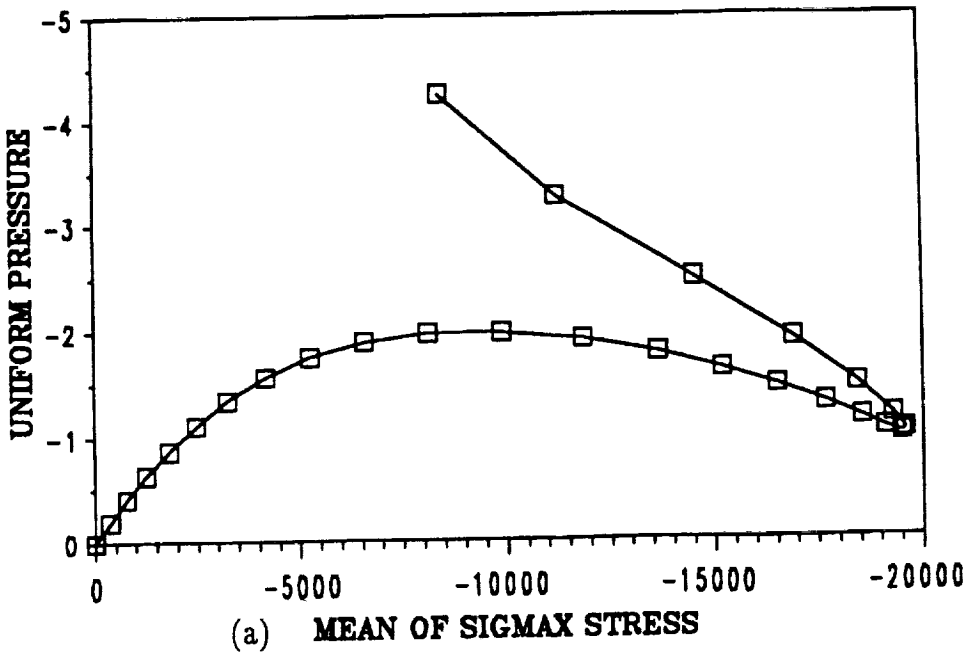

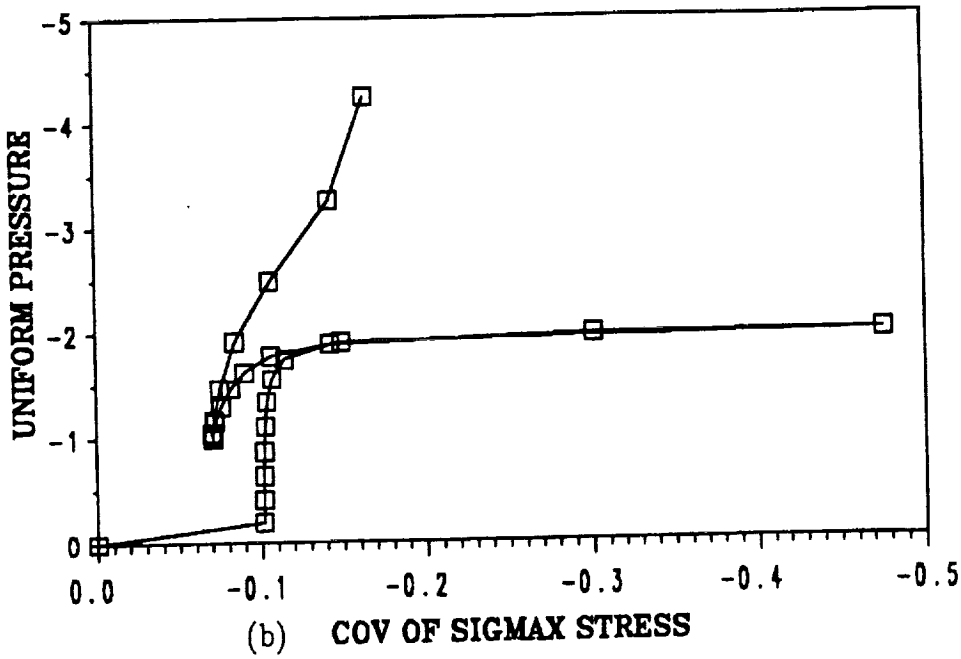

Figure 7.27 Stress postbuckling response of spherical shell using all ply–level graphite–epoxy random variables.

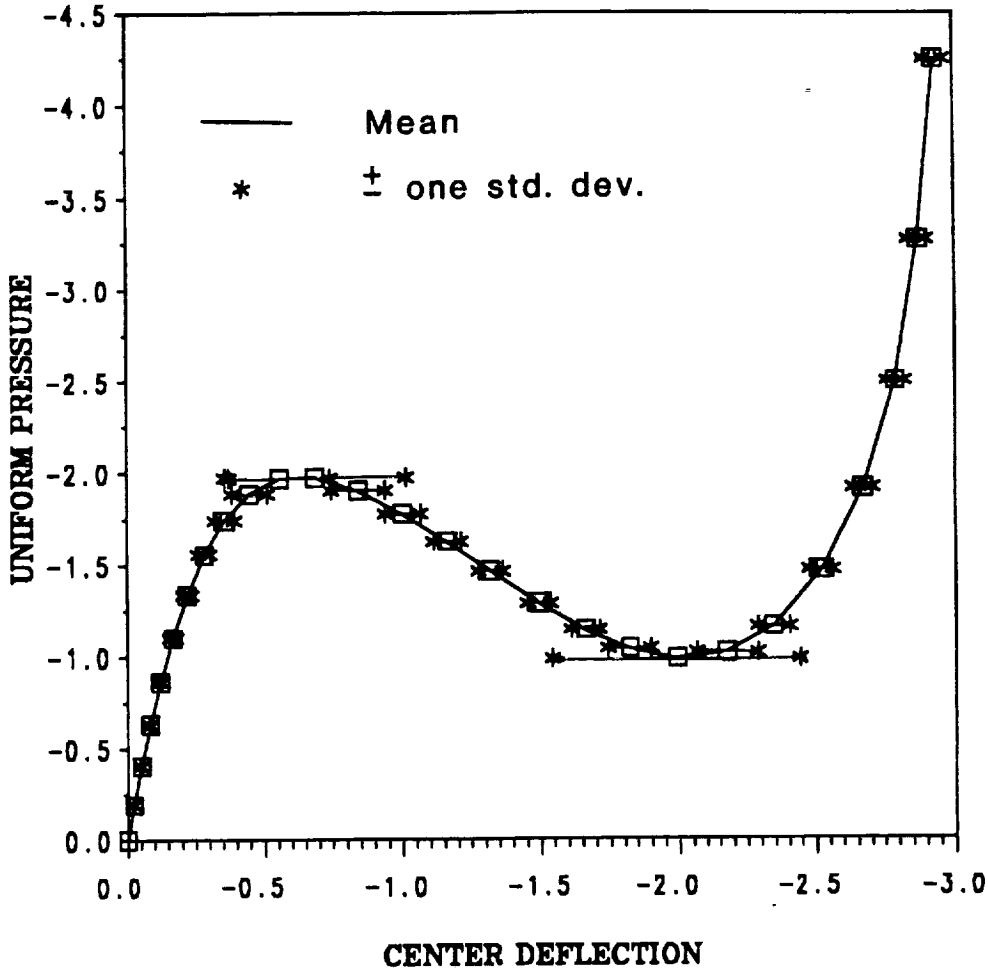

Figure 7.28 Mean center displacement w and plus or minus one standard deviation points versus load throughout postbuckling range of spherical shell.

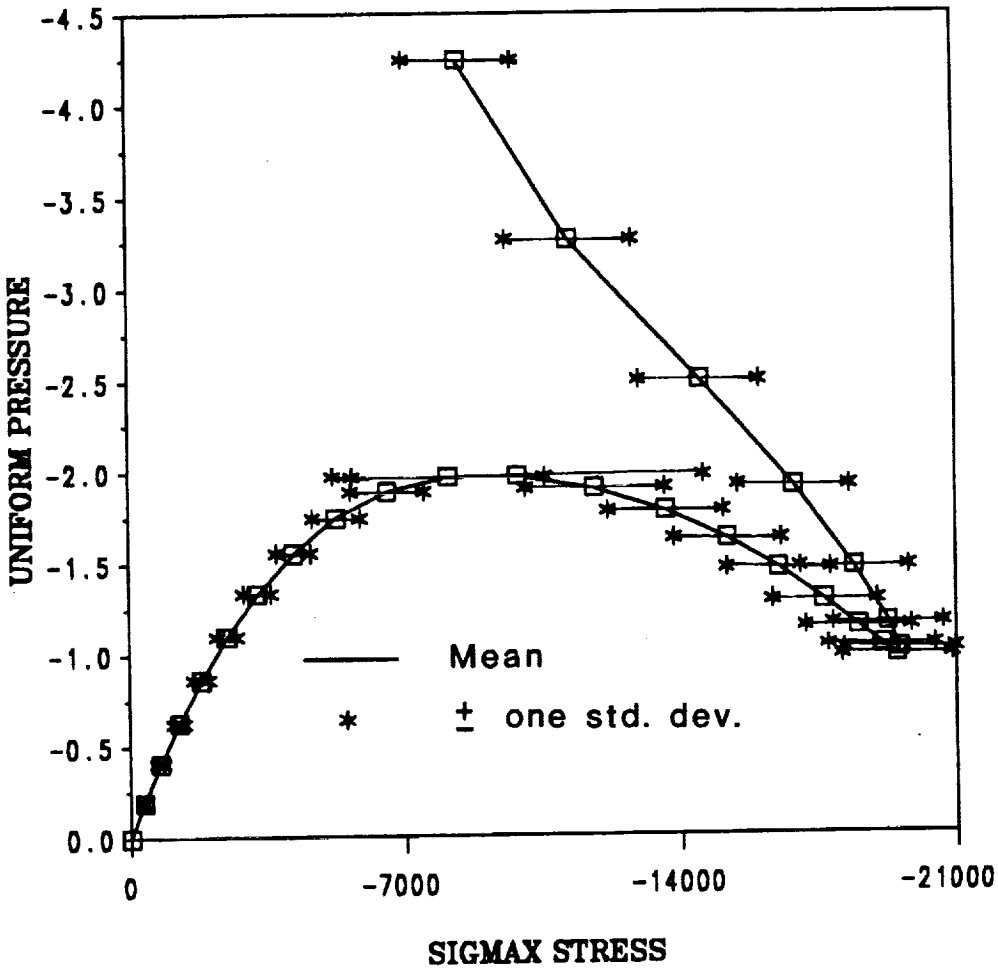

Figure 7.29 Mean σ_{xx} stress and plus or minus one standard deviation points versus load throughout postbuckling range of spherical shell.

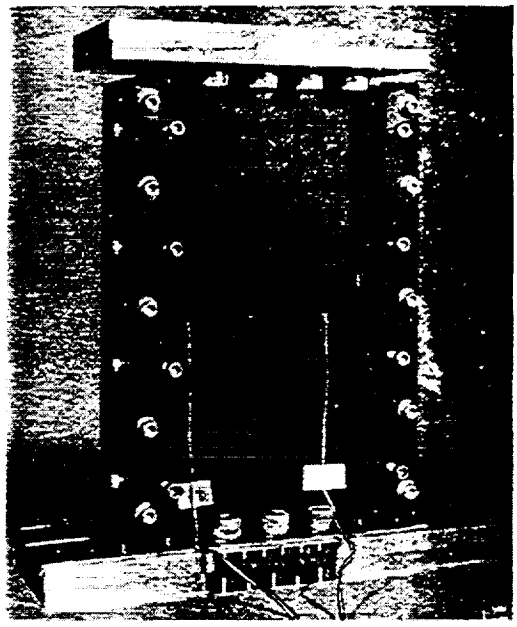

(a) Panel fixture

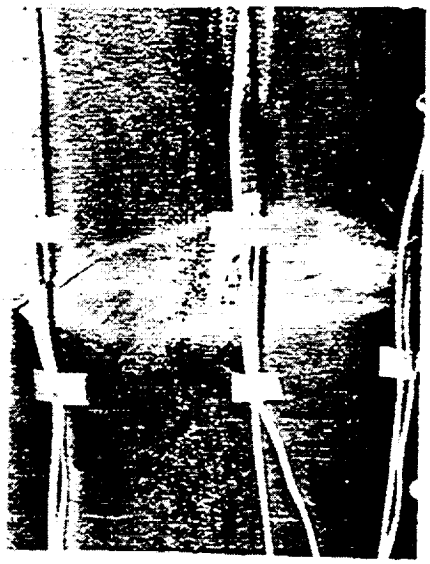

(b) Panel failure mode

Figure 7.30 Flat rectangular graphite–epoxy panel under axial compression [92].

columns. The geometry, boundary conditions, and layup are given in Figure 7.31, and the material properties and statistics are supplied in Table 7.3.

A previous deterministic analytical study was performed on the panel (denoted as Panel C4 in [92]) by this author in reference [93]. Comparisons were made between analytical and experimental results. In general the comparisons were very good, even deep in the postbuckling range. In order to pass the critical buckling load, a geometric imperfection of a small percentage of the plate thickness (typically 1 to 5) times the normalized linear buckling mode was added to the original geometry of the panel. The purpose of the previous analysis was to study the effect of shear deformation on postbuckling response and failure prediction. The purpose of this analysis is to study the variability of the panel results.

The probabilistic analysis of this panel assumed a fully correlated random field for each random function in each layer thus allowing the uniform variance solution to be used. An attempt was made to employ the random field techniques; however, the computational expense was too high due to eight random functions in 24 layers, 1625 degrees of freedom in the model, and a nonlinear analysis. The random field method took 8.3 hours per load step (on a Convex computer), whereas the uniform variance method only 5.8 minutes per load step. Since 13 load steps were required to reach the failure load and immense storage is required for the random field method with this many layers, it was concluded that for this size problem the uniform variance method was much more realistic.

The end shortening postbuckling response is shown in Figure 7.32. The load P is normalized by the analytical buckling load P_{cr}, and the end

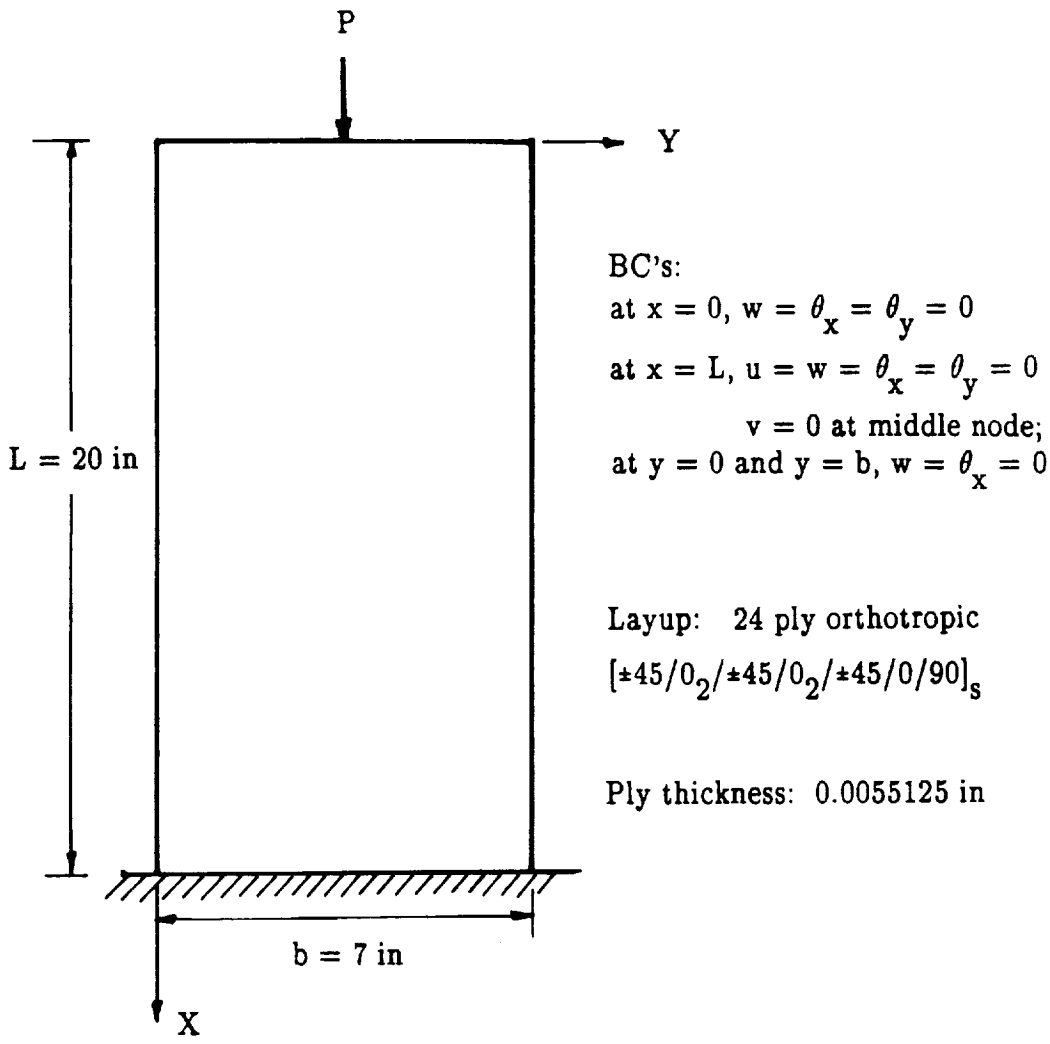

Mesh Definition:

72 nine–node Lagrange elements, uniform spacing with 12 along x direction and 6 along y; 325 nodes and 1625 DOF.

Figure 7.31 Geometry, boundary conditions, and layup for graphite–epoxy panel with axial compression.

Table 7.3

Material Properties for Graphite–Epoxy Flat Panel Under Axial Compression Problem

Random Variable	Mean	Standard Deviation	Coefficient of Variation
E_{11}	19.0×10^{6}	9.5×10^{5}	0.05
E_{22}	1.89×10^{6}	9.45×10^{4}	0.05
G_{12}	0.93×10^{6}	4.65×10^{4}	0.05
ν_{12}	0.38	1.9×10^{-2}	0.05
G_{13}	0.93×10^{6}	4.65×10^{4}	0.05
G_{23}	0.25×10^{6}	1.25×10^{4}	0.05
θ^{*}	$\pm 45^{\circ}, 0^{\circ}, 90^{\circ}$	2°	–
δ^{*}	5.5125×10^{-3}	4.167×10^{-3}	0.05

* θ indicates fiber orientation angle and δ indicates ply thickness.

The units are in psi and inches where appropriate.

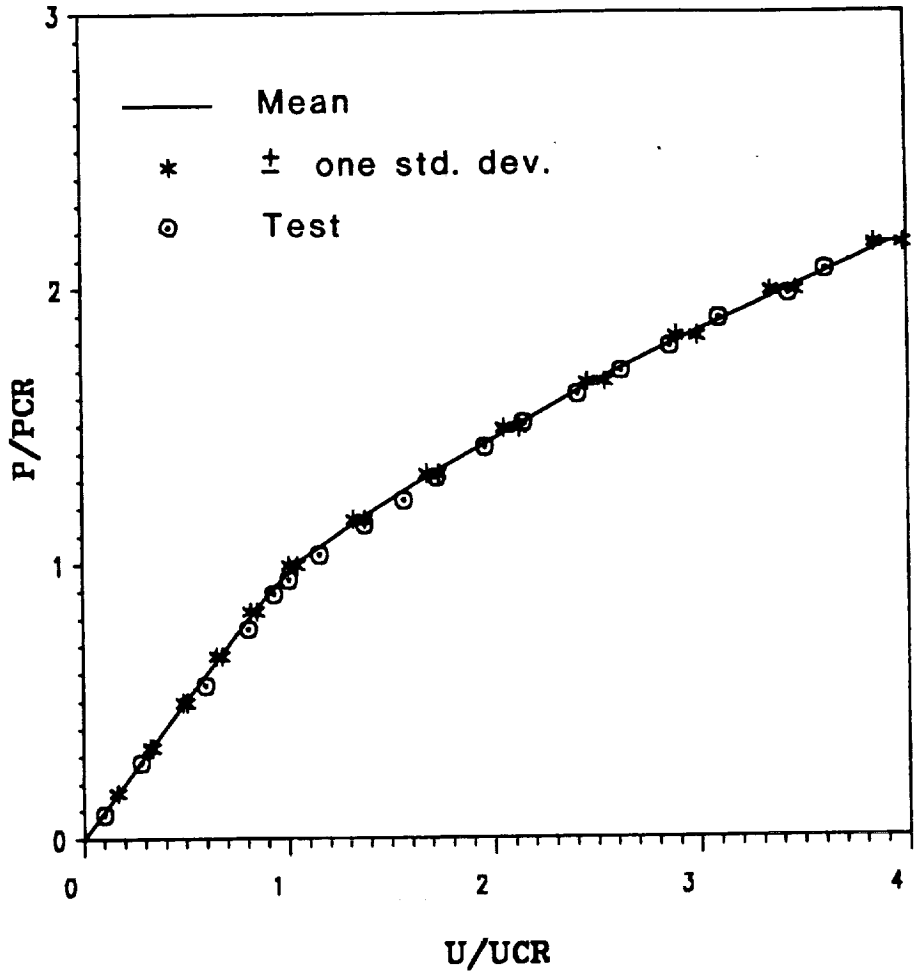

Figure 7.32 End–shortening postbuckling response of graphite–epoxy panel.

shortening deflection u by the analytical end shortening u_{cr} at buckling. A 1% plate thickness geometric imperfection was used. The analytical results compare favorably with the experimental results. In addition, the plus or minus one standard deviation points indicate the variation in the data. It should be noted that in [93], it was shown that one of the reasons for the good agreement here is the inclusion of the shear deformation in the element formulation. Figure 7.33 contains the out–of–plane deflection w near a point of maximum deflection normalized by the panel thickness t. Figure 7.34 shows the longitudinal surface strains e near a point of maximum out–of–plane deflection normalized by the analytical buckling strain e_{cr}. In this comparison only the reduced integration Gauss point closest to the experimental strain gage was used to calculate the strains. Interpolation has been shown to improve agreement with the experimental results. For all three of these plots the COV is typically around 2%, except for the w displacement prior to and at buckling which was large.

In order to understand the failure mode, it is necessary to see the nonlinear buckling mode shape. An analytical contour plot of the out–of–plane deflection at an applied load of 2.1 P_{cr} is shown in Figure 7.35a. A moire fringe pattern photograph from reference [92] of the out–of–plane deflections at the same load is shown in Figure 7.35b. Both patterns indicate two longitudinal half–waves with a buckling–mode nodal line at panel midlength.

In References 92 and 93, it was determined that the failure mode was primarily due to transverse shear stress τ_{13} (τ_{xz} in 0° ply) along the midlength (nodal line) of the panel. In later work it has been found that although τ_{13} is

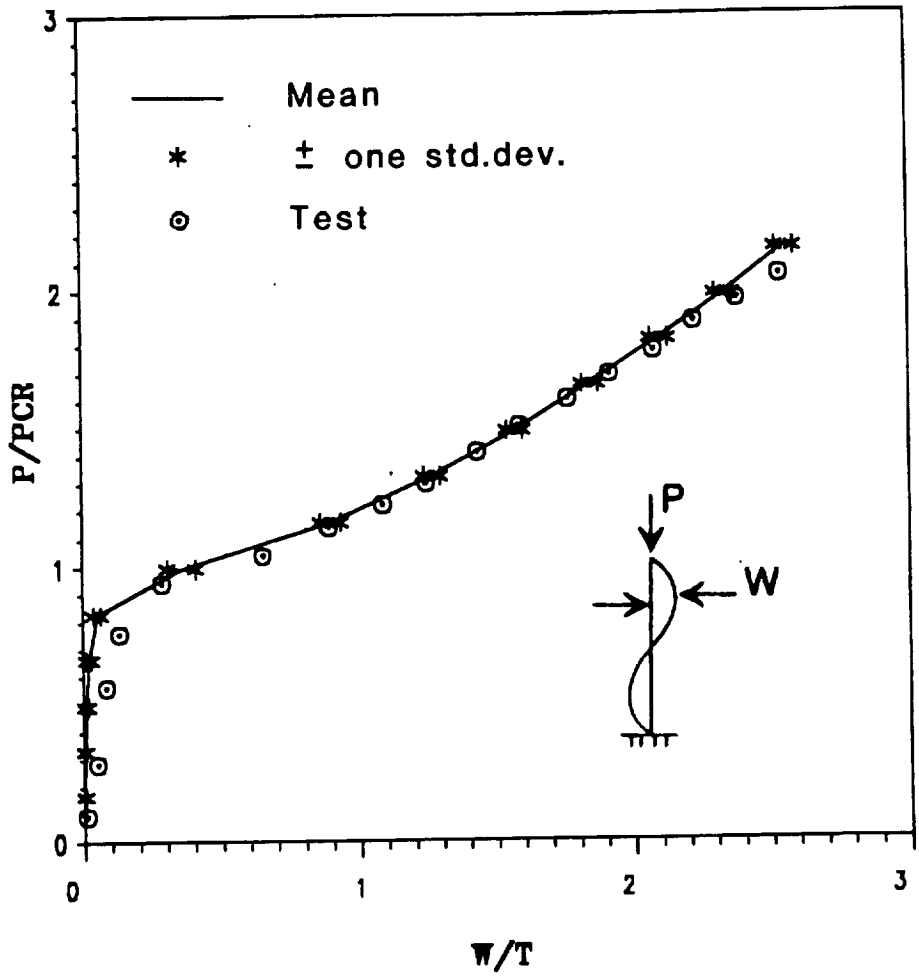

Figure 7.33 Out–of–plane displacement postbuckling response of graphite–epoxy panel.

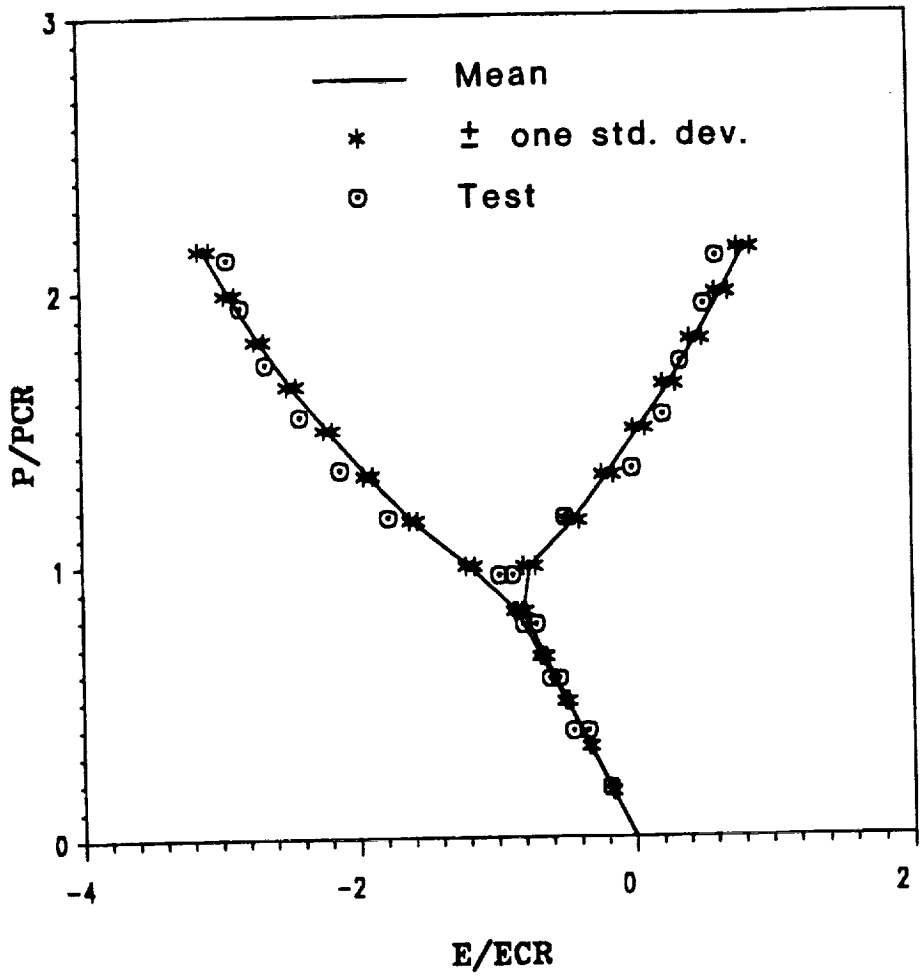

Figure 7.34 Longitudinal surface strains on opposite outer surfaces of the graphite–epoxy panel near a point of maximum out–of–plane displacement.

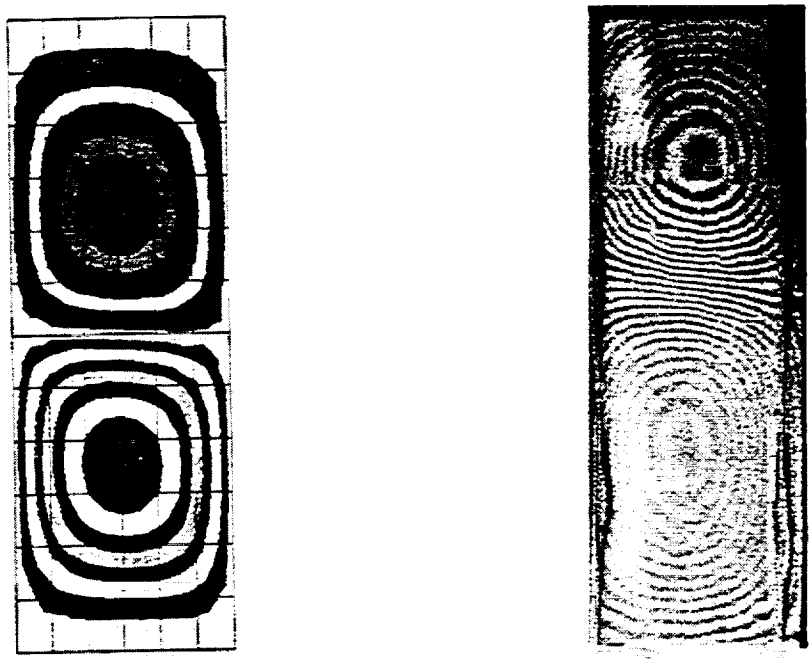

(a) Contour plot of analytical results

(b) Photograph of moire–fringe pattern

Figure 7.35 Comparison of experimental and analytical out–of–plane displacement patterns at applied load of 2.1 P_{cr} for the graphite–epoxy panel.

the primary failure mechanism, other stresses such as σ_{11} and τ_{12} also cause failure along the nodal line region in other layers.

Proceeding with the analysis, Figure 7.36a shows a contour plot of the σ_{11} stress in the third layer of the laminate (a 0° ply) at an applied load of 2.1 P_{cr}. High compressive axial stresses occur along the longitudinal edges of the panel. The redistribution of the axial (σ_{11}) stresses for this 0° ply along the panel midlength is shown in Figure 7.36b for three different load levels. The y coordinate is measured from one side of the panel and normalized by the panel width b. The longitudinal membrane strain is redistributed to the edges of the panel after buckling. Typical COV values are .05 at $P/P_{cr} = 1.0$, and range from .08 to .16 for the higher loads. The plus or minus one standard deviation points are shown in the figure. The material allowables for axial stress are 203 ksi in tension, and 165 ksi in compression, so the axial stress at this location is well below this.

The distribution of the transverse shear stress τ_{13} in the third layer of the laminate (a 0° ply) is shown in Figure 7.37a for a load of 2.1 P_{cr}. It is observed that high transverse shear stress develops along the nodal line of the panel. Figure 7.37b shows the redistribution of the τ_{13} stress for three different applied loads. At the experimental failure load of 2.1 P_{cr}, the τ_{13} stress approaches the material allowable value of 9 ksi. The COV for the τ_{13} stress was typically .055 except at the critical buckling load when it reached a value of .12.

It is of interest to determine the most significant random variables in the variance for the τ_{13} stress. Figure 7.38 contains the peak mean τ_{13} stress, along with the COV for the combined and individual random variables for

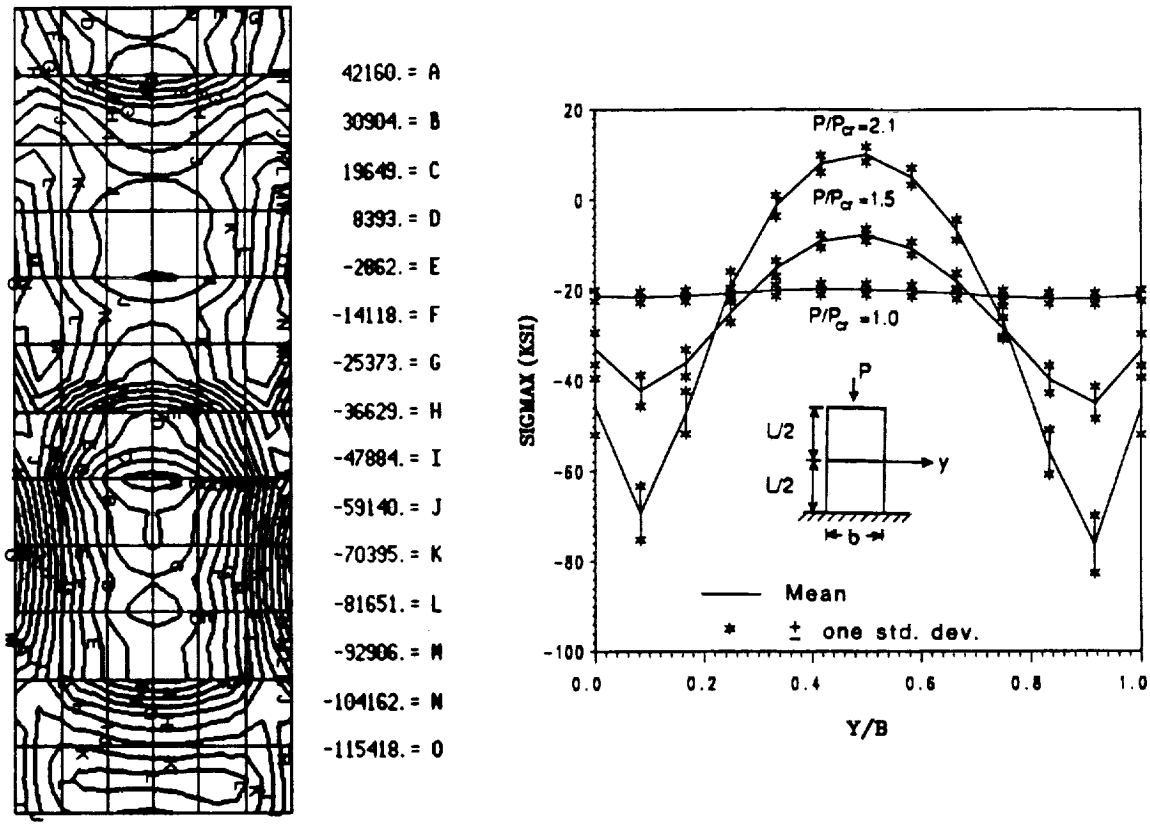

(a) Contour plot of axial stress distribution

(b) Stress distributions across panel midlength

Figure 7.36 Normal stress σ_{xx} distribution in the third–layer (0° ply) from the surface of the graphite–epoxy panel.

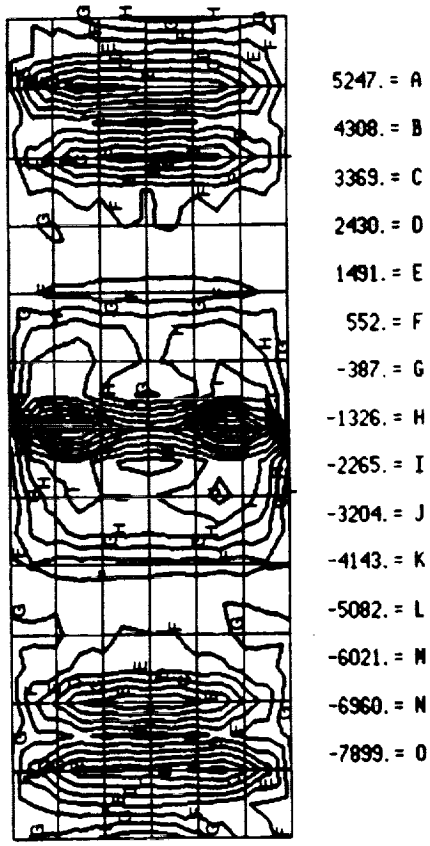

(a) Contour plot of transverse shear stress distribution

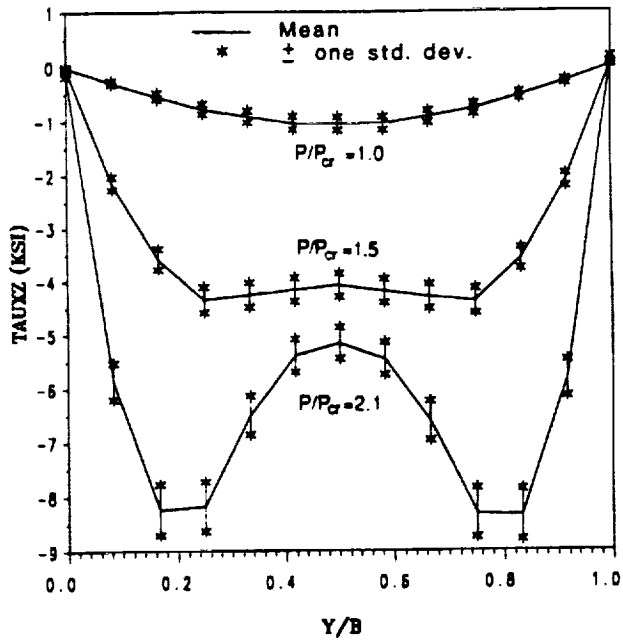

(b) Stress distributions across panel midlength

Figure 7.37 Transverse shear stress τ_{xz} distributions in the third layer (0° ply) from the surface of the graphite–epoxy panel.

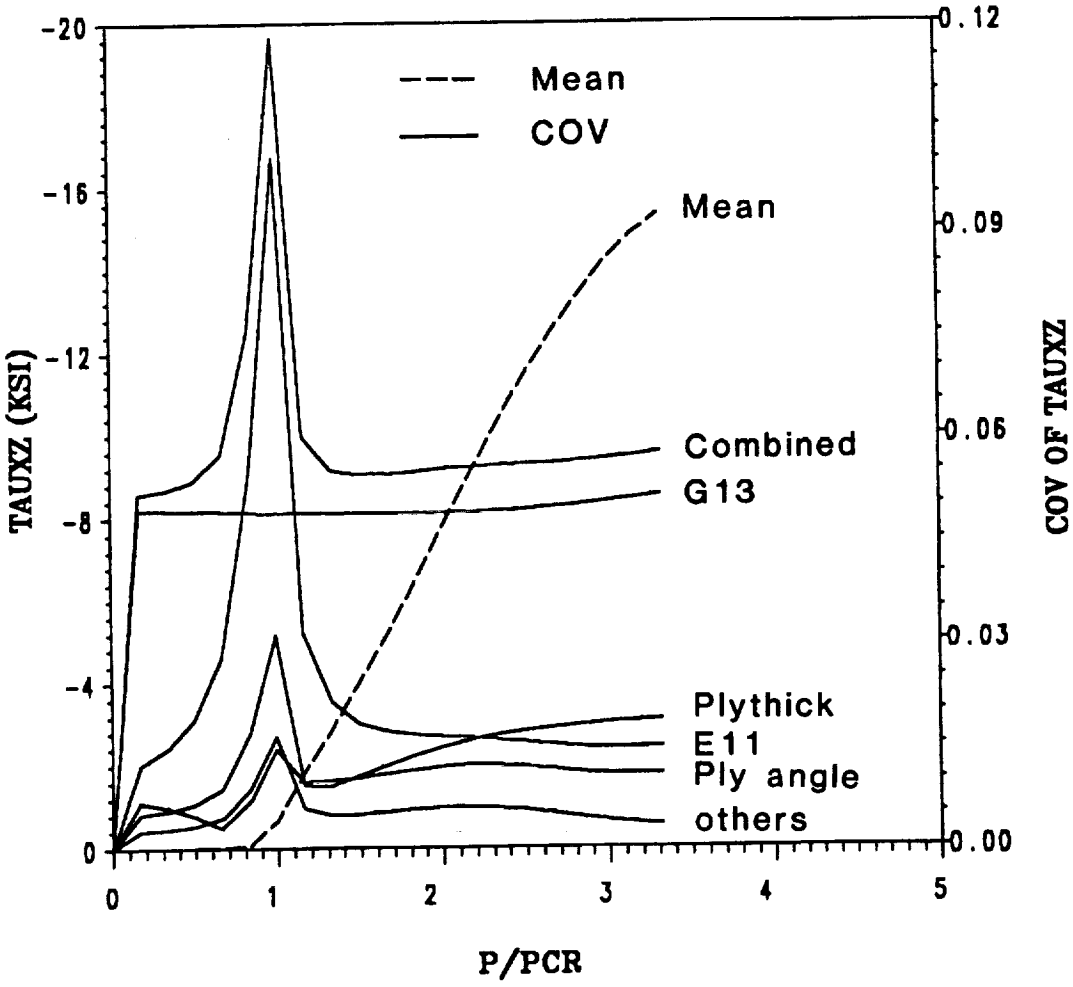

Figure 7.38 Mean and coefficient of variation (COV) of τ_{xz} stress versus load throughout postbuckling range showing the combined and individual effects of the ply–level random variables for the graphite–epoxy panel.

increasing load values. It is observed that the τ_{13} stress variance is most influenced by G_{13}, with the ply thickness effect increasing as the buckling load is passed and bending effects become more important.

Even though for this graphite–epoxy composite panel a first ply failure does not represent overall panel failure, reliability analysis was performed for first ply failure. For simplicity the maximum stress failure criterion was selected, although other failure criteria may be more suitable such as maximum strain or a quadratic polynomial criterion, such as the Tsai–Wu criterion. In this analysis, since the material allowables' accuracy was a question, a very simple example reliability calculation was determined suitable in which the failure criterion was based on exceeding the transverse shear strength of 9 ksi. The strength and stress were selected to be Normal distributed, with the stress mean and COV from the finite element results and the strength COV assumed to be 0.10. Appendix B describes the reliability theory used here [23]. Figure 7.39 is a plot of the probability of safety curve (probability of non–failure of first ply) versus load for the τ_{13} failure mode. Based on the first–order second–moment probabilistic finite element results and the assumed strength statistics, approximately 100% reliability against first ply failure exists at a load step of 1.65 P_{cr}. It is believed that the reliability analysis for first ply failure used in conjunction with a progressive failure analysis, in which the damage due to local failures is progressively accumulated, would be a very good criterion for design of these panels to exclude any failures. Another option would be to determine the system reliability, in which individual ply reliabilities are combined into the overall laminate structure reliability.

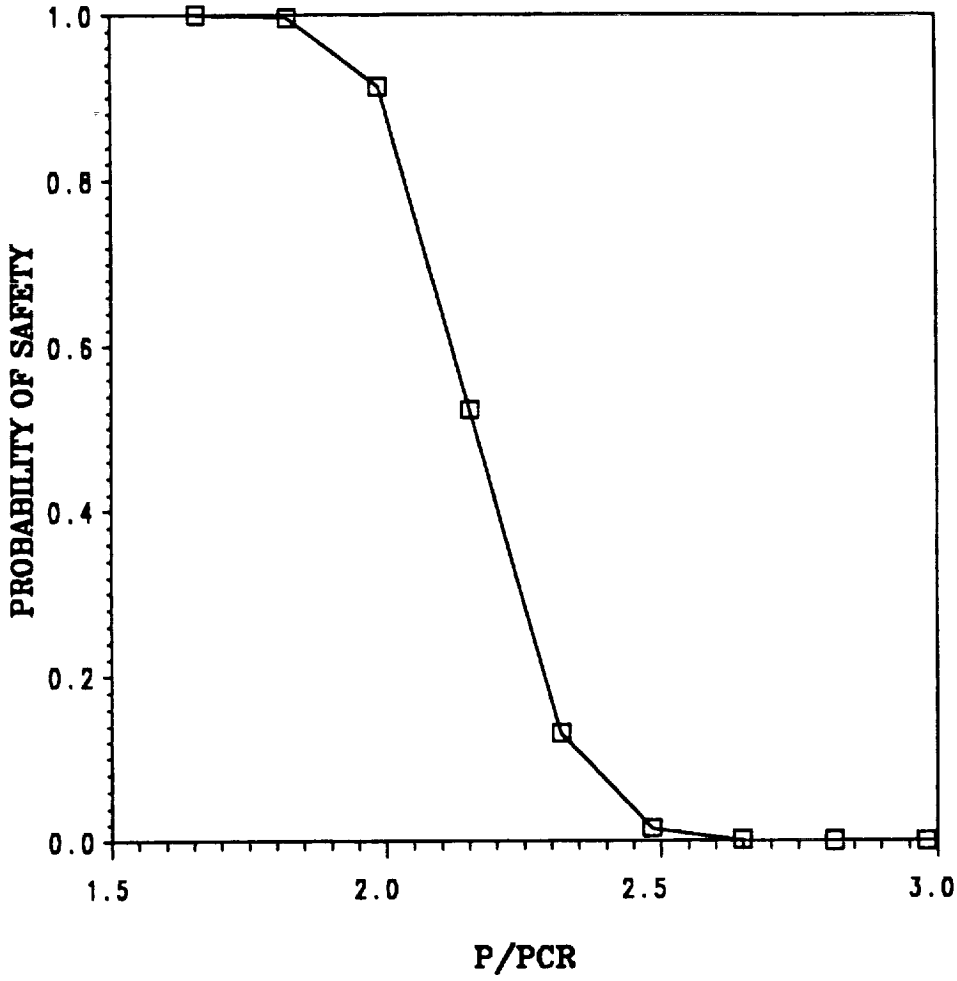

Figure 7.39 Reliability against first ply failure due to τ_{xz} stress versus load throughout postbuckling range of the graphite–epoxy panel.

7.4 Material Nonlinear Analyses

Material nonlinearity has been included in a fashion such that combined material and geometric nonlinearity can be studied. The classical example of an isotropic cylindrical shell roof under self weight is analyzed and compared with results in the literature for all three cases of geometric nonlinearity, material nonlinearity, and combined nonlinearities. The same example is then used to validate the mean and variance statistics of the first–order second–moment probabilistic method by comparison to Monte Carlo results for the combined nonlinearity case.

Two material nonlinear composites were then selected for study. First, an ARALL laminate (patented by Alcoa), composed of aramid epoxy layers in between layers of isotropic aluminum, was analyzed. Second, a single layer Boron/Aluminum composite is modeled using the orthotropic plasticity formulation. Both materials were then employed in a model of a tension specimen with a hole.

7.4.1 Cylindrical Shell Roof Under Self Weight

The cylindrical shell roof under self weight problem described in Figure 7.40 is a classical test example in the literature. The shell has free longitudinal edges and is supported at both ends on rigid diaphragms. Ideal plasticity is assumed for the material nonlinear behavior. The material properties and statistics are given in Table 7.4.

In order to validate the plasticity model shell formulation, the deterministic results for this problem are compared to those obtained by Ramm and Sattele [94]. In their work a 3x3 mesh of bicubic 16–node degenerated shell

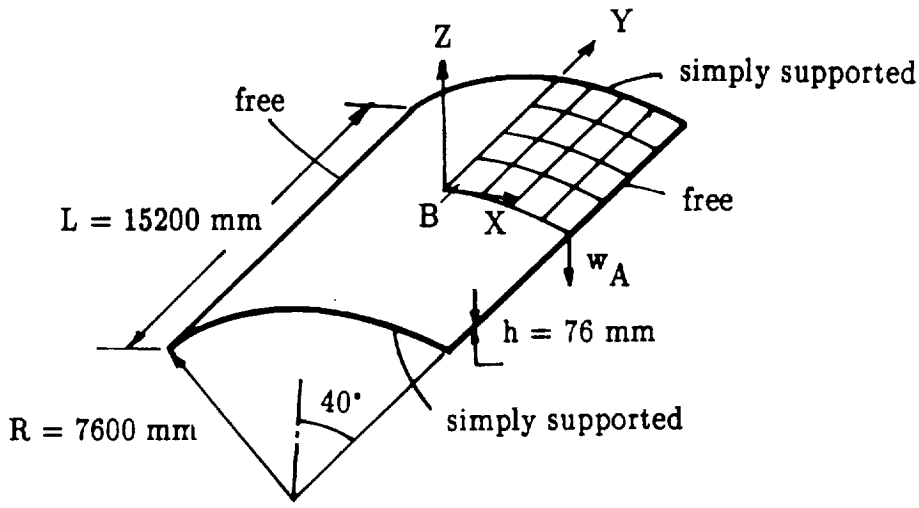

Figure 7.40 Cylindrical shell roof under self weight problem description.

Table 7.4

Material Properties and Statistics for Cylindrical Shell Roof Under Self Weight Problem

Random Variable	Mean	Standard Deviation	Coefficient of Variation	$\lambda_{\xi'}$	$\lambda_{\eta'}$
E	21000	1050	0.05	2440	3800
ν	0.0	–	–	–	–
σ_Y *	4.2	0.21	0.05	2440	3800

Material is isotropic; ν is not considered random. Units are in N/mm^2 and mm where appropriate.

* σ_Y stands for yield stress.

elements was used with a total of 441 degrees of freedom. The cubic element uses 4x4 Gauss integration in the plane of the element and a 7 point Simpson's rule integration in the thickness direction. Figure 7.41 contains the results obtained by Ramm and those for the present study for the center node deflection w_A at the free edge. Various mesh refinements of biquadratic 9–node elements were used here to study agreement with the Ramm solution. Full integration for the biquadratic element consists of 3x3 Gauss points. This element is known to have locking (over–stiffening) problems when used to model thin shells, and this is typically remedied by using either fully reduced integration on all terms (2x2) or selective reduced integration in which 3x3 integration is used for the in–plane terms and 2x2 integration for the transverse shear terms. Studying the figure, the 4x4 element mesh with full 3x3 integration obviously exhibits locking for the combined nonlinear results and thus is too stiff. Using fully reduced integration, the geometrical nonlinear elastic, and linear elastoplastic solutions agree well with the reference. However the combined nonlinear solution is too soft. By refining the mesh the locking effects are reduced such that for a 6x6 biquadratic mesh with 3x3 integration the results compare very favorably with those obtained by Ramm. The degrees of freedom in the three biquadratic meshes are as follows: 4x4 mesh – 405 d.o.f., 5x5 mesh – 605 d.o.f., and 6x6 mesh – 845 d.o.f. Eight gauss integration points through the thickness were used. In addition, it is of interest to note the stiffening effect due to the geometrical nonlinearity and the softening effect due to the elastoplasticity.

The cylindrical shell problem is used next to validate the first–order second–moment probabilistic finite element mean and variance response by

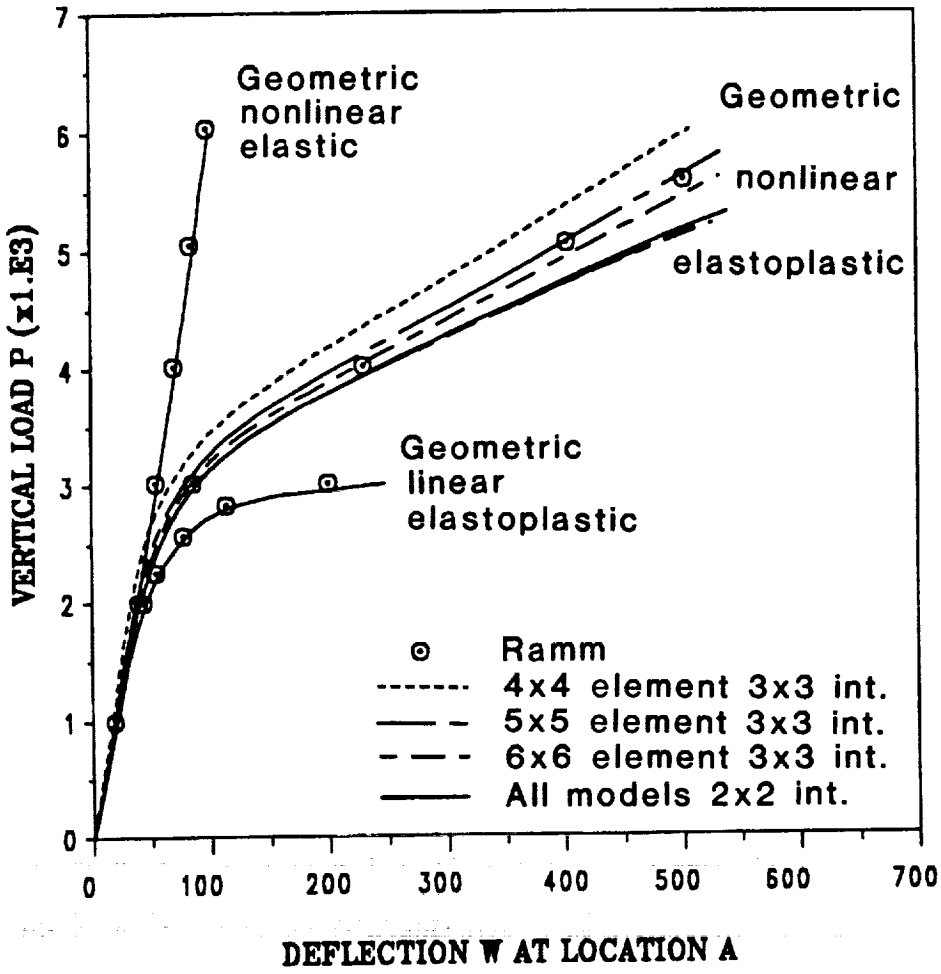

Figure 7.41 Center node displacement w at location A of cylindrical shell roof versus load for various types of nonlinearity.

comparison with Monte Carlo results. The input statistics are given in Table 7.4, and to save computation time the 4x4 model with 2x2 integration is used. The comparisons are given in Figures 7.42 – 7.45, and are made for the combined nonlinear solution, with 1500 Monte Carlo simulations. The deterministic solution yields at a load of $1.4x10^3$, and five load steps past yield are shown. More load steps are not used as the expense of the Monte Carlo solution prohibits this. The Monte Carlo solution required 43.4 hours CPU time while the first–order second–moment method only used 5.3 minutes. Obviously the perturbation method is computationally advantageous.

7.4.2 ARALL Laminate Tension Specimen with Hole

ARALL laminates are high strength hybrid composites for aerospace applications developed by Alcoa. Figure 7.46 illustrates the concept of bonding thin sheets of high strength aluminum alloys using high strength aramid fibers in a special epoxy resin. The benefits include significant increases in fatigue and fatigue crack growth properties over monolithic aluminum, and the outer aluminum layers provide impact damage and moisture protection that would be a problem for typical fiber composite materials. In addition, increases in strength and lower densities are achieved as compared to monolithic aluminum [96].

It is desired to model the nonlinear structural behavior of this hybrid composite. Figure 7.46 also shows the description of the analytical model used to represent the stiffness of this material. The aramid epoxy layers are divided into fiber–rich and resin–rich layers with stiffness given for each sublayer. Table 7.5 gives the properties and statistics for the aluminum, aramid epoxy

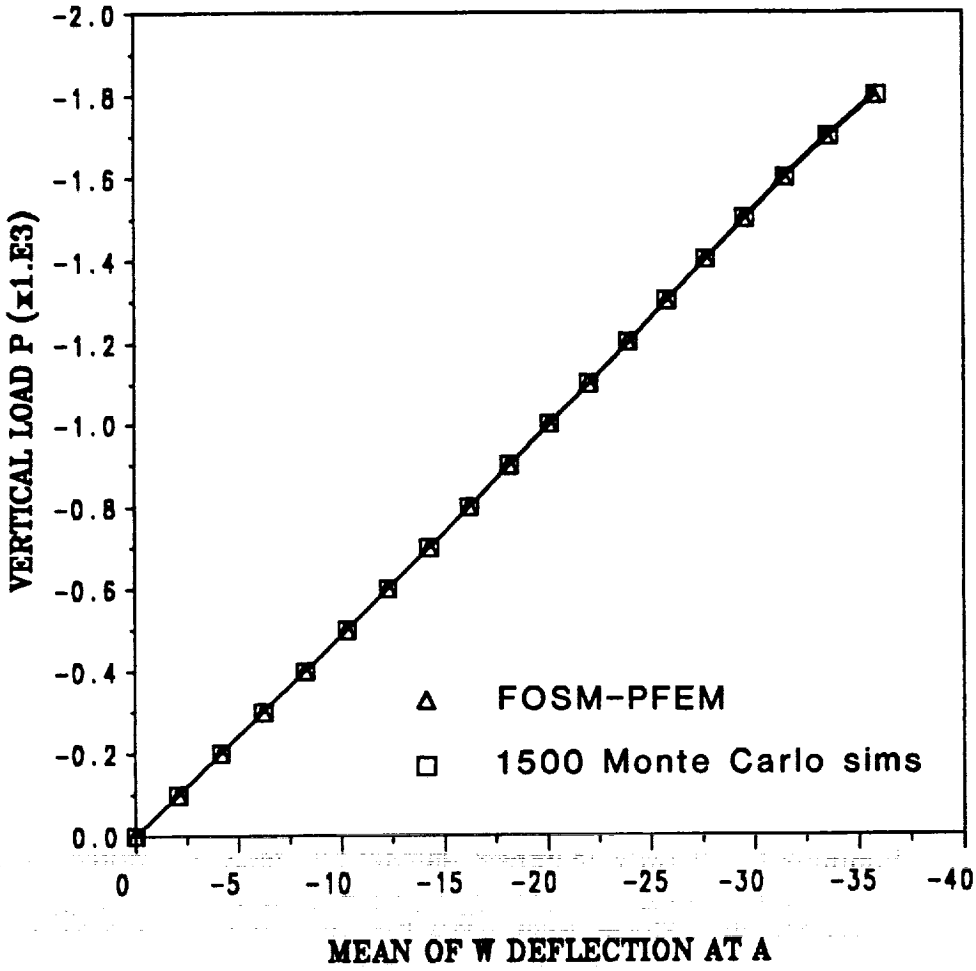

Figure 7.42 Mean center node displacement w at location A versus load for the cylindrical shell roof under self weight.

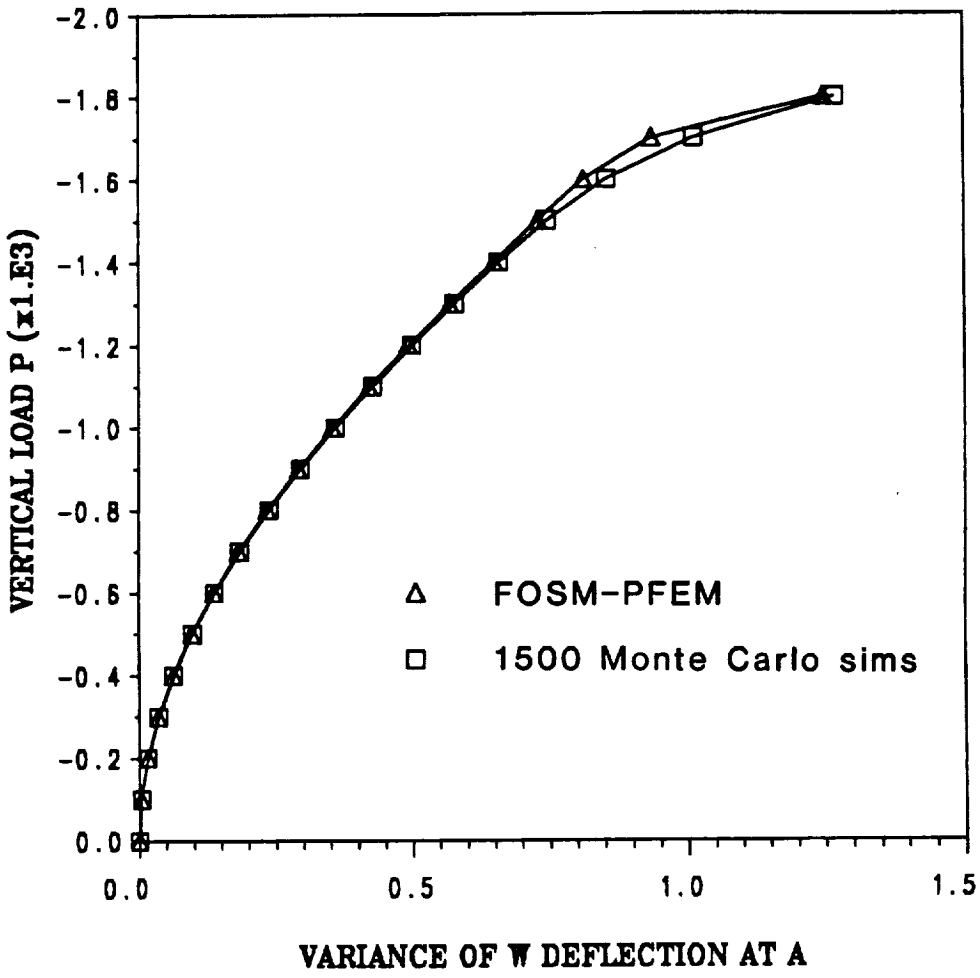

Figure 7.43 Variance of center node displacement w at location A versus load for the cylindrical shell roof under self weight.

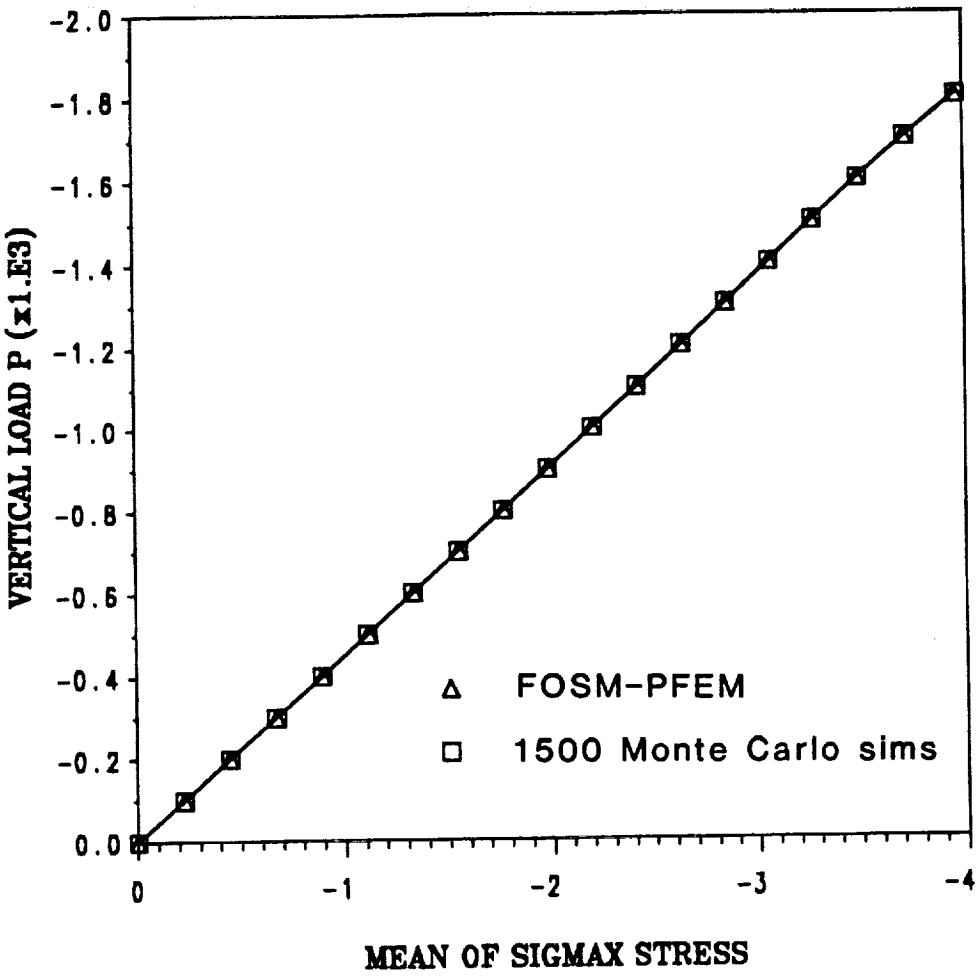

Figure 7.44 Mean σ_{xx} stress at location B versus load for the cylindrical shell roof under self weight.

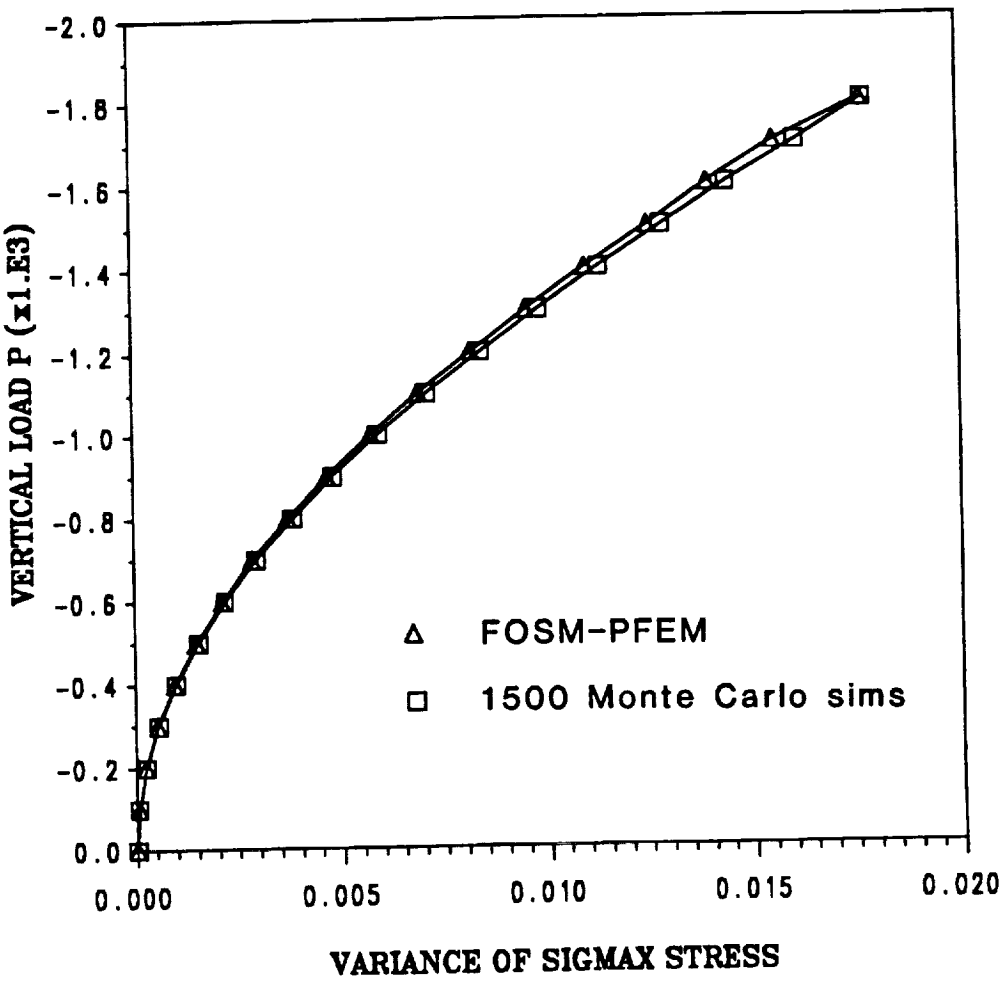

Figure 7.45 Variance of σ_{xx} stress at location B versus load for the cylindrical shell under self weight.

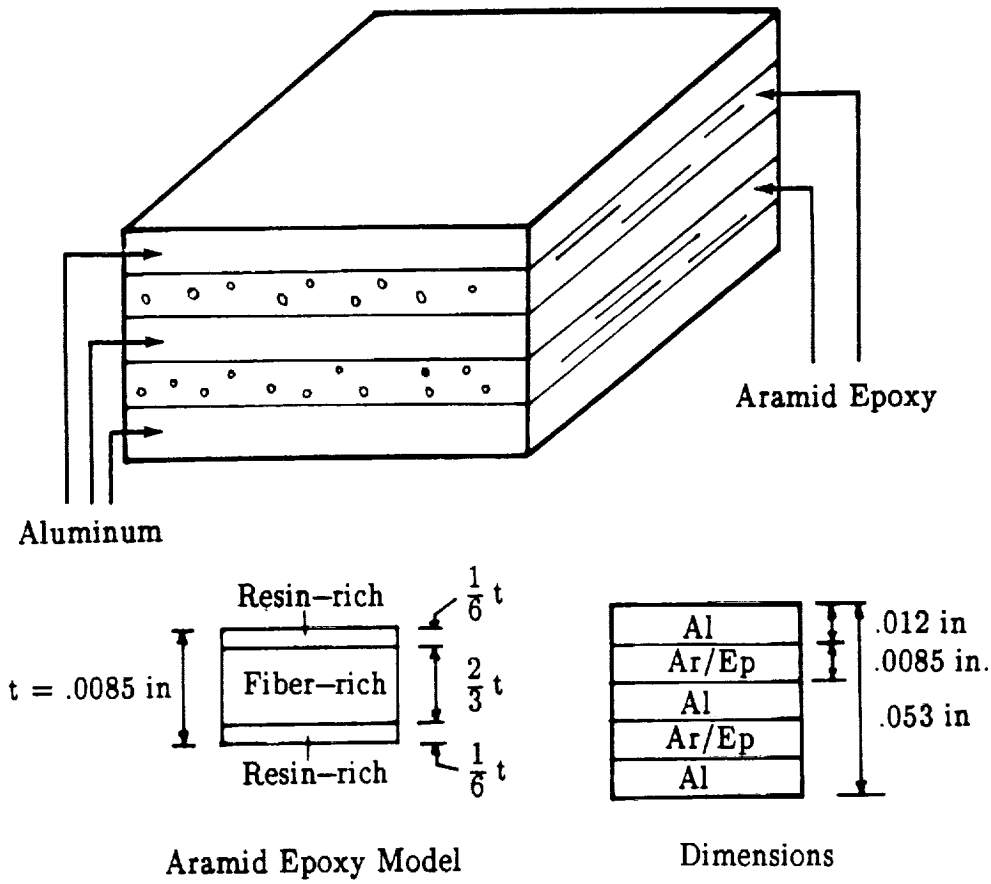

Figure 7.46 ARALL laminate layup and geometry.

Table 7.5
Material Properties and Statistics for ARALL–1 Laminate Constituents

Random Variable	Mean	Standard Deviation	Coefficient of Variation
Aluminum (7075–T6L)			
E	10.4×10^{6}	5.2×10^{5}	0.05
ν	0.3	1.5×10^{-2}	0.05
σ_Y^*	7.8×10^{4}	3.9×10^{3}	0.05
δ^*	1.2×10^{-2}	6.0×10^{-4}	0.05
Aramid Epoxy fiber–rich layers			
E_{11}	12.549×10^{6}	6.2745×10^{5}	0.05
E_{22}	0.76525×10^{6}	3.82625×10^{4}	0.05
G_{12}	0.28955×10^{6}	1.44775×10^{4}	0.05
ν_{12}	0.3458	1.729×10^{-2}	0.05
G_{13}	0.28955×10^{6}	1.44775×10^{4}	0.05
G_{23}	0.26462×10^{6}	1.3231×10^{4}	0.05
θ^*	0°,90°	2°	–
δ^*	5.6×10^{-3}	2.8×10^{-4}	0.05
Aramid Epoxy resin–rich layers			
E_{11}	2.1972×10^{6}	1.0986×10^{5}	0.05
E_{22}	0.48219×10^{6}	2.41095×10^{4}	0.05
G_{12}	0.15717×10^{6}	7.8585×10^{3}	0.05
ν_{12}	0.3749	1.8745×10^{-2}	0.05
G_{13}	0.15717×10^{6}	7.8585×10^{3}	0.05
G_{23}	0.15576×10^{6}	7.7880×10^{3}	0.05
θ^*	0°,90°	2°	–
δ^*	1.416×10^{-3}	7.08×10^{-5}	0.05

* σ_Y indicates yield stress, θ indicates fiber orientation angle, and δ indicates ply thickness.
Units are in psi and inches where appropriate.

fiber–rich, and aramid epoxy resin–rich layers. Experimental tension test results [96] are compared to the analytical results in Figure 7.47. From the figure it is observed that the aramid epoxy behavior is linear and the analytical linear comparison is very good. The 7075–T6(L) aluminum behavior is elastic perfectly–plastic and the analytical model with a yield stress of 78 ksi agrees very well except near the point of first yield. As for the ARALL–1 results (–1 indicates 7075–T6(L) aluminum is used) the analytical model with ideal plasticity for the aluminum layers and linear elastic aramid epoxy layers generally exhibits the same behavior as the experimental results except the 0 degree laminate analytical model underpredicts the stiffness after yield and the 90 degree laminate model overpredicts the stiffness after yield. For the purpose of this example the analytical model is considered acceptable and will be used to study the mean and variance response of an ARALL tension specimen with a hole.

Figure 7.48 shows the finite element model and dimensions of the tension specimen with a hole problem. The same material properties and material model from the previous discussion are used in this problem. The probabilistic analysis assumed a fully correlated random field for each random function in each layer, thus allowing the uniform variance technique to be used here. Again the computational expense of discretized random fields in each layer in a nonlinear analysis forced this assumption. Figure 7.49 contains the mean and standard deviation of the longitudinal ϵ_{yy} strain at the hole edge (point A in Figure 7.48) for the case where all aramid epoxy layers are aligned at 90 degrees to the load. The figure also shows the breakdown of standard deviations for all the significant random variables. Since the fibers are 90 degrees to the load and

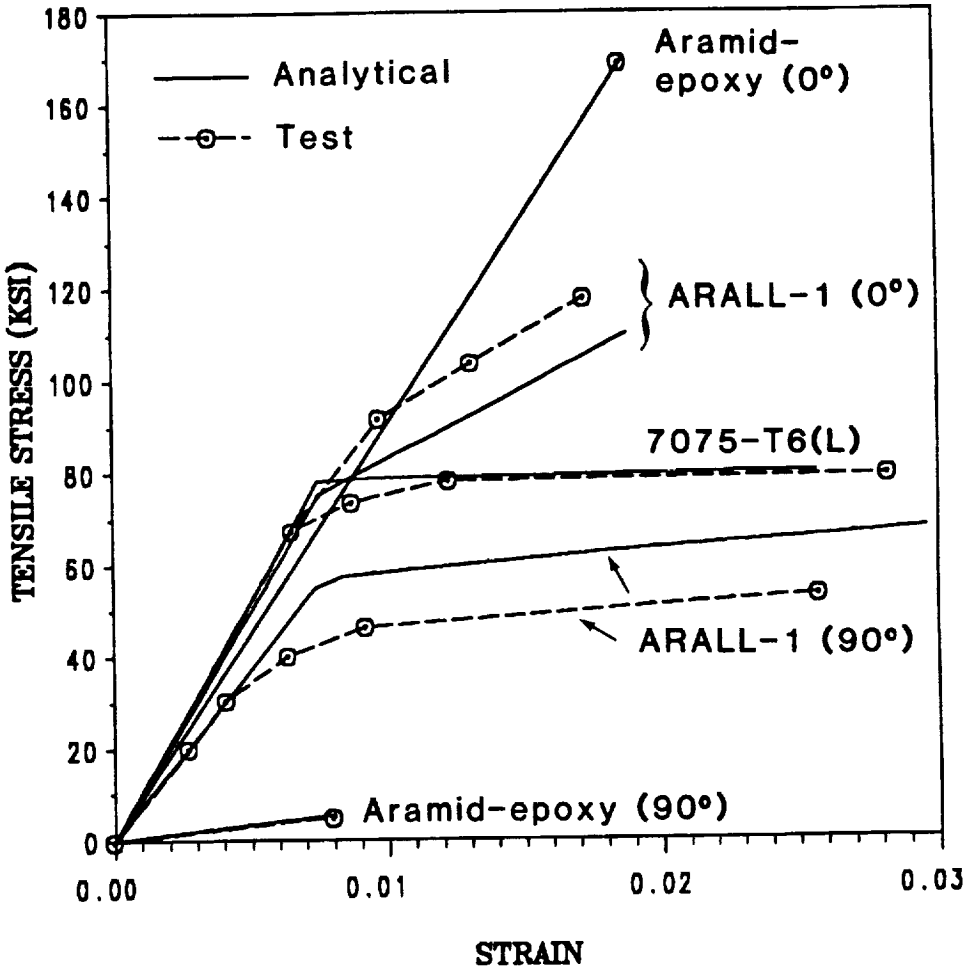

Figure 7.47 ARALL tension test experimental and analytical comparisons.

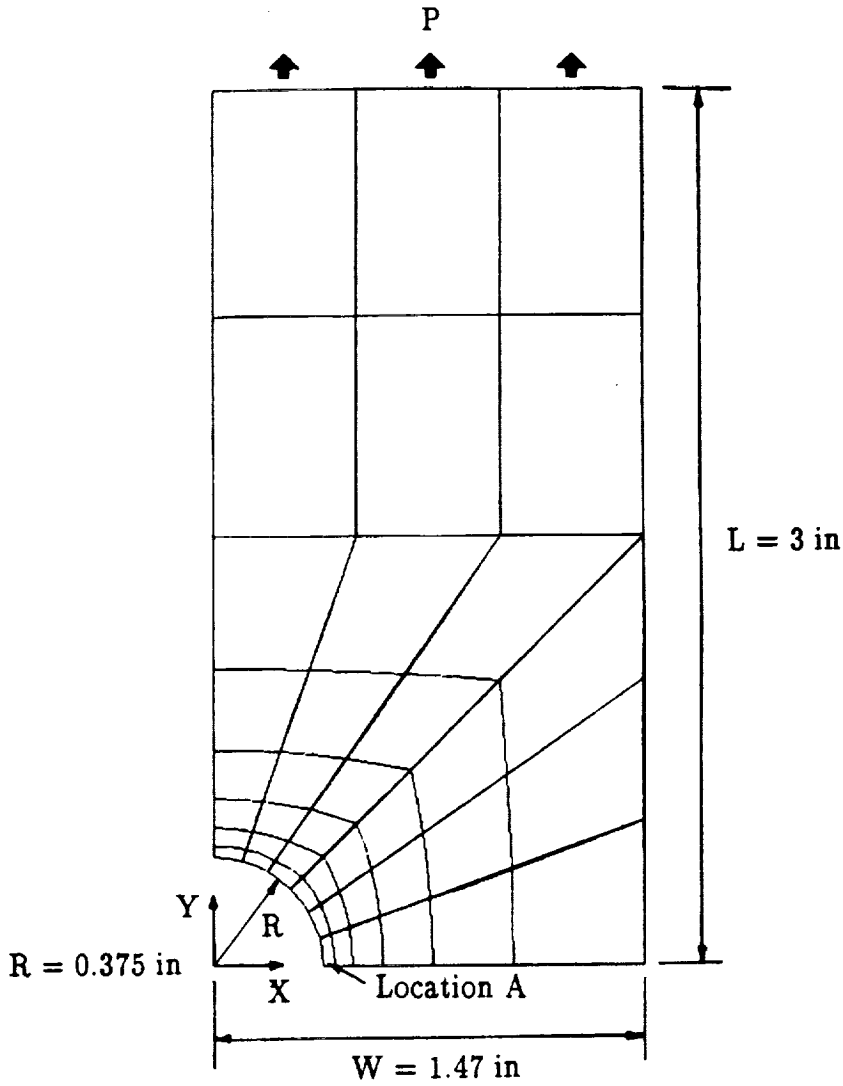

BC's: at x = 0 u = 0
at y = 0 v = 0
at y = L u = 0

Figure 7.48 Finite element model and dimensions of ARALL tension specimen with hole.

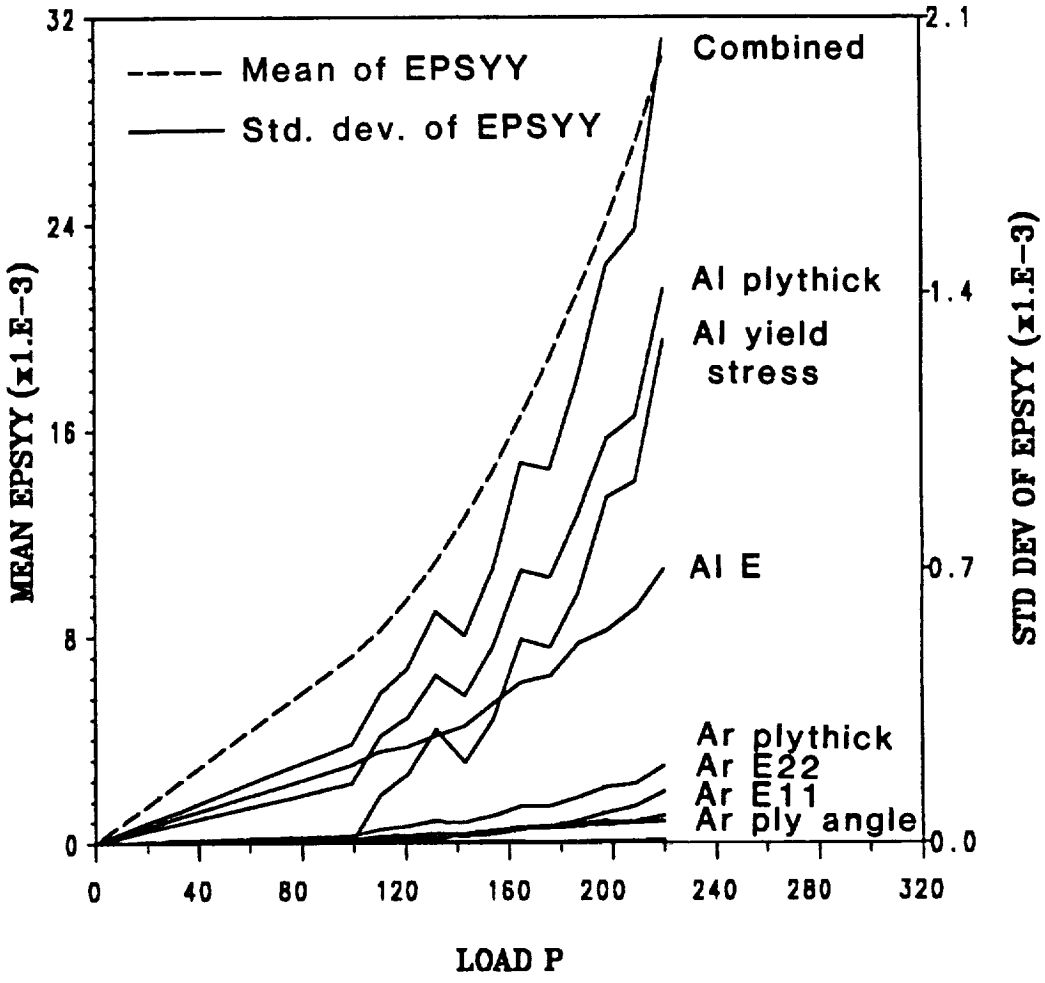

Figure 7.49 ARALL tension specimen with hole; mean and standard deviation of ϵ_{yy} strain at the hole edge (point A) versus load for the case where the fibers are 90° to the load; included are the combined and individual effects of the ply–level random variables.

to the strain ϵ_{yy}, then the aluminum properties tend to dominate. It is interesting to note that even though no bending occurs in this problem, the ply thickness of the aluminum layers is dominant after yield. The aluminum yield stress and elastic modulus are also important. Figure 7.50 contains similar results except now the fibers are aligned with the loading direction. While the aluminum yield stress and ply thickness random variables are still significant, the aramid E_{11} and ply thickness random variables are now equally important. These results illustrate the role the individual random variables play in the total variability of this type of ARALL structure.

7.4.3 Boron/Aluminum Tension Specimen with Hole

A Boron/Aluminum laminate was selected to illustrate the use of the macroscopic orthotropic plasticity formulation. The same problem dimensions (except for thickness) were used as in the last example, however, as shown in Figure 7.51, a different mesh was used that placed gauss points along the x–axis. Rizzi, Leewood, Doyle, and Sun [75] conducted an experimental and analytical study of this specimen, and provided experimental measurements for the orthotropic elastic constants as well as the a_{ij} values in the yield criterion and the hardening parameters in the isotropic work hardening model. These values are all stated in Table 7.6 and are used in the present analytical model. It should be noted that the a_{ij} values used in this study differ from those given in the reference by a factor of 2/3 due to a minor difference in the formulations. Figure 7.52 contains a comparison of the analytical results from the present study and experimental results from reference [75] for the longitudinal strain ϵ_{yy} along a radial line (x–axis) 90 degrees to the loading. The agreement is

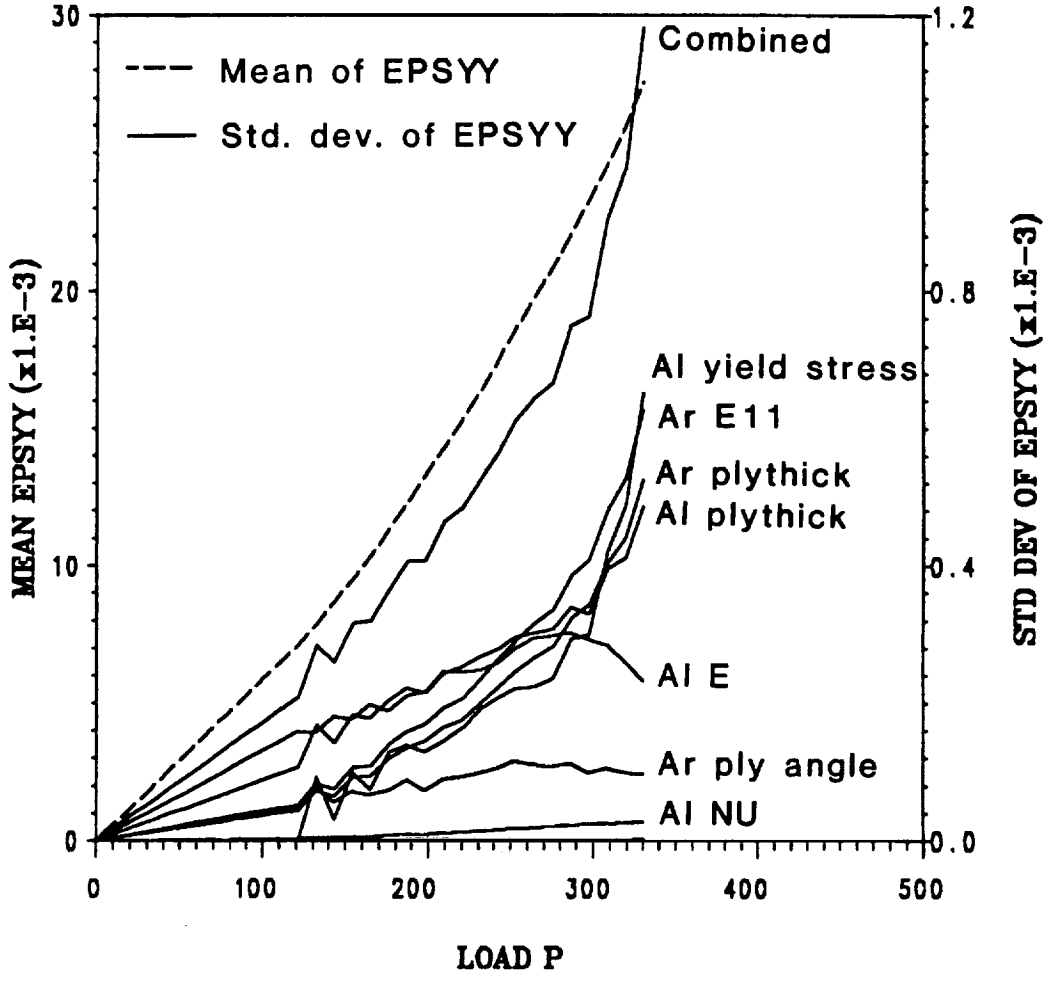

Figure 7.50 ARALL tension specimen with hole; mean and standard deviation of ϵ_{yy} strain at the hole edge (point A) versus load for the case where the fibers were alligned with the load; included are the combined and individual effects of the ply–level random variables.

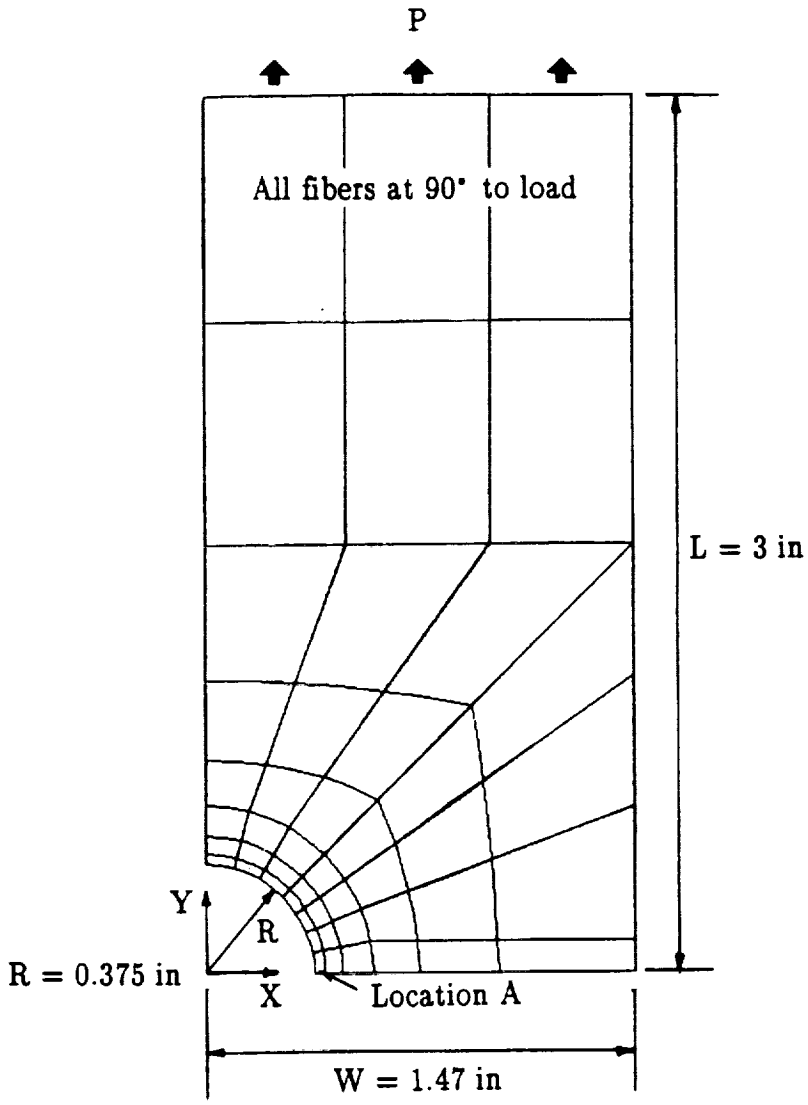

Figure 7.51 Finite element model and dimensions of Boron/Aluminum tension specimen with hole.

Table 7.6

Material Properties and Statistics for Boron/Aluminum Laminate

Random Variable	Mean	Standard Deviation	Coefficient of Variation
E_{11}	29.4×10^6	1.47×10^6	0.05
E_{22}	19.1×10^6	9.55×10^5	0.05
G_{12}	7.49×10^6	3.745×10^5	0.05
ν_{12}	0.169	8.45×10^{-3}	0.05
G_{13}	7.49×10^6	3.745×10^5	0.05
G_{23}	7.49×10^6	3.745×10^5	0.05
σ_Y^*	13.5×10^3	6.75×10^2	0.05
$\bar{H}^*$	60.0×10^3	3.0×10^3	0.05
θ^*	0°	2.0°	–
δ^*	7.95×10^{-2}	–	0.05

* σ_Y indicates yield stress, $\bar{H}$ indicates hardening modulus, θ indicates ply orientation angle, δ indicates ply thickness.

The values of the a_{ij} constants in the yield criterion are:

$$\frac{3}{2} a_{11} = 0.001 \quad \frac{3}{2} a_{22} = 1.0 \quad \frac{3}{2} a_{12} = -0.01$$

$$\frac{3}{2} a_{44} = \frac{3}{2} a_{55} = \frac{3}{2} a_{66} = 1.9$$

The hardening model used was $Y(\alpha) = \bar{H}[\alpha + [\frac{\sigma_Y}{\bar{H}}]^{\lambda}]^{1/\lambda}$

$$\lambda = 5.8$$

Units are in psi and inches where appropriate.

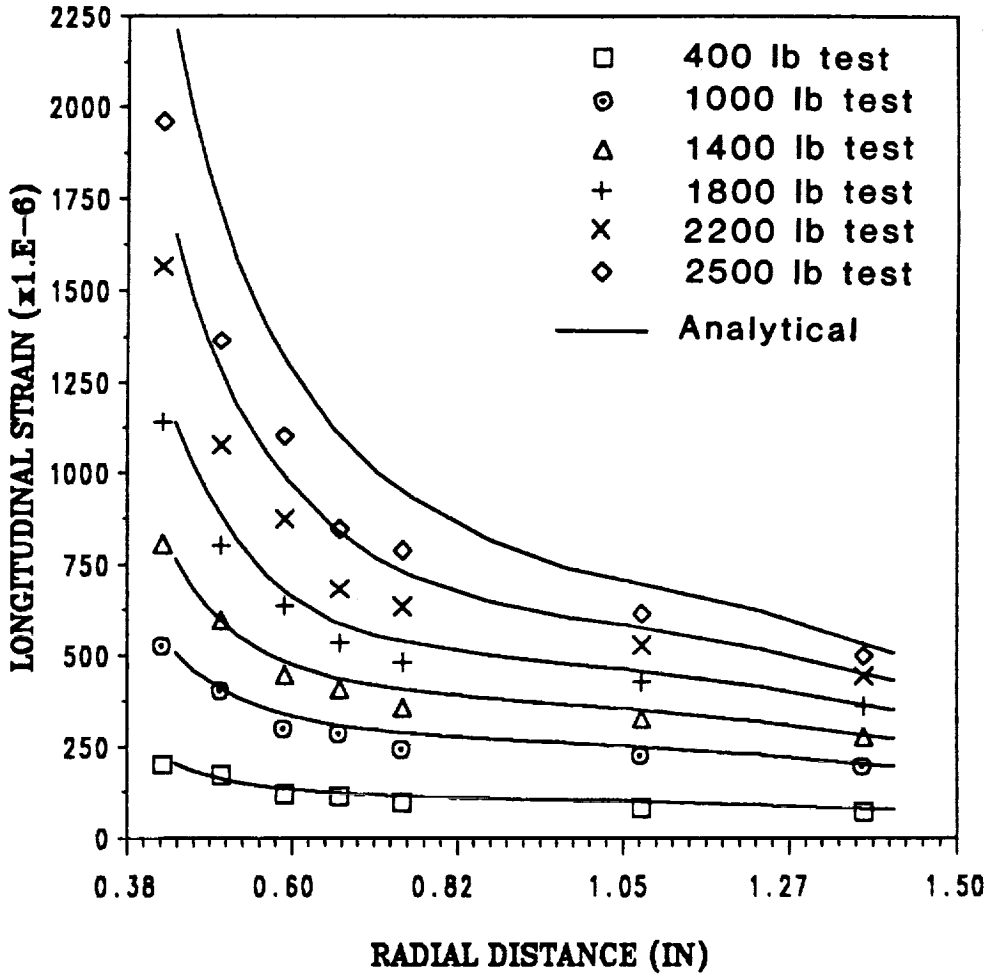

Figure 7.52 Analytical and experimental comparison of the longitudinal strain ϵ_{yy} along a line 90° to the loading for the Boron/Aluminum laminate tension specimen with hole.

slightly worse than that obtained in [75], but is probably due to the difference in element formulations and the classical incremental plastic stress routine used versus the radial return algorithm used here. Yielding occurs after 1000 lbs, and the agreement worsens as the loading is increased. However, the results are still considered quite good.

Using the random variable statistics stated in Table 7.6, the first–order second–moment probabilistic method was used to evaluate the mean and variance of the ϵ_{yy} strain response. Once again the probabilistic analysis assumed a fully correlated random field for each random function which allowed the uniform variance technique to be used here. Figure 7.53 shows the analytical mean ϵ_{yy} strain for the 2500 lb and 1000 lb load values with the plus or minus one standard deviation points included. It is obvious that the sensitivity of ϵ_{yy} to the random variables increases both with the load and as the location moves closer to the hole. Figure 7.54 is a plot of both the mean and standard deviation of the ϵ_{yy} strain at the location A on the model versus load. The breakdown for each random variable is presented as well. Since only a single layer is used, then the ply thickness could not be considered a variable here. The most significant random variable is the plastic hardening modulus $\bar{H}$, with E_{22} and the yield stress important as well. Note that E_{22} is significant since the fibers are 90 degrees to both the loading direction and to ϵ_{yy}. This example could obviously be extended to include the a_{ij} plastic yield coefficients and the hardening parameter λ as random variables since they are also experimentally measured quantities with uncertainties.

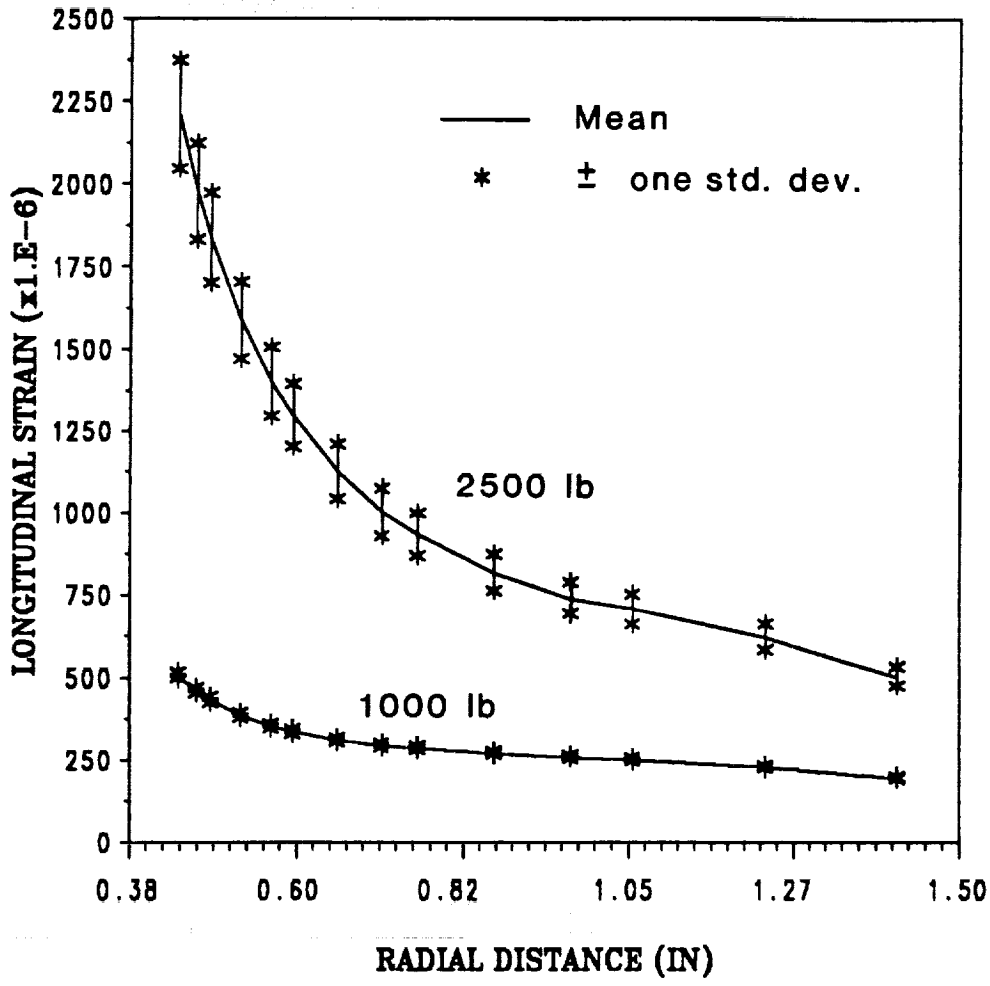

Figure 7.53 Analytical results for the longitudinal strain ϵ_{yy} along a line 90° to the loading for the Boron/Aluminum laminate tension specimen with hole.

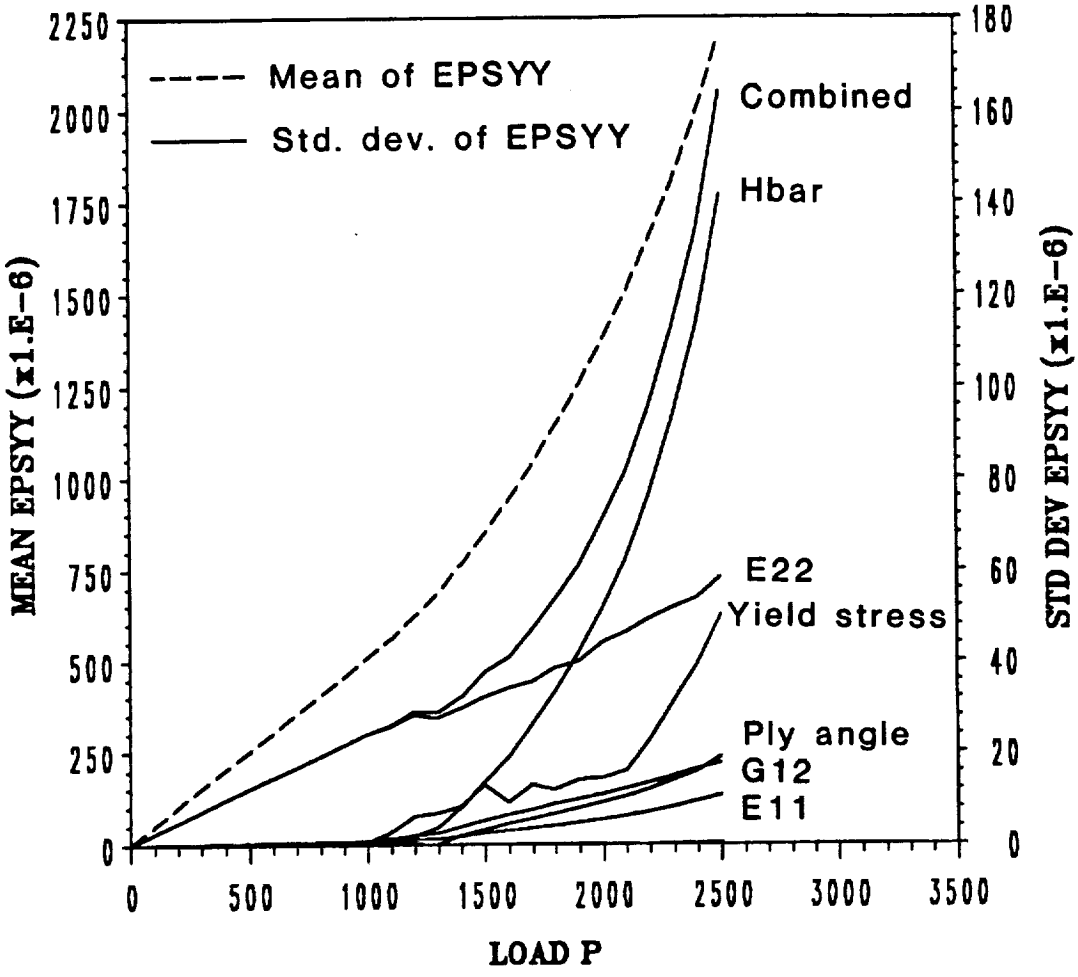

Figure 7.54 Boron/Aluminum tension specimen with hole; mean and standard deviation of ϵ_{yy} longitudinal strain at the hole edge (point A) versus load; included are the combined and individual effects of the ply–level random variables.

8. CONCLUSIONS AND RECOMMENDATIONS

8.1 Summary and Conclusions

A probabilistic finite element analysis procedure for laminated composite shells is developed. Full geometric nonlinearity for large deformation and rotation and rate–independent anisotropic plasticity are included. A degenerated 3–D laminated composite shell element with first–order shear deformable kinematics and a total Lagrangian finite element formulation is used in the deterministic analysis. The first–order second–moment technique for probabilistic finite element analysis of random fields is employed to determine mean and variance of displacement, strain, and stress fields. Random variables built into the model include ply stiffnesses, orientation angles, and ply thicknesses. Fiber and matrix stiffnesses and volume ratios can be selected as random variables with the use of the Aboudi micromechanics model. Monte Carlo simulation was used to verify selected results.

Many problems were investigated either to verify the second–moment method's accuracy or to investigate and quantify variability in certain structures. It was concluded very early that the second–order perturbation of the second–moment method required too much computational expense and storage and returned only a slight correction to the mean values. By comparing the results with the Monte Carlo method, it is concluded that the first–order second–moment method for estimating structural response mean and variance is quite accurate as long as the input coefficient of variations are less than 0.15. The method maintains this accuracy when a significant number of independent random variables are assumed, as is typically the case in layered composite problems. A few large degree of freedom and large number of layer nonlinear

problems were studied to test the probabilistic method's ability to deal with practical (aerospace industry) size models. The random field techniques for the larger models become far too costly both from computational and storage viewpoints. However, the assumption of a fully correlated field for each random variable in each layer (uniform variance) led to more realistic computational expense.

The inclusion of transverse shear deformation proved to be critical in modeling laminated composites, especially into the postbuckling range. It was demonstrated that the modified Riks arc length method works quite well with the second–moment probabilistic method and allowed mean and variance calculations to be made beyond zero–slope limit points, which often exist in shell structures.

As for material nonlinear problems, the radial return algorithm was installed in a manner such that combined geometric and material nonlinear problems can be solved quite efficiently. The plasticity analysis is performed here in combination with the geometric nonlinearity and resulted in very little increase in iterations per load step. ARALL and Boron/Aluminum plasticity problems were investigated and the variability of these composites were quantified for a tension specimen with a hole.

An approximate reliability calculation against first ply failure was made for a composite panel loaded in axial compression into its postbuckled state. By assuming the stress and strength to have Normal distributions, the mean and variance of the stress could be used directly in a linear (maximum stress) performance function to estimate probability of safety.

8.2 Recommendations

The natural and most important step to be added to the computational procedure developed herein is to efficiently and optimally integrate it with the first and second–order reliability estimation methods. Thus calculation of the mean and variance response would become optional if reliability computations are desired. The sensitivity derivatives already computed in the program would simply be used directly to compute the safety indices, and in this way the original random variables can be assumed to be any known distribution functions with specified mean, variance, and correlation. The loss in accuracy in calculating small probabilities of failure by using the mean and variance response directly would be avoided in this manner.

With the improved reliability algorithm installed, more detailed and accurate laminated composite reliability calculations could be made. More generally accepted failure criteria, such as the Tsai–Wu, Tsai–Hill, and maximum strain criteria could be used. Laminate failure could be studied by combining the individual first ply failure probabilities into a system reliability problem. More detailed stress analysis may be required, leading to a global–local approach combining other theories such as the layer–wise theories of Reddy [97]. Stiffener elements could be added to model the effects of stiffened composite plates and shells. Also, design optimization could be performed by optimizing the reliability index, with selected random variables used as design variables.

The generality of the formulation could be improved by broadening the range of loading and problem types. The addition of thermal loads, random loads and geometry, and transient analysis are obvious extensions. The

inclusion of plasticity and other nonlinear behavior at the constituent level of a micromechanics theory is also a possibility. Due to the realization that the mechanics of the interphase region in a metal matrix composite is very critical, a micromechanics theory which includes this region is essential.

ACKNOWLEDGEMENTS

The financial support provided by NASA Lewis Research Center in funding this research is gratefully acknowledged (Grant NAG–3–933). In particular, the authors thank Mr. Dale Hopkins, the NASA Grant monitor.

REFERENCES

1. Law, A. M. and Kelton, W. D., *Simulation Modeling and Analysis*, McGraw–Hill Book Co., 1982.

2. McKay, M. D., Beckman, R. J. and Conover, W. J., "A Comparison of Three Methods for Selecting Values of Input Variables in the Analysis of Output from a Computer Code," *Technometrics*, Vol. 21, No. 2, 1979.

3. Vanmarcke, E., *Random Fields, Analysis and Syntheses*, MIT Press, second printing, 1984.

4. Ma, F. and Wei, M. S., "On the Synthesis of Porous Random Fields for Groundwater Flow," *Computer–Aided Engineering*, ASME PVP, Vol. 98, No. 5, 1985, p. 237.

5. Shinozuka, M. and Dasgupta, G., "Stochastic Finite Element Methods in Dynamics," *Proceedings of the 3rd Conference on Dynamic Response of Structures*, Los Angeles, CA, March 31–April 2, 1986, p. 44.

6. Yamazaki, F., Shinozuka, M. and Dasgupta, G., "Neumann Expansion for Stochastic Finite Element Analysis," *Stochastic Mechanics*, Vol. 1, M. Shinozuka, (ed.), Dept. Civil Eng. and Eng. Mechanics, Columbia University, New York, June 1987.

7. Contreras, H., "The Stochastic Finite Element Method," *Computers and Structures*, Vol. 12, 1980, p. 341.

8. Spanos, P., "Stochastic Linearization in Structural Dynamics," *Applied Mech. Reviews*, Vol. 34, 1981, p. 1.

9. Wen, Y. K., "Equivalent Linearization of Hysteretic Systems Under Random Excitation," *J. Applied Mechanics*, 1980, p. 150.

10. Mohammadi, J. and Amin, M., "Nonlinear Stochastic Finite Element Analysis of Pipes on Hysteretic Supports Under Seismic Excitation," *Computational Probabilistic Methods*, presented at The Joint ASME/SES Applied Mechanics and Engineering Sciences Conference, Berkeley, CA, June 20–22, 1988, p. 123.

11. Casciati, F. and Faravelli, L., "Stochastic Equivalent Linearization for Dynamic Analysis of Continuous Systems," *Computational Probabilistic Methods*, presented at The Joint ASME/SES Applied Mechanics and Engineering Sciences Conference, Berkeley, CA, June 20–22, 1988, p. 205.

12. Faravelli, L., Casciati, F., and Singh, M. P., "Stochastic Equivalent Linearization Algorithms and Their Applicability to Hysteretic Systems," *Meccanica*, Vol. 23, 1988, p. 107.

13. Casciati, F. and Faravelli, L., "Stochastic Finite Element Analysis of Nonlinear Media," *ASME Pressure Vessels and Piping Division*, PVP Vol. 176, 1989, p. 133.

14. Casciati, F. and Faravelli, L., "Nonlinear Stochastic Finite Element Analysis of Continua," *Proc. ICOSSAR '89, 5th Int. Conf. on Structural Safety and Reliability*, San Francisco, CA, 1989, p. 1105.

15. Casciati, F. and Faravelli, L., "Stochastic Equivalent Linearization of Hysteretic Behavior," *Proc. Eighth Int. Conf. on Offshore Mechanics and Arctic Engineering*, The Hague, 1989, p. 383.

16. Chen, C. C. T., and Yang, H. T. Y., "Random Vibrations of Geometrically Nonlinear Finite Element Plates and Shells," *Proc. ICOSSAR '89, 5th Int. Conf. on Structural Safety and Reliability*, San Francisco, CA, 1989, p. 1303.

17. Faravelli, L., "Stochastic Finite Elements by Response Surface Techniques," *Computational Probabilistic Methods*, presented at The Joint ASME/SES Applied Mechanics and Engineering Sciences Conference, Berkeley, CA, June 20–22, 1988, p. 197.

18. Faravelli, L. and Bigi, D., "Stochastic Finite Elements for Automotive Impact," *ASME Pressure Vessels and Piping Division*, PVP, Vol. 176 1989, p. 55.

19. Chryssanthopoulos, M., Baker, M. J. and Dowling, P. J., "Reliability–Based Design of Stringer–Stiffened Cylinders Under Axial Compression," *Proc. Sixth Int. Offshore Mechanics and Arctic Engineering Symposium*, Vol. 2, 1987, p. 403.

20. Larder, R. A., "The Stochastic Finite Element Simulation of Parallel Fiber Composites," *J. Composite Materials*, Vol. 10, January 1976, p. 21.

21. Deodatis, G. and Shinozuka, M., "Spatial Strength Variation of Laminated Orthotropic Composites," *J. of Composite Materials*, Vol. 23, 1989, p. 1256.

22. Ditlevsen, O., Bjerager, P., Olesen, R., and Hasofer, A. M., "Directional Simulation in Guassian Processes," *Probabilistic Engineering Mechanics*, Vol. 3, No. 4, 1988, p. 207.

23. Ang, A. H. S. and Tang, W. K., *Probability Concepts in Engineering Planning and Design, Volumes I and II, Basic Principles*, Wiley, 1984.

24. Handa, K. and Andersson, K., "Application of Finite Element Methods in Statistical Analysis of Structures," *Proc. ICOSSAR '81, 3rd Int. Conf. Structural Safety and Reliability*, Trondheim, Norway, 1981, p. 409.

25. Hisada, T. and Nakagiri, S., "Stochastic Finite Element Method Developed for Structural Safety and Reliability," *Proc. ICOSSAR '81, 3rd Int. Conf. Structural Safety and Reliability*, Trondheim, Norway, 1981, p. 395.

26. Nakagiri, S., Takabatake, H. and Tani, S., "Uncertain Eigenvalue Analysis of Composite Laminated Plates by the Stochastic Finite Element Method," *ASME J. of Engineering for Industry*, Vol. 109, No. 1, February 1987, p. 9.

27. Tani, S., Nakagiri, S. and Higashino, T., "Assessment of the Reliability Indices of CFRP Laminated Plate," *Computational Probabilistic Methods*, presented at The Joint ASME/SES Applied Mechanics and Engineering Sciences Conference, Berkeley, CA, June 20–22, 1988, p. 27.

28. Tani, S. and Nakagiri, S., "Reliability Synthesis of CFRP Laminated Plate," *Proc. ICOSSAR '89, 5th Int. Conf. on Structural Safety and Reliability*, San Francisco, CA, 1989, p. 2079.

29. Sato, Y., Watanabe, K. and Nakagiri, S., "Stochastic Finite Element Analysis of Stresses in FRP Pressure Vessels," *ASME Pressure Vessels and Piping Division*, PVP Vol. 177, 1989, p. 181.

30. Lawrence, M. A., "Basis Random Variables in Finite Element Analysis," *Int. J. for Numerical Methods in Engineering*, Vol. 24, 1987, p. 1849.

31. Lawrence, M. A., "Probability–Based Tools for Interactive Computer–Aided Design," *Computational Probabilistic Methods*, presented at The Joint ASME/SES Applied Mechanics and Engineering Sciences Conference, Berkeley, CA, June 20–22, 1988, p. 37.

32. Ghanem, R. and Spanos, P. D., "Galerkin–Based Response Surface Approach for Reliability Analysis," *Proc. ICOSSAR '89, 5th Int. Conf. on Structural Safety and Reliability*, San Francisco, CA, 1989, p. 1081.

33. Liu, W. K., Belytschko, T., and Mani, A., "Random Field Finite Elements," *Int. J. for Numerical Methods in Engineering*, Vol. 23, 1986, p. 1831.

34. Liu, W. K., Belytschko, T. and Mani, A., "Probabilistic Finite Elements for Nonlinear Structural Dynamics," *Computer Methods in Applied Mechanics and Engineering*, Vol. 56, 1986, p. 61.

35. Liu, W. K., Besterfield, G. and Belytschko, T., "Transient Probabilistic Systems," *Computer Methods in Applied Mechanics and Engineering*, Vol. 67, 1988, p. 27.

36. Liu, W. K., Besterfield, G. and Belytschko, T., "Variational Approach to Probabilistic Finite Elements," *J. Engineering Mechanics*, Vol. 114, No. 12, December, 1988, p. 2115.

37. Liu, W. K., Belytschko, T. and Mani, A., "Applications of Probabilistic Finite Element Methods in Elastic/Plastic Dynamics," *Transactions of the ASME*, Vol. 109, February 1987, p. 2.

38. Liu, W. K., Mani, A. and Belytschko, T., "Finite Element Methods in Probabilistic Mechanics," *Probabilistic Engineering Mechanics*, Vol. 2, No. 4, 1987, p. 201.

39. Liu, W. K., Belytschko, T. and Mani, A., "Probabilistic Finite Elements for Transient Analysis in Nonlinear Continua," *Advances in Aerospace Structural Analysis*, AD–09, ASME, O. H. Burnside and C. H. Parr, (eds.), New York, 1985, p. 9.

40. Mani, A., *Probabilistic Finite Element Methods*, Ph.D. Dissertation, Mechanical Engineering Department, Northwestern University, Evanston, Illinois, August 1987.

41. Liu, W. K., Besterfield, G., Lawrence, M. and Belytschko, T., "Kuhn–Tucker Optimization Based Reliability Analysis for Probabilistic Finite Elements," *Computational Probabilistic Methods*, presented at The Joint ASME/SES Applied Mechanics and Engineering Sciences Conference, Berkeley, CA, June 20–22, 1988, p. 135.

42. Besterfield, G. H., Liu, W. K., Lawrence, M. A., and Belytschko, T. B., "Fatigue Crack Growth Reliability by Probabilistic Finite Elements," *Computational Mechanics of Probabilistic and Reliability Analysis*, W. K. Liu and T. Belytschko, (eds.), Northwestern University, Evanston, Ill., Elme Press Int., Lusanne, Wa., 1989, p. 343.

43. Liu, W. K., Chen, J. S., and Lu, Y. Y., "Probabilistic Analysis of a Fluid–Shell System with Random Imperfections," *Computational Mechanics of Probabilistic and Reliability Analysis*, W. K. Liu and T. Belytschko, (eds.), Northwestern University, Evanston, Ill., Elme Elme Press Int., Lusanne, Wa., 1989, p. 543.

44. Arnbjerg–Nielsen, T. and Bjerager, P., "Finite Element Reliability Method with Improved Efficiency by Sensitivity Analysis," *Computational Probabilistic Methods*, presented at The Joint ASME/SES Applied Mechanics and Engineering Sciences Conference, Berkeley, CA, June 20–22, 1988, p. 15.

45. Der Kiureghian, A. D. and Ke, J.–B., "The Stochastic Finite Element Method in Structural Reliability," *Probabilistic Engineering Mechanics*, Vol. 3, No. 2, 1988, p. 83.

46. Liu, P.–L. and Der Kiureghian, A. D., "Finite Element Reliability of Two Dimensional Continua with Geometric Nonlinearity," *Proc. ICOSSAR '89, 5th Int. Conf. on Structural Safety and Reliability*, San Francisco, CA, 1989, p. 1089.

47. Gorman, M., "Structural Resistance Moments by Quadratures," *Structural Safety*, Vol. 2, 1984, p. 73.

48. Tokada, T. and Shinozuka, M., "Local Integration Method in Stochastic Finite Element Analysis," *Proc. ICOSSAR '89, 5th Int. Conf. on Structural Safety and Reliability*, San Francisco, CA, 1989, p. 1073.

49. Weiqiu, Z. and Weiqiang, W., "Applications of Stochastic FEM Based on the Local Average of Random Field in Random Eigenvalue Problems," *Chinese J. of Aeronautics*, Vol. 3, No. 1, 1990, p. 1.

50. Dias, J. B. and Nagtegaal, J. C., "Efficient Algorithms for Use in Probabilistic Finite Element Analysis," *Advances in Aerospace Structural Analysis*, AD–09, ASME, 1985, p. 37.

51. Dias, J. B. and Nakazawa, S., "An Approach to Probabilistic Finite Element Analysis Using a Mixed–Iterative Formulation," *Computational Probabilistic Methods*, presented at The Joint ASME/SES Applied Mechanics and Engineering Sciences Conference, Berkeley, CA, June 20–22, 1988, p. 75.

52. Cruse, T. A., Burnside, O. H., Wu, Y.–T., Polch, E. Z. and Dias, J. B., "Probabilistic Structural Analysis Methods for Select Space Propulsion System Structural Components (PSAM)," *Computers and Structures*, Vol. 29, No. 5, 1988, p. 891.

53. Cruse, T. A., Wu, Y.–T., Dias, J. B. and Rajagopal, K. R., "Probabilistic Structural Analysis Methods and Applications," *Computers and Structures*, Vol. 30, No. 1/2, 1988, p. 163.

54. Rajagopal, K. R., DebChaudhury, A. and Newell, J. F., "Verification of Nessus Code on Space Propulsion Components," *Proc. ICOSSAR '89, 5th Int. Conf. on Structural Safety and Reliability*, San Francisco, CA, 1989, p. 2299.

55. Millwater, H. R., Wu, Y.–T., Dias, J. B., McClung, R. C., Raveendra, S. T. and Thacker, B. H., "The Nessus Software System for Probabilistic Structural Analysis," *Proc. ICOSSAR '89, 5th Int. Conf. on Structural Safety and Reliability*, San Francisco, CA, 1989, p. 2283.

56. Liu, W. K. and Belytschko, T., (eds.), *Computational Mechanics of Probabilistic and Reliability Analysis*, Elme Press Int., Lusanne, WA, 1989.

57. Sugiyama, T., Ukon, H. and Matsumoto, T., "Probabilistic Analysis of Soil Structures Using Finite Element Method," *Proc. ICOSSAR '89, 5th Int. Conf. on Structural Safety and Reliability*, San Francisco, CA, 1989, p. 1113.

58. Ishii, K. and Suzuki, M., "Stochastic Finite Element Analysis for Spatial Variations of Soil Properties Using Kriging Technique," *Proc. ICOSSAR '89, 5th Int. Conf. on Structural Safety and Reliability*, San Francisco, CA, 1989, p. 1161.

59. Hisada, T. and Noguchi, H., "Sensitivity Analysis for Nonlinear Stochastic FEM in 3D Elasto–Plastic Problems," *ASME Pressure Vessels and Piping Division*, PVP Vol. 177, 1989, p. 175.

60. Hisada, T. and Noguchi, H., "Development of a Nonlinear Stochastic FEM and its Application," *Proc. ICOSSAR '89, 5th Int. Conf. on Structural Safety and Reliability*, San Francisco, CA, 1989, p. 1097.

61. Millwater, H. R., Wu, Y.–T. and Fossum, A. F., "Probabilistic Analysis of a Materially Nonlinear Structure," *A Collection of Technical Papers from the AIAA/ASME/ASCE/AHS/ASC 31st Structures, Structural Dynamics and Materials Conference*, Part 2, 1990, p. 1048.

62. Harren, S. V., "Probabilistic Analysis of Structures Composed of Path Dependent Materials," *Proc. ICOSSAR '89, 5th Int. Conf. on Structural Safety and Reliability*, San Francisco, CA, 1989, p. 2291.

63. Arenburg, R. T., *Analysis of Metal Matrix Composite Structures Using a Micromechanical Constitutive Theory*, Ph.D. Dissertation, Engineering Mechanics, Virginia Polytechnic Institute and State University, Blacksburg, VA, December 1988.

64. Aboudi, J., "Closed Form Constitutive Equations for Metal Matrix Composites," *Int. J. Engineering Science*, Vol. 25, No. 9, 1987, p. 1229.

65. Bodner, S. R., "Review of a Unified Elastic–Viscoplastic Theory," *Unified Constitutive Equations for Plastic Deformations and Creep of Engineering Alloy*, A. K. Miller, (ed.), Elsevier Applied Sciences Publishers, 1986.

66. Griffin, O. H., *Three–Dimensional Inelastic Finite Element Analysis of Laminated Composites*, Ph.D. Dissertation, Virginia Polytechnic Institute and State University, Blacksburg, Virginia, 1980.

67. Hill, R., "A Theory of the Yielding and Plastic Flow of Anisotropic Metals," *Proc. Roy. Soc.*, Vol. 193, No. 1033, 1948, p. 189.

68. Hill, R., *The Mathematical Theory of Plasticity*, Oxford University Press, 1950.

69. Lin, T. H., Salinas, D., and Ito, Y. M., "Effects of Hydro–Static Stress on the Yielding of Cold–Rolled Metals and Fiber–Reinforced Composites," *J. of Composite Materials*, Vol. 6, 1972, p. 409.

70. Chandrashekhara, K., "Geometric and Material Nonlinear Analysis of Laminated Composite Plates and Shells," Ph.D. Dissertation, Virginia Polytechnic Institute and State University, Blacksburg, Virginia, 1985.

71. Valanis, K. C., "Fundamental Consequences of a New Intrinsic Time Measure: Plasticity as a Limit of the Endochronic Theory," *Arch. of Mech.*, Vol. 32, 1980, p. 171.

72. Pindera, M. J. and Herakovich, C. T., "An Endochronic Model for the Response of Unidirectional Composites Under Off–Axis Tensile Loads," *Mechanics of Composite Materials: Recent Advances*, Proceedings of the IUTAM Symposium on Mechanics of Composite Materials, Z. Hashin and C. T. Herakovich, (eds.), Virginia Polytechnic Institute and State University, Blacksburg, Virginia, 1982.

73. Kachanov, L. M., *Fundamentals of the Theory of Plasticity*, Mir Publishers, Moscow, 1984.

74. Kenaga, D., Doyle, J. F. and Sun, C. T., "The Characterization of Boron/Aluminum Composite in the Nonlinear Range as an Orthotropic Elastic–Plastic Material," *J. of Composite Materials*, Vol. 21, 1987, p. 516.

75. Rizzi, S. A., Leewood, A. R., Doyle, J. F., and Sun, C. T., "Elastic–Plastic Analysis of Boron/Aluminum Composite Under Constrained Plasticity Conditions," *J. of Composite Materials*, Vol. 21, 1987, p. 734.

76. Sun, C. T. and Chen, J. K., "Effect of Plasticity on Free Edge Stresses in Boron–Aluminum Composite Laminates," *J. of Composite Materials*, Vol. 21, 1987, p. 969.

77. Leewood, A. R., Doyle, J. F. and Sun, C. T., "Finite Element Program for Analysis of Laminated Anisotropic Elastoplastic Materials," *Computers and Structures*, Vol. 25, No. 5, 1987, p. 749.

78. Hasofer, A. M. and Lind, N. C., "Exact and Invariant Second–Moment Code Format," *J. of the Engineering Mechanics Division*, ASCE, Vol. 100, No. EM1, February 1974, p. 111.

79. Rackwitz, R. and Fiessler, B., "Structural Reliability Under Combined Random Load Sequences," *J. of Computers and Structures*, Vol. 9, 1978, p. 489.

80. Chen, X. and Lind, N. C., "Fast Probability Integration by Three Parameter Normal Tail Approximation," *Structural Safety*, Vol. 1, 1983, p. 169.

81. Wu, Y.–T. and Wirsching, P. H., "A New Algorithm for Structural Reliability Estimation," *J. of Engineering Mechanics*, ASCE, 1985.

82. Wu, Y.–T., "Demonstration of a New Fast Probability Integration Method for Reliability Analysis," *Proc. of Symposium on Probabilistic Structural Design and Analysis*, ASME, 1985.

83. Wirsching, P. H. and Wu, Y.–T., "Advanced Reliability Methods for Structural Evaluation," *J. of Engineering for Industry*, ASME, Vol. 109, p. 19.

84. Wu, Y.–T., *Efficient Methods for Mechanical and Structural Reliability Analysis and Design*, Ph.D. Dissertation, The University of Arizona, April 1984.

85. Wu, Y.–T., Millwater, H. R., and Cruse, T. A., "An Advanced Probabilistic Structural Analysis Method for Implicit Performance Functions," *A Collection of Technical Papers from the AIAA/ASME/ASCE/AHS/ASC 30th Structures, Structural Dynamics and Materials Conference*, Part 4, 1989, p. 1852.

86. Liao, C.–L., *An Incremental Total Lagrangian Formulation for General Anisotropic Shell–Type Structures*, Ph.D. Dissertation, Department of Engineering Mechanics, Virginia Polytechnic Institute and State University, Blacksburg, VA, June 1987.

87. Reddy, J. N., *An Introduction to the Finite Element Method*, McGraw–Hill, New York, 1984.

88. Chao, W. C. and Reddy, J. N., "Analysis of Laminated Composite Shells Using a Degenerated 3–D Element," *Int. J. Numerical Methods in Engineering*, Vol. 20, 1984, p. 1991.

89. Simo, J. C. and Hughes, T. J. R., *Elastoplasticity and Viscoplasticity Computational Aspects*, Draft of book unpublished, 1988.

90. Simo, J. C. and Taylor, R. L., "A Return Mapping Algorithm for Plane Stress Elastoplasticity," *Int. J. for Numerical Methods in Engineering*, Vol. 22, No. 3, 1986, p. 649.

91. Crisfield, M. A., "A Fast Incremental/Iterative Solution Procedure that Handles "Snap–Through"," *Computers and Structures*, Vol. 13, 1980, p. 55.

92. Starnes, J. H., Jr., and Rouse, M., "Postbuckling and Failure Characteristics of Selected Flat Rectangular Graphite–Epoxy Plates Loaded in Compression," AIAA Paper No. 81–0543, 1981.

93. Engelstad, S. P., Knight, N. F., Jr., and Reddy, J. N., "Interlaminar Shear Stress Effects on the Postbuckling Response of Graphite–Epoxy Panels," *Advances in Structural Testing, Analysis, and Design*, Tata McGraw–Hill, New Delhi, 1990, p. 102.

94. Ramm, E. and Sattele, J. M., "Elasto–Plastic Large Deformation Shell Analysis Using Degenerated Elements," *Nonlinear Finite Element Analysis of Plates and Shells*, T. J. R. Hughes, A. Pifko, and A. Jay, (eds.), AMD–48, ASME, 1981, p. 265.

95. Dupuis, G. A., Hibbitt, H. D., McNamara, S. F. and Marcal, P. V., "Nonlinear Material and Geometric Behavior of Shell Structures," *Computers and Structures*, Vol. 1, 1971, p. 223.

96. Bucci, R. J. and Mueller, L. N., "ARALL Laminate Performance Characteristics," presented at ARALL Laminates Technical Conference, Seven Springs Resort, Champion, PA, 1987.

97. Reddy, J. N., "On New Developments in the Refined Theories of Laminated Composite Plates," Presented at the *International Conference on New Developments in Structural Mechanics*, Catania, Italy, July 1990.

APPENDIX A

In this appendix, a few relevant terms are defined and the basic method for determining reliability is described. This brief review is only meant as an aid to the reader. Most of the definitions involved in the initial part of this section are based on material from reference [56].

In general terms, a random variable is one whose value is uncertain or undetermined. For this reason problems without random variables are often considered to be deterministic. The distribution function controls the probability of a random variable having certain values. Two distribution functions are of major importance: the cumulative distribution function (CDF), and the probability density function (PDF). The CDF of a random variable U is given by

$$F_U(u) \equiv P[U \leq u] \tag{A.1}$$

which means the probability that the random variable U is less than or equal to some deterministic value u. The PDF is defined as

$$f_U(u) \equiv \frac{dF_U(u)}{du} \tag{A.2}$$

so that

$$P[U \leq u] = F_U(u) = \int_{-\infty}^{u} f_U(z)dz$$

The weighted averages or moments of random variables can also be used to describe their distribution. The expected value of a function r(U) is defined

as

$$E[r(U)] \equiv \int_{-\infty}^{\infty} r(u) f_U(u) du \tag{A.3}$$

Using this definition, important moments can be defined such as mean and variance. The first moment, called the mean, is the central measure of the PDF and is given by

$$E[U] = \mu_U = \int_{-\infty}^{\infty} u f_U(u) du \tag{A.4}$$

The second moment (central), called the variance, is a measure of the dispersion or spread of the distribution from its mean and is defined as

$$Var(U) \equiv E[U - \mu_U]^2 = \int_{-\infty}^{\infty} (u - \mu_U)^2 f_U(u) du \tag{A.5}$$

The standard deviation and coefficient of variation are parameters which are often utilized. The standard deviation is given by

$$\sigma_U \equiv \sqrt{Var(U)} \tag{A.6}$$

and the coefficient of variation (COV) by

$$COV \equiv \frac{\sigma_U}{\mu_U} \tag{A.7}$$

When two random variables have a probabilistic relationship, this becomes a family and the relationship is defined by their joint distribution functions. For example, the joint CDF of two random variables U and V is defined as

$$F_{UV}(u,v) \equiv P[U \leq u, V \leq v] \tag{A.8}$$

where the comma indicates the intersecting areas of the individual CDFs. Moments can also be defined for two random variables. The expectation of a function of U and V (first moment) is given by

$$E[r(U,V)] \equiv \int_{-\infty}^{\infty}\int_{-\infty}^{\infty} r(u,v) f_{UV}(u,v)dv \tag{A.9}$$

The second central moment, or covariance,

$$Cov(U,V) \equiv E[(U-\mu_U)(V-\mu_V)] = \int_{-\infty}^{\infty}\int_{-\infty}^{\infty}(u-\mu_U)(v-\mu_V) f_{UV}(u,v)dv \tag{A.10}$$

and corresponding correlation coefficient,

$$\rho_{UV} \equiv \frac{Cov(U,V)}{\sigma_U \sigma_V}$$

are dimensional and dimensionless measures of linear dependence between the two random variables.

A random function is an extension of these ideas in which this function varies with one or more variables but for specific values of the variables its value is uncertain. If the variable is restricted to time only, then the random function is called a random process. If the variables are only spatial coordinates, then the function is called a random field. In the present study random fields are the focus, however it is also shown that if a random field becomes very highly correlated, this reduces to or becomes equivalent to a single random variable. A random function has an infinite number of distribution functions, often referred to by "orders", which imply moments. For example, the second–order CDF of a random field U(x), where x refers to spatial coordinates, evaluated at x_1 and x_2 is given by

$$F_{U_1U_2}(u_1,u_2,x_1,x_2) = P[U_1 = U(x_1) \leq u_1, U_2 = U(x_2) \leq u_2] \tag{A.11}$$

A homogeneous (or stationary if x refers to time) random function U(x) of order two is one whose second–order CDF and PDF are dependent only on the difference (x_1-x_2) and not on the actual values of x_1 and x_2. When the function has a constant mean and an autocovariance dependent only on this difference (x_1-x_2), then it is termed homogeneous in the wide sense.

Autocovariance refers to the covariance of a single random function evaluated at two points, given mathematically by

$$\mathrm{Cov}(U(x_1),U(x_2)) = \int_{-\infty}^{\infty}\int_{-\infty}^{\infty} f_{U_1U_2}(u_1,u_2;x_1,x_2)du_1du_2 \tag{A.12}$$

In the present study only random fields which are homogeneous in the wide sense have been considered. However, the methods can easily be applied to inhomogeneous fields in which the mean is a function of the actual spatial coordinates, for example.

Having defined some basic probabilistic principles and terms, the next step is to describe the framework typically used to estimate reliability. The description to follow is modeled after the original ideas developed by Hasofer and Lind [78] and discussed by Wirsching and Wu [83]. Let $g(U_i) = 0$ be the limit state function in which U_i are the random variables. Each U_i is transformed to a reduced coordinate u_i according to

$$u_i = (U_i - \mu_i)/\sigma_i \tag{A.13}$$

where (μ_i,σ_i) are the mean and standard deviation respectively of U_i. Equation (A.13) is then substituted into $g(U_i)$ so that the limit state function is now expressed in terms of the reduced coordinates, $g_1(u_i)$. The generalized safety index β is defined as the minimum distance from the origin of the reduced coordinates to the limit state surface. Thus in mathematical terms the problem becomes the following constrained minimization problem

$$\beta = \min \sqrt{\Sigma u_i^2} \tag{A.14}$$

subject to the constraint $g_1(u_i) = 0$. The design point is also defined as the point on $g_1(u_i) = 0$ closest to the origin. Typically, various optimization schemes are employed to solve the problem stated above.

The probability of failure P_f can be easily determined using the safety index β and the standardized Normal cumulative distribution tables (ϕ) as

$$P_f = \phi(-\beta) \tag{A.15}$$

If $g(U_i)$ is linear in the U_i, and all U_i are Normal, then P_f is exact. Otherwise P_f is only an approximation.

Extensions to the above basic method have been developed by Rackwitz and Fiessler [79], Chen and Lind [80], and Wu [81–85] which provide improvements to the estimate of P_f. These improvements allow for other distributions than the Normal, and also nonlinear limit state functions. The recent Wu method has proven to be the most accurate and also the most complex.

In the process of solving the constrained minimization problem, derivatives of the limit state function with respect to random variables are required. Since the limit state function is typically a function of the structural response (e.g. displacement, strain, stress, etc.), then by the chain rule of differentiation, derivatives of the response with respect to the random variables are needed. Since the latter derivatives are already determined in the process of calculating the variance using the second–moment probabilistic finite element

method, then they can now be used directly to estimate reliability. In this way an efficient procedure for reliability estimation incorporating the probabilistic finite element method is achieved.

APPENDIX B

The Monte Carlo simulation method is considered to be a mature subject, with widespread use since the onset of rapid computers. The term "simulation", as used in the present context, is the technique of using a computer to evaluate a given deterministic model numerically. Monte Carlo simulation, in a general sense, can be defined as any simulation involving the use of random numbers for solving certain stochastic problems. In the following paragraphs, a brief description of the Monte Carlo simulation method is presented. Most of the content of this review is based on the material in reference [1].

Using the Monte Carlo simulation procedure, the computer is used to generate n independent statistical samples for each random variable, which are then fed into the model. Each sample can be thought of as an independent deterministic experiment, which is processed by the model to yield the results of the experiment. Each "sample" is drawn from a pre–selected probability distribution, so that the sample distribution is appropriate. After the simulation process, the output data is statistically analyzed to estimate the true characteristics of the model.

Many probability distribution functions exist in the statistical literature. In this study the random variables were all assumed to follow the Normal distribution, whose probability density function (PDF) is defined as

$$f_U(u) = \frac{1}{\sqrt{2\pi}\ \sigma_U} \exp\left[\frac{-(u - \mu_U)^2}{2\sigma_U^2}\right] \qquad (B.1)$$

where μ_U and σ_U are the mean and standard deviation of the random variable U. In the process of generating random numbers, the Uniform distribution becomes important. This distribution gives an equal probability of any number within the prescribed interval, and its PDF is defined as

$$f_U(u) = \frac{1}{b-a} \qquad \text{if } a \leq u \leq b \qquad \text{(B.2)}$$

$$0 \qquad \text{elsewhere}$$

Therefore once independent random numbers have been generated from the Uniform distribution, they can be transformed into random variables from any other distribution. Many random number generators and distribution sampling schemes exist in the literature, and the reader is therefore referred to [1].

When correlation between random variables exist, such as in the case of a random field, then the independent random variable samples produced from the random number generator/sampling scheme must be transformed into correlated random variable samples. In this study a method proposed by Shinozuka [6] is used, in which the Choleski decomposition of the covariance matrix is utilized to perform this transformation.

Since in the present work the mean and variance are the distribution parameters of the structural response under study, then it is necessary to estimate these moments using Monte Carlo techniques. With this in mind, the sample mean is defined as

$$\bar{U}(n) \equiv \frac{\sum_{i=1}^{n} u_i}{n} \tag{B.3}$$

such that $\bar{U}(n)$ is an unbiased estimator of the actual mean μ_U. The sample variance is defined as

$$s^2(n) \equiv \frac{\sum_{i=1}^{n} [u_i - \bar{U}(n)]^2}{n - 1} \tag{B.4}$$

such that $s^2(n)$ is an unbiased estimator of the actual variance σ_U^2. The strong law of large numbers guarantees if a sufficiently large sample size n is taken, that $\bar{U}(n) \cong \mu_U$ will be true. Thus it is obvious that the Monte Carlo simulation method requires a large sample size to be accurate, so that when this method is combined with the finite element method, considerable computational expense is the result. For this reason the Monte Carlo method is not attractive in performing probabilistic finite element analysis. However, it is considered quite accurate when large enough samples are taken, and for this reason it is used to check selected results of the second–moment probabilistic finite element method.

REPORT DOCUMENTATION PAGE

Form Approved
OMB No. 0704-0188

1. AGENCY USE ONLY (Leave blank)	2. REPORT DATE	3. REPORT TYPE AND DATES COVERED
	February 1993	Final Contractor Report

4. TITLE AND SUBTITLE

Nonlinear Probabilistic Finite Element Models of Laminated Composite Shells

5. FUNDING NUMBERS

WU-510-01-50
NAG3-933

6. AUTHOR(S)

S.P. Engelstad and J.N. Reddy

7. PERFORMING ORGANIZATION NAME(S) AND ADDRESS(ES)

Virginia Polytechnic Institute and State University
Blacksbury, Virginia 24061-02

8. PERFORMING ORGANIZATION REPORT NUMBER

E-7579

9. SPONSORING/MONITORING AGENCY NAMES(S) AND ADDRESS(ES)

National Aeronautics and Space Administration
Lewis Research Center
Cleveland, Ohio 44135-3191

10. SPONSORING/MONITORING AGENCY REPORT NUMBER

NASA CR-191069

11. SUPPLEMENTARY NOTES

Project Manager, Dale A. Hopkins, Structures Division, NASA Lewis Research Center, (216) 433-3260.

12a. DISTRIBUTION/AVAILABILITY STATEMENT

Unclassified - Unlimited
Subject Category 24

12b. DISTRIBUTION CODE

13. ABSTRACT *(Maximum 200 words)*

A probabilistic finite element analysis procedure for laminated composite shells has been developed. A total Lagrangian finite element formulation, employing a degenerated 3-D laminated composite shell element with the full Green-Lagrange strains and first-order shear deformable kinematics, forms the modeling foundation. The first-order second-moment techniques for probabilistic finite element analysis of random fields is employed and results are presented in the form of mean and variance of the structural response. The effects of material nonlinearity are included through the use of a rate-independent anisotropic plasticity formulation with the macroscopic point of view. Both ply-level and micromechanics-level random variables can be selected, the latter by means of the Aboudi micromechanics model. A number of sample problems are solved to verify the accuracy of the procedures developed and to quantify the variability of certain material type/structure combinations. Experimental data is compared in many cases, and the Monte Carlo simulation method is used to check the probabilistic results. In general, the procedure is quite effective in modeling the mean and variance response of the linear and nonlinear behavior of laminated composite shells.

14. SUBJECT TERMS

Finite element method, Nonlinear analysis, Probabilistic analysis, Composite laminates, Shell structures, Structural reliability

15. NUMBER OF PAGES

200

16. PRICE CODE

A09

17. SECURITY CLASSIFICATION OF REPORT	18. SECURITY CLASSIFICATION OF THIS PAGE	19. SECURITY CLASSIFICATION OF ABSTRACT	20. LIMITATION OF ABSTRACT
Unclassified	Unclassified	Unclassified	